

DESIGN AND MANUFACTURING OF A QUAD TILT ROTOR  
UNMANNED AIR VEHICLE

A THESIS SUBMITTED TO  
THE GRADUATE SCHOOL OF NATURAL AND APPLIED SCIENCES  
OF  
MIDDLE EAST TECHNICAL UNIVERSITY

BY

AHMET CANER KAHVECİOĞLU

IN PARTIAL FULFILLMENT OF THE REQUIREMENTS  
FOR  
THE DEGREE OF MASTER OF SCIENCE  
IN  
AEROSPACE ENGINEERING

SEPTEMBER 2014



Approval of the thesis:

**DESIGN AND MANUFACTURING OF A QUAD TILT ROTOR  
UNMANNED AIR VEHICLE**

submitted by **AHMET CANER KAHVECİOĞLU** in partial fulfillment of the requirements for the degree of **Master of Science in Aerospace Engineering Department, Middle East Technical University** by,

Prof. Dr. Canan Özgen

Dean, Graduate School of **Natural and Applied Sciences**

Prof. Dr. Ozan Tekinalp

Head of Department, **Aerospace Engineering**

Prof. Dr. Nafiz Alemdaroğlu

Supervisor, **Aerospace Engineering Dept., METU**

**Examining Committee Members:**

Prof. Dr. Serkan Özgen

Aerospace Engineering Dept., METU

Prof. Dr. Nafiz Alemdaroğlu

Aerospace Engineering Dept., METU

Prof. Dr. Altan Kayran

Aerospace Engineering Dept., METU

Prof. Dr. Yusuf Özyörük

Aerospace Engineering Dept., METU

Prof. Dr. Kahraman Albayrak

Mechanical Engineering Dept., METU

Date:

**I hereby declare that all information in this document has been obtained and presented accordance with academic rules and ethical conduct. I also declare that, as required by these rules and conduct, I have fully cited and referenced all material and results that are not original to this work.**

Name, Last name: Ahmet Caner KAHVECİOĞLU

Signature:

# **ABSTRACT**

## **DESIGN AND MANUFACTURING OF A QUAD TILT ROTOR UNMANNED AIR VEHICLE**

Kahveciođlu, Ahmet Caner  
M.S., Department of Aerospace Engineering  
Supervisor: Prof. Dr. Nafiz Alemdarođlu

September 2014, 145 pages

This thesis presents the design and manufacturing process of a mini class quad tilt rotor unmanned air vehicle (UAV). An optimal design procedure is conducted to satisfy a set of pre-determined requirements, which ensure a competitive aircraft platform performing primarily intelligence, surveillance and reconnaissance missions in UAV market.

The aircraft has four electric motors with tilting capability in one axis, which gives it the opportunity to combine the vertical take-off and landing capabilities with long endurance and good maximum cruise speed. In addition, as a result of the physical concept and the modular design of the aircraft, wing and tail parts of the aircraft can be demounted, so that the aircraft is converted to a highly maneuverable quad-rotor, which has a longer hovering time capacity than the full aircraft and is more appropriate for missions requiring stealth.

The thesis includes the construction of a mathematical model which calculates all of the weight estimation parameters and geometrical and performance outputs; generation of different design cases using this mathematical model and the procedure for an optimal design choice; construction of the outer geometry and inner structure

of the aircraft; manufacturing of the molds and the composite skins of the aircraft; and assemblage of the aircraft. Outputs of the mathematical model are compared with computational fluid dynamics (CFD) solutions to justify the analytical calculations. Besides, static loading tests are conducted to examine the structural design of the airframe.

The main objective of the study is to give an idea about the feasibility of developing a new concept of a mini class UAV.

Keywords: Unmanned Air Vehicle, Tilt-rotor, Optimization, Design, Manufacture

## ÖZ

### **DÖRT DÖNER ROTORLU BİR İNSANSIZ HAVA ARACININ TASARIM VE ÜRETİMİ**

KAHVECİOĞLU, AHMET CANER

Yüksek Lisans, Havacılık ve Uzay Mühendisliği Bölümü

Tez Yöneticisi: Prof. Dr. Nafiz Alemdaroğlu

Eylül 2014, 145 sayfa

Bu tez, dört tilt rotorlu mini sınıf bir insansız hava aracının (İHA) tasarım ve üretim sürecini konu almaktadır. Ağırlıklı olarak istihbarat, keşif ve gözlem görevlerini yürütecek bu hava aracını İHA pazarında rekabet edebilir kılacak, önceden belirlenmiş bir gereksinimler bütünü, optimal bir tasarım prosedürü uygulanarak karşılanmaya çalışılmıştır.

Hava aracı dört adet tilt edilebilen- öne ve yukarı döndürülebilen- elektrik motoruna sahiptir. Bu özelliği ona dikey iniş-kalkış imkânını, uzun uçuş süresi ve yüksek azami seyir hızı yetenekleri ile birleştirme olanağı sunmuştur. Bunun yanında hava aracının fiziksel konsepti ve modüler tasarımı, kanat ve kuyruk parçalarının çıkarılarak; onun yüksek manevra kabiliyetli bir dört pervaneli helikoptere dönüşmesini sağlar. Böylece hava aracı daha uzun bir dikey uçuş havada kalma süresine sahip olur ve ayrıca dikkat çekmemesi gereken görevlere daha uygun hale gelir.

Bu tez, tüm ağırlık tahmini, geometri ve performans parametrelerinin hesaplandığı bir matematiksel modelin oluşturulması; bu model kullanılarak farklı tasarım alternatiflerinin oluşturulması ve optimum tasarım tercihinin yapılmasına dair

yöntem; uçağın dış geometrisi ve iç yapısının oluşturulması; uçağın kalıpların ve kompozit yüzeylerinin üretilmesi ve uçağın montajı konularını kapsamaktadır. Matematiksel modelden alınan sonuçlar, hesaplamalı akışkanlar dinamiği (HAD) çözümlerinden alınan veriler ile kıyaslanmış ve analitik hesaplar doğrulanmıştır. Hava aracının yapısal tasarımı, uygulanan statik yükleme testleri ile kontrol edilmiştir.

Bu çalışmanın temel amacı yeni bir konseptte sahip, mini sınıf bir İHA'nın geliştirilmesinin yapılabilirliği hakkında fikir vermektir.

Anahtar Kelimeler: İnsansız Hava Aracı, Tilt-rotor, Optimizasyon, Tasarım, Üretim

*To Olic...*

## **ACKNOWLEDGMENTS**

I am grateful to my supervisor Prof. Dr. Nafiz Alemdarođlu due to his support, advice and encouragements through my thesis work. I would like to thank Prof. Dr. Altan Kayran for his help in manufacturing process. I also want to thank Mr. Ender Özyetiř and Mr. Güçlü Özcan for their help in the testing phase. Besides I am very grateful to my family for their support and encouragements.

## TABLE OF CONTENTS

ABSTRACT .....	v
ÖZ .....	vii
ACKNOWLEDGMENTS .....	x
TABLE OF CONTENTS .....	xi
LIST OF TABLES .....	xv
LIST OF FIGURES .....	xvi
1. INTRODUCTION .....	1
1.1 The Concept of Tilt Rotor .....	2
1.2 The Concept of Convertible Mini Quad Tilt Rotor UAV .....	2
1.3 The Design Philosophy .....	5
1.4 Literature Survey .....	6
Competitor Study .....	9
1.5 Determination of Requirements .....	11
Mission Profile .....	11
Cruise Speed .....	13
Payload .....	13
Operational Altitude .....	13
Weight .....	14
Stall Speed .....	14
Wing Span .....	14
Power Unit .....	14
Endurance .....	14
2. CONCEPTUAL DESIGN PROCEDURE .....	17

2.1	Structure of MS Excel and Ansys Workbench Design Exploration Toolbox Coupled Design Study.....	17
2.2	Construction of the MS Excel File .....	19
	Input Parameters.....	20
	Weight Estimation Parameters .....	26
	Drag Estimation Parameters.....	33
	Geometrical Output Parameters .....	34
	Performance Output Parameters.....	36
2.3	Determination of Inputs, Outputs and Optimization Criteria .....	40
2.4	Procedure in Ansys Workbench Design Exploration Toolbox .....	45
	Design of Experiments .....	45
	Response Surface .....	47
	Optimization.....	48
3.	OUTCOME OF THE OPTIMIZATION AND DECISION OF THE FINAL CONFIGURATION .....	49
3.1	Important Correlations and Graphs .....	49
	Local Sensitivities .....	49
	Response Curves .....	51
	Trade off Charts .....	59
3.2	The Decision of the Final Design .....	63
3.3	The Numerical Outputs .....	67
	Geometrical Outputs .....	67
	Weight Outputs .....	68
	Aerodynamic and Performance Outputs .....	68
3.4	Constructing the Outer Geometry.....	71
	Fuselage.....	71

Wing.....	72
Booms .....	72
Tails.....	72
3.5    Structure of the Components and Inner Placement .....	75
Fuselage.....	75
Wing.....	76
Horizontal and Vertical Tails .....	77
Placement inside the Fuselage .....	78
3.6    Static Margin Calculation.....	79
4.    MANUFACTURING.....	83
4.1    Constructing a Manufacturable Geometry .....	83
Carrying the Numerical Values of the Design Output to the CAD .....	83
Splitting the Geometry and Drawing the Female Molds .....	85
4.2    Manufacturing of the Molds.....	88
Defining the Tool-paths and Generating the Numerical Code.....	88
Machining the Molds .....	88
Surface Finish Treatments.....	90
4.3    Manufacturing of the Composite Skins and Inner Structural Frames .....	91
Methodology .....	91
Fuselage.....	92
Wing and Tail.....	94
Inner Structural Frames.....	95
Weights of the Produced Parts .....	96
4.4    Assemblage .....	96
Fuselage.....	96
Wing.....	98

Tails.....	100
Weights of the Assembled Parts.....	102
Preparation of the Aircraft for Future Work .....	105
5. CONCLUSION.....	109
REFERENCES.....	113
APPENDICES .....	119
A.COST ANALYSIS .....	119
B.MOTOR DATASHEET .....	121
C.JUSTIFICATION OF AERODYNAMICAL OUTPUTS BY CFD CALCULATIONS .....	123
D.CONCEPTUAL PROBLEM: DRAG FORCE ON MOTOR BOOMS.....	131
E.JUSTIFICATION OF THE STRUCTURAL DESIGN OF THE AIRCRAFT BY STATIC LOADING.....	141

## LIST OF TABLES

Table 1.1 Competitor Study .....	10
Table 2.1 Airfoil Comparison @ $Re=200000$ [41] .....	23
Table 2.2 Defined Parameters in Optimization Toolbox and Optimization Criteria .	44
Table 2.3 Output of Design of Experiments .....	46
Table 2.4 Goodness of Fit Table .....	47
Table 3.1 Geometrical Outputs .....	67
Table 3.2 Weight Outputs .....	68
Table 3.3 Aerodynamic and Performance Outputs .....	68
Table 3.4 Weight Distribution of the Fixed Wing Mode .....	80
Table 4.1 Comparison of the Calculated and Measured Weights of the Composite Skin Parts .....	96
Table 4.2 Comparison of the Calculated and Measured Weights of the Assembled Parts.....	103
Table A.1 Costs of the Components .....	119
Table B.1 Performance of the Motor with Different Propellers .....	121
Table C.1 Drag Force Comparison of CFD Results with Analytical Calculations..	128
Table D.1 Drag Forces on Components at 20 m/s with zero angle of attack.....	131
Table E.1 Loads at the Stations in 1g Static Wing Loading Test .....	142
Table E.2 Loads at the Stations in 3g Static Wing Loading Test .....	143

## LIST OF FIGURES

Figure 1.1 Conceptual Sketch of the Aircraft (Quad-rotor Mode).....	3
Figure 1.2 Conceptual Sketch of the Aircraft (Fixed Wing Mode) .....	4
Figure 1.3 Flow-field of Tilting Rotors Mounted on the Wing (Out of Ground Effect) (from [3]).....	4
Figure 1.4 Flow-field of Tilting Rotors Mounted on the Wing (In Ground Effect) (from [3]).....	5
Figure 1.5 Schematic of the Conceptual Design Methodology .....	6
Figure 1.6 Experimental Prototype in [15] (from [15]) .....	7
Figure 1.7 AeroVironment Shrike.....	8
Figure 1.8 IAI Ghost .....	8
Figure 1.9 IAI Mini Panther .....	9
Figure 1.10 IAI Bird Eye 500.....	9
Figure 1.11 Primary Mission Profile (Mission 4) .....	13
Figure 2.1 Flowchart of the Optimization Procedure (Green and Yellow Blocks are Excel and Ansys Part Respectively).....	17
Figure 2.2 Analysis and Project Schematics in Ansys Workbench .....	18
Figure 2.3 Defining Objectives and Constraints in the Optimization Section .....	19
Figure 2.4 Scheme of MS Excel File .....	20
Figure 2.5 Polars of SD7062 @ Re=200000[41] .....	23
Figure 2.6 Fuselage Skin Plies (without -on the left hand side- and with reinforcement -on the right hand side-) .....	27
Figure 2.7 Wing Skin Plies (without -on the left hand side- and with reinforcement - on the right hand side-).....	28
Figure 2.8 Horizontal and Vertical Tail Skins Plies (without -on the left hand side- and with reinforcement -on the right hand side-) .....	28

Figure 2.9	Defined Parameters in Excel Interface of Ansys Workbench .....	40
Figure 2.10	The Procedure in Design of Experiments Phase .....	45
Figure 2.11	Accuracy of Response Surface .....	48
Figure 3.1	Local Sensitivity Bars @W/S=140, AR_wing=9.5, V=20m/s.....	50
Figure 3.2	W/S and AR_wing Response of ENDURANCE_4 @V=20 m/s.....	52
Figure 3.3	Wing Loading and Wing Aspect Ratio Responses of ENDURANCE_4 @V=25m/s.....	52
Figure 3.4	Velocity Response of ENDURANCE_4 @W/S=140 N/m <sup>2</sup> , AR_wing=9,5 .....	53
Figure 3.5	Wing Aspect Ratio Response of Design Take-off Weight @W/S=140 N/m <sup>2</sup> , V=20 .....	54
Figure 3.6	Wing Loading Response of Design Takeoff Weight @AR_wing=9.5, V=20m/s.....	54
Figure 3.7	Wing Loading Response of Stall Speed @AR_wing=9.5, V=20m/s.....	55
Figure 3.8	Wing Loading and Wing Aspect Ratio Responses of ENDURANCE_1 @V=20m/s.....	56
Figure 3.9	Velocity Response of ENDURANCE_1@W/S=140 N/m <sup>2</sup> , AR_wing =9.5 .....	57
Figure 3.10	Wing Loading and Wing Aspect Ratio Response of ENDURANCE_2	58
Figure 3.11	Wing Loading and Wing Aspect Ratio Response of ENDURANCE_3	58
Figure 3.12	Wing Loading and Wing Aspect Ratio Response of Wing Span .....	59
Figure 3.13	Trade-off Between W/S and AR_wing.....	60
Figure 3.14	Trade-off between W_0 and ENDURANCE_4 .....	61
Figure 3.15	Trade-off Between Stall Speed and ENDURANCE_4 .....	61
Figure 3.16	Trade-off Between Stall Speed and W_0 .....	62
Figure 3.17	Trade-off Between The Wing Span and Aspect Ratio .....	62
Figure 3.18	The candidate Points.....	63

Figure 3.19	ENDURANCE_4 Values of the Candidates (units are in minutes).....	64
Figure 3.20	Design Take-off Weight Values of the Candidates (units are in grams) .	64
Figure 3.21	Stall Speed Values of the Candidates (units are in m/s) .....	65
Figure 3.22	Wing Span Values of the Candidates (units are in meters) .....	65
Figure 3.23	ENDURANCE_3 Values of the Candidates (units are in minutes).....	66
Figure 3.24	ENDURANCE_1 Values of the Candidates (units are in minutes).....	66
Figure 3.25	Variation of Maximum Load Factor with Velocity .....	70
Figure 3.26	Variation of Power Required and Power Available with Velocity.....	70
3.27	Rate of Climb Variation with Velocity .....	71
Figure 3.28	Isometric View of the Quad-rotor Mode of the Aircraft .....	73
Figure 3.29	Isometric View of the Fixed Wing Mode of the Aircraft (Horizontal Flight Mode).....	73
Figure 3.30	Isometric View of the Fixed Wing Mode of the Aircraft (Vertical Flight Mode) .....	74
Figure 3.31	The Front, Top and Right Views of the Fixed Wing Mode of the Aircraft .....	75
Figure 3.32	Inner Structure of the Fuselage .....	76
Figure 3.33	Inner Structure of the Wing .....	77
Figure 3.34	Inner Structure of the Horizontal Tail.....	77
Figure 3.35	Inner Structure of the Vertical Tail.....	78
Figure 3.36	Placement of the Components (Fixed Wing Mode) .....	79
Figure 3.37	Placement of the Components (Quad-rotor Mode).....	79
Figure 4.1	Construction of the Wing Surface .....	83
Figure 4.2	Manufacturing Steps .....	84
Figure 4.3	Guiding Curves and Reference Cross-Sections of the Fuselage.....	85
Figure 4.4	An Example of Adverse Slope on Molds .....	86
Figure 4.5	CAD Drawing of the Molds (one side only).....	87

Figure 4.6 An Example of Tool-Paths (Left Wing Lower Surface Finishing Tool-Path) .....	88
Figure 4.7 Machining the Fuselage Mold .....	89
Figure 4.8 Scenes from Machining of the Molds (Finishing of the wing and horizontal tail; roughening of the vertical tail) .....	89
Figure 4.9 Scenes from Surface Finishing Treatments (Polyester putty on fuselage mold, applying primer on wing molds and varnished molds).....	90
Figure 4.10 Vacuum Bagging Wet Lay-up Method (from [51]) .....	92
Figure 4.11 Manufacturing of the Fuselage Skins .....	93
Figure 4.12 Manufacturing of the Wing Skins.....	94
Figure 4.13 All of the Composite Skins Parts of the Aircraft.....	95
Figure 4.14 Manufacturing of the Inner Structural Frames .....	95
Figure 4.15 Assemblage Steps of the Fuselage.....	97
Figure 4.16 Assembled Fuselage .....	98
Figure 4.17 Front Spar of the Wing .....	98
Figure 4.18 Preparing the Upper Wing Surface.....	99
Figure 4.19 Assembled Wings .....	99
Figure 4.20 Inner Structure of the Tail Surfaces.....	100
Figure 4.21 Horizontal Tail Adhered to the End of the Tail Boom.....	100
Figure 4.22 Positioning and Adhering the Vertical Tail.....	101
Figure 4.23 Assembled Horizontal and Vertical Tails.....	101
Figure 4.24 Views of the Assembled Aircraft .....	104
Figure 4.25 Electronic Equipment and Cabling Installed on the Prototype.....	105
Figure 4.26 Radio Receiver, Flight Controller, Servo Multiplexer Card and Cabling Installed on the Aircraft .....	106
Figure 4.27 Tilt Mechanism Installed on the Aircraft.....	106
Figure 4.28 View of the Equipped Aircraft (Fixed Wing Mode) for R/C Flight.....	107

Figure 4.29 View of the Equipped Aircraft (in Quad-rotor mode) for R/C Flight ..	107
Figure 4.30 A Scene From Vertical Flight in Quad-rotor Mode.....	108
Figure C.0.1 Boundary Mesh on the Wall Surfaces.....	124
Figure C.0.2 Computational Domain .....	124
Figure C.0.3 Cross-section of the motor boom in computational mesh.....	125
Figure C.0.4 Lift Coefficient Variation of the Full Aircraft with Angle of Attack ..	125
Figure C.0.5 Drag Coefficient Variation of the Full Aircraft with Angle of Attack	126
Figure C.0.6 Static Pressure Contours at 20 m/s and Zero Angle of Attack.....	127
Figure C.0.7 Body-y Moment Coefficient Variation of the Full Aircraft with Angle of Attack (In Stability Axes [56]) .....	129
Figure C.0.8 Body-z Moment Coefficient Variation of the Full Aircraft with Angle of Attack (In Stability Axes [56]).....	129
Figure C.0.9 Static Pressure Contours at 20 m/s and 10° Side-slip Angle .....	130
Figure D.0.1 Velocity Vectors around the Motor Boom at 20 m/s with zero angle of attack .....	132
Figure D.0.2 Static Pressure Contours around the Motor Boom at 20 m/s with zero angle of attack .....	132
Figure D.0.3 Static Pressure Contours of the Aircraft Version without Motor Booms at 20 m/s with zero angle of attack.....	133
Figure D.0.4 Separation Points on several 2-d elliptical and Jukowsky shapes determined by theoretical analysis of the boundary layer flow (from [45]) .....	133
Figure D.0.5 A Possible Tilting-Fairing Solution to Reduce the Form Drag (Upper configuration in horizontal flight and lower configuration in hovering) .....	134
Figure D.0.6 Delay Separation on Golf Ball (from [57]).....	135
Figure D.0.7 The Mechanism of Flow Separation Delaying by Dimples on Surface (from [58]).....	135
Figure D.0.8 Drag Coefficient Variation of Some Geometries with Reynolds Number ([from[58]) .....	136

Figure D.0.9 Sketch of the Experimental Flow Geometry [59] (from [59]).....	136
Figure D.0.10 Flow Visualization of the Experiment in [59] (from [59]) .....	137
Figure D.0.11 Influence of Splitter Plates on Drag Coefficients of Several Geometries (from [45]) .....	138
Figure D.0.12 Effects of Splitter Plates upon $St_v$ and Localised Pressure Coefficient (from [61]).....	139
Figure E.0.1 1g Static Wing Loading Test (about 2.5kg at each wing).....	141
Figure E. 0.2 1g Static Wing Loading Test (about 2.5kg at each wing).....	142
Figure E. 0.3 Wing Deformation in 1g Static Wing Loading Test .....	143
Figure E.0.4 3g Static Wing Loading Test (about 7.5 kg at each wing).....	144
Figure E.0.5 Wing Deformation in 1g Static Wing Loading Test .....	144
Figure E.0.6 Static Loading of Motor Booms.....	145



# **CHAPTER 1**

## **INTRODUCTION**

The zeitgeist of the moment gives prominence to the unmanned air vehicles (UAV's) in many areas of aviation. Countless applications have been realized so far, and many others still have their potentials. Lower manufacturing and operation costs and more flexible mission profiles due to the absence of pilot make UAV's more preferable in many military and civil applications. In macro scale, there is a trend to replace the manned air vehicles with UAV's having the same mission profiles. Similarly, in smaller scales, autonomous controls take the place of the remotely piloting and eliminate many handicaps like hardship of performing some manoeuvres or human fatigue. In addition to this, small scale aircraft have started to become important in completely new military and civil areas by means of developing hardware and software technologies.

As the application areas expand, new requirements arise. For the last few decades, the micro and mini class UAV's have not been seen as remotely piloted hobby toys. They have become today's most versatile vehicles for surveillance, mapping, target tracing and search-rescue operations. In addition to that other missions including target demolishing, electronic warfare and establishing data link are done by small UAV's. One of the most important factor for small scale UAV's to have a wide operation spectrum is their low manufacturing and operating cost. For many operations, they are considered as disposable or expendable.

Many small scale UAV's are used as a part of a man portable system on the field. As they are carried by men, these systems are light-weight and less complicated. Also, these aircraft generally do not need runway to take-off. Some of them have VTOL capabilities; and the others are launched by hand or by using catapults. For recovery, some of the ones without VTOL capabilities use parachute or airbag; or both. Other

methods like belly landing, deep stall, catching by a net or hook are also used in these systems.

## **1.1 The Concept of Tilt Rotor**

The tilt rotor concept is a combination of horizontal flight of a fixed wing and VTOL capabilities of a rotary wing. It has good endurance and forward velocity properties while it does not need a runway. At the instances of take-off and landing, the axes of the rotors are perpendicular to the ground; and parallel during the horizontal flight. The rotors are tilted when transition between vertical and horizontal flights is performed.

In general, for all scales the most obvious advantage of the tilt rotor concept is to eliminate the need for a runway. For mini class UAV's, it may be thought that it is unnecessary to add complication for that feature; as they already do not need runway. On the other hand, firstly for take-off many of these systems include catapults, which have a certain weight. Secondly, in many operations precision of the landing point is very important. Parachute recovery may have problem with that issue in case of windy weathers. Belly landing and catching by net are more difficult methods to perform, including the risk of damaging the aircraft.

A mini class rotary wing UAV has other problems. Firstly, rotary wings are more fragile to the wind conditions. Their flight conditions are more limited with respect to the fixed wing aircraft. In addition to that, their forward speed is significantly lower than fixed wings. Also their endurances are very low comparing with the fixed UAV's.

Apart from those, tilt rotor concept brings completely different operational capabilities to a fixed wing aircraft. Mode transition from horizontal flight to hovering during mission becomes possible, which is very critical for reconnaissance operations.

## **1.2 The Concept of Convertible Mini Quad Tilt Rotor UAV**

The subject of this study is a mini class quad tilt rotor UAV, whose tail and wing can be demounted optionally. When its tail and wing are demounted, the aircraft becomes a highly manoeuvrable quad-rotor with same payload. There are two

advantages of this: Firstly the aircraft gets rid of the weights of the tail and wing; and an extra battery can be loaded instead. So a significant increase in endurance is obtained. Secondly, for some special missions where stealth is an issue, the aircraft gets rid of its long wing and tail; and for search and rescue operations, it enables the aircraft to enter some narrower spaces like inside of a building or a cave. Briefly, these are the main motivations for developing this aircraft concept. In addition to enhancing the operational capabilities, charging battery from the electric poles may be possible with new technological developments in battery technologies in future. Such a development would make this concept very advantageous in the market.

The quad-rotor mode and the fixed wing mode of the aircraft are shown in Figure 1.1 and Figure 1.2 respectively.

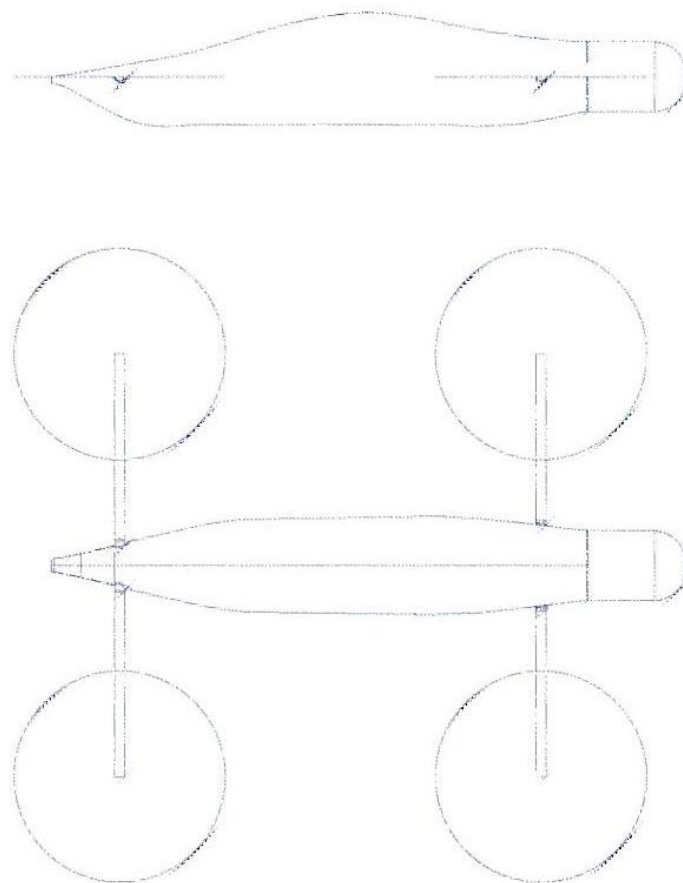


*Figure 1.1 Conceptual Sketch of the Aircraft (Quad-rotor Mode)*

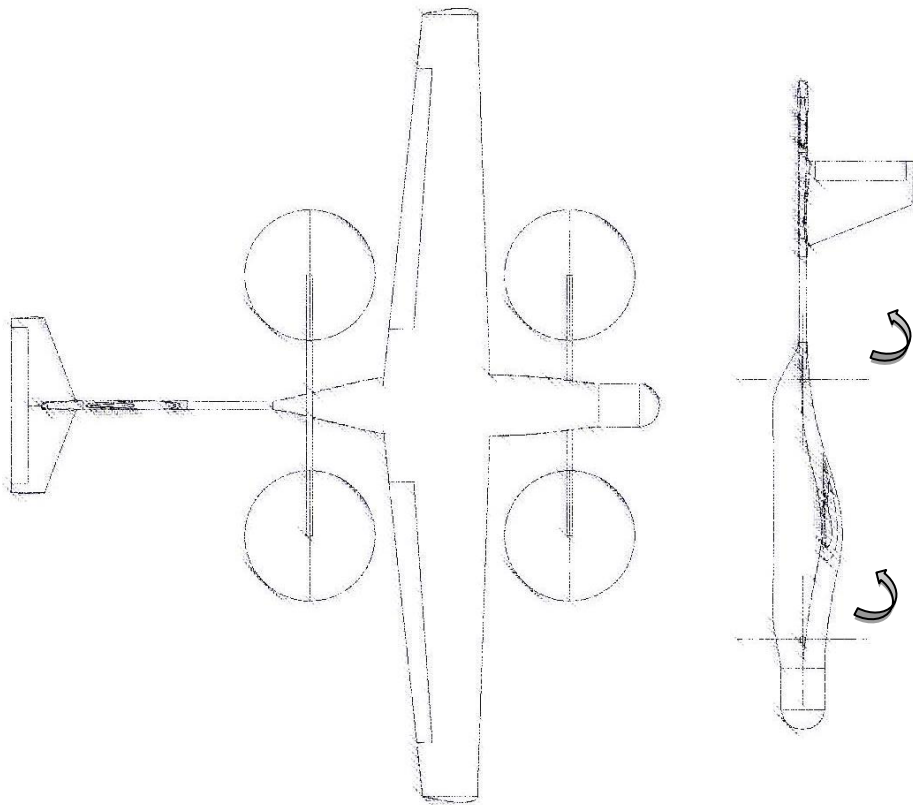


Figure 1.2 Conceptual Sketch of the Aircraft (Fixed Wing Mode)

A tandem wing configuration, where the tilting rotors are mounted on the wings, like the other QTR's [1], [2] is not chosen for some reasons. Although it may turn into an advantage in ground effect condition; the rotor wake towards the upper wing surface causes a high download force, which decreases the aircraft's lifting capacity out of ground effect [3]. The situation is shown in Figure 1.3 and Figure 1.4.

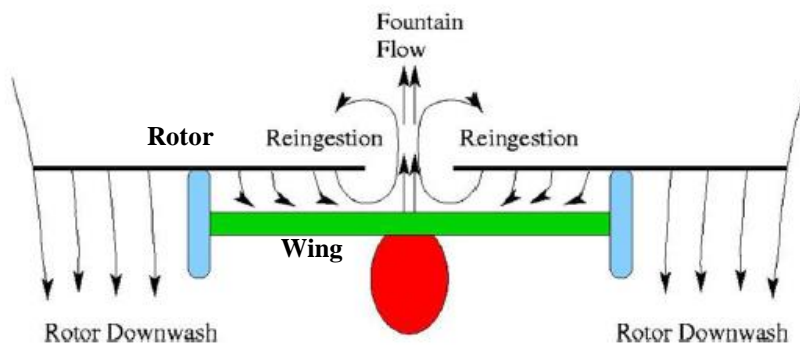


Figure 1.3 Flow-field of Tilting Rotors Mounted on the Wing (Out of Ground Effect) (from [3])

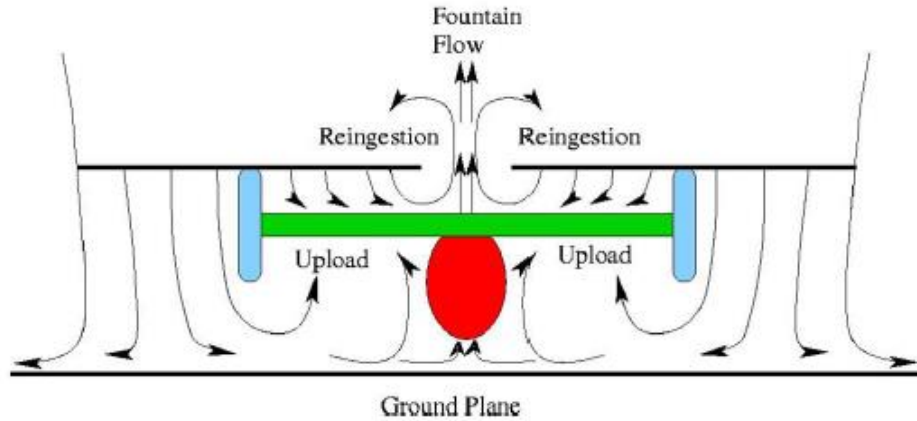


Figure 1.4 Flow-field of Tilting Rotors Mounted on the Wing (In Ground Effect) (from [3])

In this study's concept, instead of the wing upper surface, only boom sees the rotor wake. So during the vertical flight download due to the rotor wake is reduced. On the other hand, as a weakness of this study's concept, in horizontal flight, motor booms directly see the free stream, which increases the drag dramatically. This issue is discussed in APPENDIX D.

Another option to prevent this adverse effect is to use a ducted fan. However, the ducts themselves create significant drag and in addition to this the ducts increase the weight of the aircraft. [4]

This aircraft concept is genuine with its option to convert tilt rotor aircraft into quad-rotor. By demounting the wing and the tail, not only the weight is decreased, but also the manoeuvrability is enhanced by decreasing the moment of inertias of the aircraft significantly.

### 1.3 The Design Philosophy

A design study is making a chain of decisions to create something acceptable for requirements. Generally there are many ways to reach a goal. Moreover, some of these ways may also contain decisions without good reasoning. On the other hand, some initial decisions and acceptances without good reasoning may lead non-optimal solutions. The very basic notion behind this design study is that good reasoning is tried to be made for every single design choice. Therefore, a multi-objective optimization tool is used at the conceptual design level.

Only empirical formulas are used to conduct the iterative calculations, but no CFD or FEM analyses data is used in conceptual design phase considering the calculation costs.

As the study includes manufacturing, any unrealistic result may affect the credibility of the whole study. So, manufacturability is always considered in decisions.

In practice, a mathematical model, which is specific for this concept, is constructed in MS EXCEL. In this model, structural and aerodynamic calculations are conducted iteratively. In Ansys Workbench’s Design Optimization Toolbox, desired requirements and objectives are defined and let the toolbox choose the best combinations of design choices by using the MS EXCEL as solver.

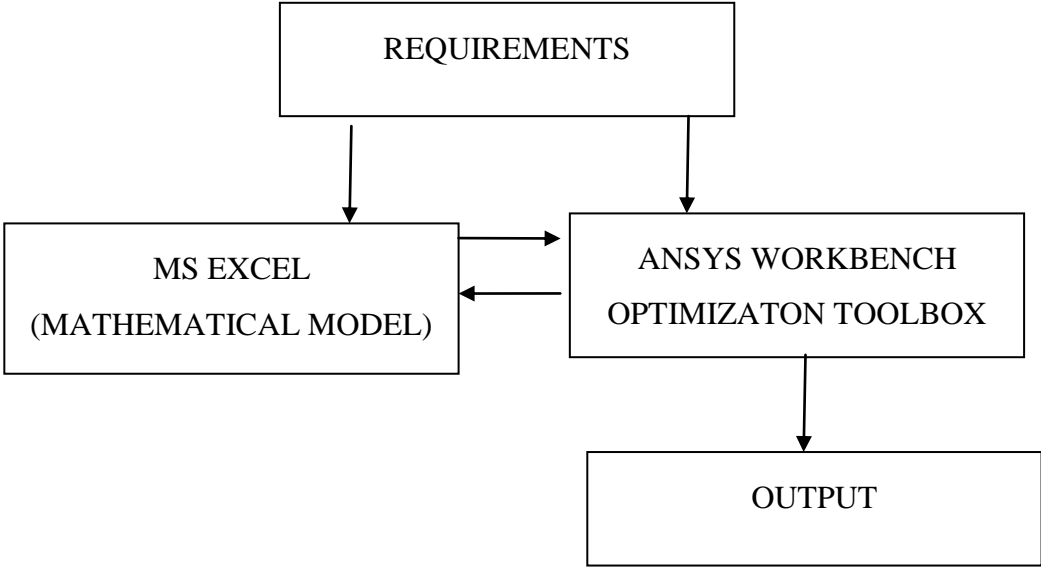


Figure 1.5 Schematic of the Conceptual Design Methodology

### 1.4 Literature Survey

In large scale, The Bell Boeing V-22 Osprey [5] is the most known example of the tilt rotor concept. It is a manned aircraft and widely used in military operations. A smaller version of V-22, The AW609 [6] is another manned tilt rotor aircraft mainly used in civil operations. These two aircraft have two rotors having swash blades and hinge mechanisms [4]. The Bell X-22 can be shown as an example of manned quad tilt rotor aircraft, whose program was cancelled in late 80’s. [1] Today “Bell Boeing Quad Tilt Rotor” [2], which is C-130 sized cargo aircraft, is an on-going project.

Boeing Phantom Swift [7] is another on-going tilt rotor project. It shows that the tilt rotor concept is still alive in large scale.

The Bell Eagle Eye [8], IAI Panther [9] and KARI Smart UAV [10] are mid-scale UAV's. TURAC [11], which is a tilt rotor with three motors, is also an on-going project from Turkey. Koker 1 [12] is another quad tilt wing developed in Iran having similar scales.

In small scale, there are many VTOL aircraft in market, which are mainly helicopters and multi-copters. Only IAI Mini Panther [13] is a tilt rotor UAV, which is the closest concept for this study. In academic side, in recent years, SUAVI, which is a tilt wing UAV, is developed in small scales [14]. In addition, the aircraft mentioned in [15] has the same physical concept to this study. In [15], the modelling and control aspects of this concept are examined.

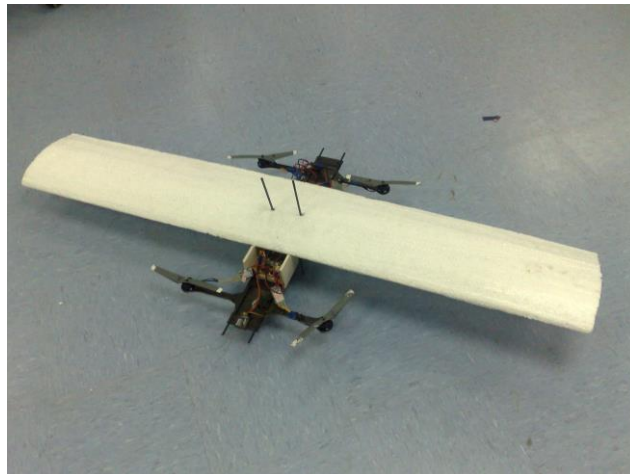


*Figure 1.6 Experimental Prototype in [15] (from [15])*

Interest on this subject is very extensive nowadays. There are also many individual developers in VTOL aircraft area. The most of these individual efforts are on small scales. However, these valuable works are mostly remotely piloted aircraft with no payload; and their specifications are not available. So, they cannot be considered in competitor study. On the other hand, the fixed wing aircraft in same class are taken into account in competitor study, as they have similar mission profiles.

In competitor study, numerous aircraft with same objectives are examined, and some of them are listed. Besides, some of them are more important than other, which shape the concept of the aircraft.

AeroVironment SHRIKE: This is a quad-rotor with a camera as payload. It answers the need of stealth UAV capable of perching and staring. [16] Shrike has a very good endurance. It is ideal for intelligence operations. It is small enough to be carried in a backpack.



*Figure 1.7 AeroVironment Shrike*

IAI GHOST: It is another stealthy UAV that can operate day and night. It also has good endurance. It is especially optimized to operate in urban areas. [17] It has twin rotor configuration and it is a very stable aircraft even in case of side-winds and gusts.



*Figure 1.8IAI Ghost*

IAI MINI PANTHER: It is a tilt rotor with three electric motors. It has a wide range of mission capabilities combining the bests of rotary wing and fixed wing concepts [13]. Despite of being slightly larger, it is the closest aircraft to this study's concept in UAV market.



*Figure 1.9 IAI Mini Panther*

IAI BIRD-EYE 500: As a fixed wing aircraft, the physical properties are expected to be very similar with this aircraft. It is again used mainly in intelligence, surveillance, reconnaissance (ISR) missions. The whole system including two aircraft, one ground control station (GCS) is carried in two backpacks and operated by two unskilled soldiers. [18] It is launched by hand or bungee.



*Figure 1.10 IAI Bird Eye 500*

## **Competitor Study**

Some important aircraft having similar objectives are listed. Except RQ-16 T-Hawk, which has piston motor, all of the competitors have electric driven motors. Some of the data of the aircraft are missing and could not be found in literature.

Table 1.1 Competitor Study

COMPETITOR	CONCEPT	MTOW	SPAN	LENGTH	OPRT. RANGE	ENDURANCE	CRUISE SPEED	PAYLOAD WEIGHT	OPRT. ALTITUDE
Raven (RQ-11B) [19]	Fixed Wing	1.9 kg	1.3 m	1.09 m	10 km	60-90 min	16 m/s	-	-
Puma (RQ-20) [20]	Fixed Wing	5.9 kg	2.8 m	1.4 m	15 km	120 min	10-23 m/s	-	-
EMT Aladin[21]	Fixed Wing	3.2 kg	1.46 m	1.53 m	> 15 km	30-60 min	45-90 m/s	-	-
Orbiter[22]	Fixed Wing	6.5 kg	2.2 m	1 m	15 km	120-180 min	10-38 m/s	-	5500 m
Skylite B[23]	Fixed Wing	6 kg	2.4 m	1.15 m	10 km	> 90 min	20-33 m/s	750 gr	100-600 m (AGL)
Bird-Eye 400[24]	Fixed Wing	5.6 kg	2.2 m	0.8 m	10-15 km	60 min	15-25 m/s	1.2 kg	1000 m (AGL)
Bird-Eye 500[18]	Fixed Wing	5 kg	2 m	1.6 m	10 km	60 min	10-30 m/s	850 gr	500 m (AGL)
Casper 200[25]	Fixed Wing	2.3 kg	2 m	1.3 m	10 km	90 min	10-25 m/s	240 gr	250 m (AGL)
DP-6 Whisperer[26]	Tandem Helicopter	23 kg	2m	2m	80 km	60-30 min	35 m/s	1-7kg	5000 m
Ghost[17]	Tandem Helicopter	4 kg	-	0.75 x 1.45 m	-	30 min	0-18 m/s	600 gr	Dozens of meters
Shrike[16]	Quadrotor	2.5 kg	N/A	-	5 km	40 min	15 m/s	-	-
HeliSpy II[27]	VTOL	2 kg	0.28 m	0.7 m	-	-	> 34 m/s	-	-
Datron Scout[28]	Quadrotor	1.3 kg	N/A	0.8 x.08 x 0.2 m	3 km	20 min	14 m/s	-	500 m (AGL)
RQ-16 T-Hawk[29]	Ducted Fan VTOL	8.4 kg	N/A	-	11 km	40 min	36 m/s	-	3200 m
Oviwun[30]	Ducted Fan VTOL	2.5 kg	64.7 cm	41.1 cm	1.6 km	20 min	14 m/s	0.5-3 kg	5875 m
Mini Panther [13]	Tilt Rotor	12 kg	3.2 m	-	20 km	90 min	20 m/s	2 kg	1500 m (AGL)
Turac [11]	Tilt Rotor	47 kg	4.2 m	1.8 m	-	85 min	20 m/s	8 kg	-

All the competitors carry optical sensors in normal, and they are mainly used for reconnaissance and surveillance missions. However, none of them is so similar to

this study's concept; so that the requirements of the aircraft for being a competitive option cannot be determined directly. Moreover, the numbers may not show everything and some qualitative properties can make an aircraft preferable. Therefore some basic requirements are accepted as is; and some of them are used to get an idea.

First of all, the payload and data-video links are roughly determined by the competitor study only. These kinds of aircraft stream video up to 15 km, and the gimbal-optical sensor combination has some standards. So these are going to be determined accordingly. So even without knowing exactly which cameras are used in those aircraft, it can be said that the payload to be chosen is going to weigh around these values.

The weights and the sizes of the aircraft vary in a range. The average values are taken into account.

The endurance values give a rough idea. The fixed wing aircraft have endurances above one hour. The rotary wing aircraft have endurances up to 40 minutes, except DP-6 Whisperer, which is a relatively larger scale aircraft.

All the candidates use electric motors. This choice is somehow obvious for this scale considering the acoustic emission and maintenance issues.

Last but not least, the cruise speed is going to be determined considering these numbers. The cruise speed should be a reason for preference for choosing this concept instead of a rotary wing.

## **1.5 Determination of Requirements**

### **Mission Profile**

There are some mission profile options determined for this aircraft. These are:

- Horizontal Flight Fixed Wing Mode (MISSION 1)
- Vertical Flight in Fixed Wing Mode (MISSION 2)
- Vertical Flight in Quad-Rotor Mode (MISSION 3)
- Combined Flight in Fixed Wing Mode (MISSION 4)

These mission profiles are represented by some formulas in prepared MS Excel file. Their endurance values are calculated and parameterized in optimization phase.

The horizontal flight in fixed wing mode refers the mission including:

- i. Vertical Take-Off for 15 seconds with a vertical velocity about 1 m/s
- ii. Transition to horizontal flight mode (rotors are perpendicular to the ground) and climb to the operational altitude
- iii. Loiter
- iv. Descend and transition to vertical flight mode (rotors are parallel to the ground)
- v. Vertical Landing for 15 seconds with a vertical velocity about 1 m/s

The vertical flight in fixed wing and quad-rotor modes refer the same mission profile, but in different modes:

- i. Vertical Take-Off for 15 seconds with a vertical velocity about 1 m/s
- ii. Vertical Flight to operation zone, execute the mission
- iii. Vertical Landing for 15 seconds with a vertical velocity about 1 m/s

The combined flight in fixed wing mode is the primary mission profile, and the endurance of this mission profile is going to be maximized during the optimization based design procedure.

- i. Vertical Take-Off for 15 second with a vertical velocity about 1 m/s
- ii. Transition to horizontal flight mode and climb to the operational altitude
- iii. Loiter
- iv. Transition to vertical flight mode, hovering above the target for 5 min and collecting detailed data
- v. Transition to horizontal flight mode and loiter
- vi. Descend and transition to vertical flight mode
- vii. Vertical Landing for 15 seconds with a vertical velocity about 1 m/s

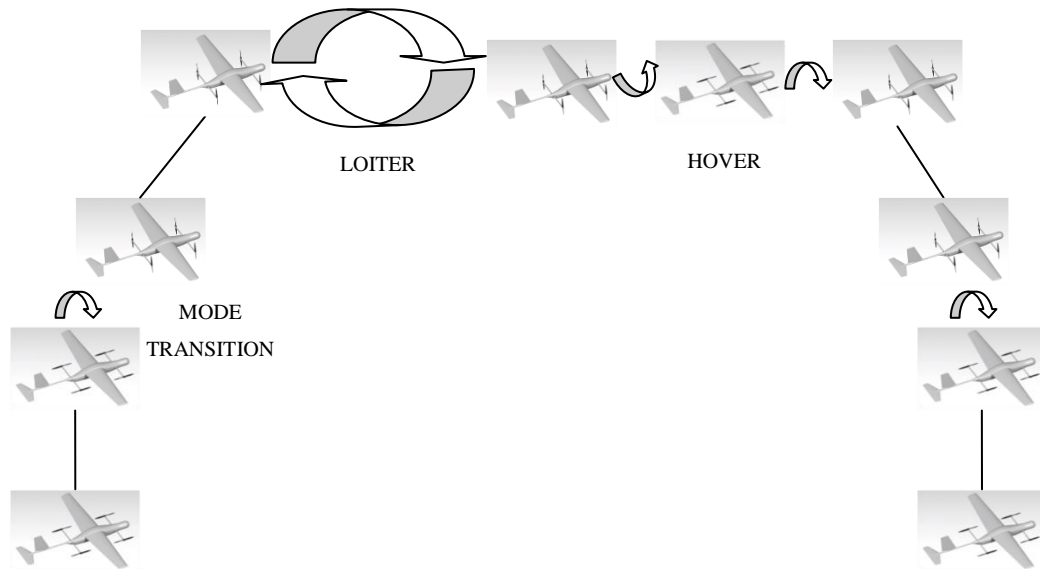


Figure 1.11 Primary Mission Profile (Mission 4)

### Cruise Speed

The cruise speed should be an advantage over the rotary wing aircraft. So design cruise speed should not be too low. On the other hand, increasing the cruise velocity dramatically decreases the endurance. Looking at the competitor study ([11], [13], [23]) a design cruise speed of 20 m/s is determined to be a good compromise.

### Payload

Payload is a gimbal with optical sensors. For the design procedure, only physical properties of the payload are necessary; and different designs can be made for different payloads. In addition to that, the optimization procedure can be conducted to maximize the payload weight. In this study, a commercial gimbal carrying electro-optical daylight and infrared sensors is chosen. [31]

### Operational Altitude

Operational altitude is determined by the properties of the payload and desired level of image detail. It can be deduced from the competitor study that [23], for various missions, the operational altitude varies between 100m - 600m AGL. For the design calculations altitude of 1100 m is used. The aircraft is thought to be used in urban

areas more than rural areas in general. The average altitude of the cities in Turkey is 695 m. [32], and assuming an average operational above ground level of 400 m results in an operation altitude of 1100 m.

### **Weight**

The total weight is crucial for a VTOL aircraft. First of all, because of the nature of the tilt rotor concept, the aircraft should carry a bigger motor than a one necessary for horizontal flight. Thrust to weight ratios are roughly 0.3 and 1.3 for horizontal and vertical flight respectively [11]. Therefore as the aircraft gets heavier, the amount of excess thrust increases and thereby the motor weight unneeded in horizontal flight increases. Secondly, thinking at system level, the aircraft is going to be a man portable system. It means that a system including two or three aircraft, ground control station, antennas and spare parts is going to be packed into one or two bags; and carried by men. There is always a weight carrying limit for a person; so the maximum take-off weight of the aircraft is limited to be 5000 gr. Any design heavier than this value is going to be eliminated in the optimization process.

### **Stall Speed**

The maximum value for the stall speed is determined to be 14 m/s, which is roughly 2/3 of the cruise speed. The aircraft is going to be automatically controlled but during the mode transition phase, low stall speed is a reason for preference.

### **Wing Span**

The maximum wing span is limited to be 2 meters for considerations about structure of the wing and modularity.

### **Power Unit**

Considering the acoustic emission, thereby stealth issues, electric motors are used. Lithium-Polymer batteries are used due to their unrivalled combination of energy density and discharge rate.

### **Endurance**

For primary mission profile (Mission 4) minimum 60 minutes of endurance, which is typical for this kind of an aircraft, is determined. By this way the endurance

standards are reached besides that vertical take-off and landing and some hovering time is added to the mission. For horizontal flight mission (Mission 1) a minimum 90 minutes of loiter time is determined. For quad-rotor mode, minimum 20 minutes of hovering time is determined.



## CHAPTER 2

### CONCEPTUAL DESIGN PROCEDURE

#### 2.1 Structure of MS Excel and Ansys Workbench Design Exploration Toolbox Coupled Design Study

Conceptual design procedure is conducted by coupling the abilities of the two commercial programs namely Microsoft Office Excel and Ansys Workbench. The design strategy is such that all the mathematical and physical correlations, which are necessary for conceptual design, are formulated in the Excel file, and then the desired key parameters like wing loading, stall velocity etc. are determined to create various design cases using Ansys Workbench's Design Exploration Toolbox. The flowchart of the procedure is shown by Figure 2.1.

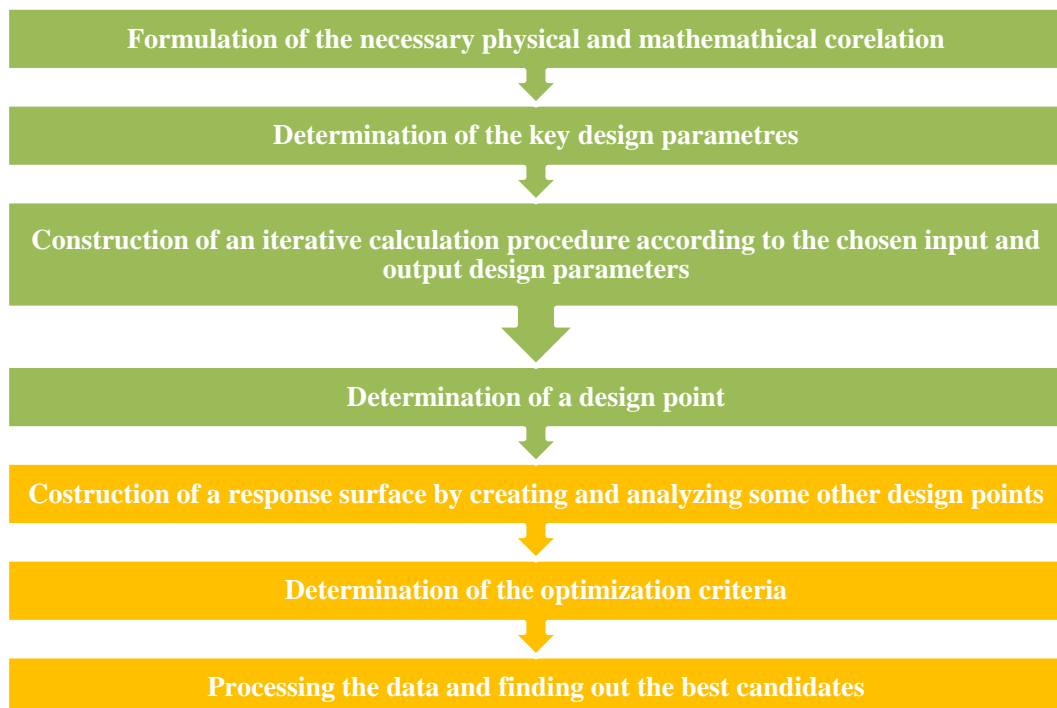


Figure 2.1 Flowchart of the Optimization Procedure (Green and Yellow Blocks are Excel and Ansys Part Respectively)

There is an Excel add-in in Ansys Workbench environment, so Ansys Workbench can directly communicate with MS Excel when the file is uploaded. Desired parameters in MS Excel file are chosen and given special names so that Ansys Workbench can identify them. After the Excel file is loaded to the Ansys Workbench, these desired parameters are defined as input or output, and these parameters can be read by Design Exploration Toolbox.

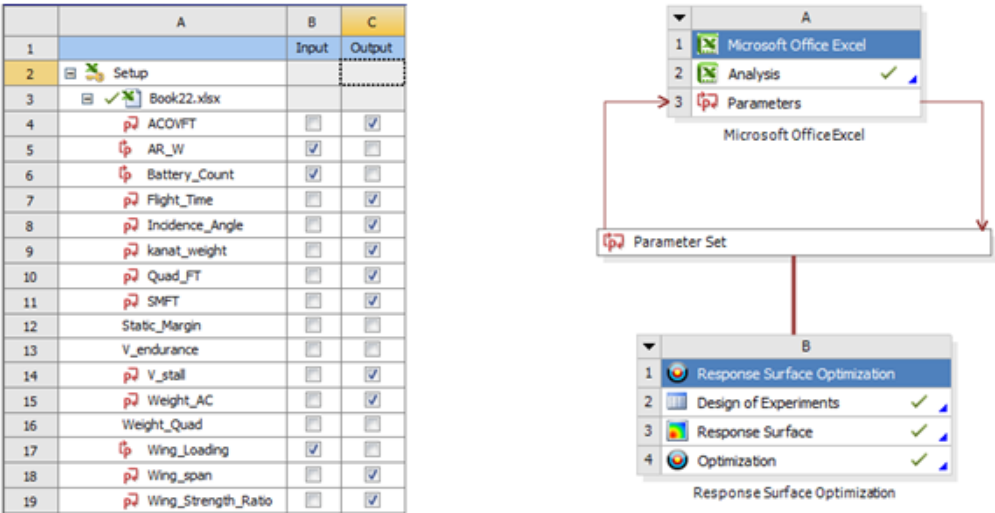


Figure 2.2 Analysis and Project Schematics in Ansys Workbench

In the design optimization process, Ansys Workbench uses MS Excel as solver to do the necessary calculations and to create all the desired cases. Then, Design Exploration Toolbox draws the values of the key parameters and establishes correlations between them. Therefore, all the responses of the output parameters to the variations of the input parameters are explored.

After completing the response analysis, desired objectives and constraints are defined in the optimization section of the toolbox. Hence, Design Exploration Toolbox can find the most suitable candidates for these criteria.

	A	B	C
1		Enabled	Monitoring
2	☑ Optimization		
3	☑ Objectives and Constraints		
4	🎯 Maximize P9		
5	🎯 Maximize P6; P6 >= 120		
6	🎯 Minimize P11; P11 <= 5000		
7	🎯 Minimize P13		
8	🎯 Minimize P10; P10 <= 14		
9	🎯 Seek P15 = 2,5		
10	☑ Domain		
11	☑ Microsoft Office Excel (A1)		
12	🔗 P1 - AR_W	<input checked="" type="checkbox"/>	
13	🔗 P2 - Battery_Count	<input checked="" type="checkbox"/>	
14	🔗 P3 - Wing_Loading	<input checked="" type="checkbox"/>	
15	Parameter Relationships		
16	☑ Results		
17	☑ Candidate Points		
18	☑ Tradeoff		
19	☑ Samples		

Figure 2.3 Defining Objectives and Constraints in the Optimization Section

## 2.2 Construction of the MS Excel File

In this work, all the necessary formulas are embedded in the MS excel file (mathematical model) and all of the output parameters are calculated in an iterative manner. In MS Excel file, there are three types of parameters. First of all is the input parameter. These types of parameters are not calculated and they are just set beforehand. When setting the optimization process in the Ansys Workbench side, only these parameters are defined as input and they are not defined as output. In MS Excel file, there are few input variables which are the key design parameters like wing loading, aspect ratio etc., and the physical constants like the density of the adhesive material or diameter of the gimbal. Proceeding with the Ansys Workbench side, only the desired key design parameters are taken and used to create different design cases.

Secondly, as the calculations are iterative, most of the parameters are both input and output in the MS Excel file. These parameters are calculated and they are not imposed externally, so they are not defined as input parameters in Ansys Workbench side. On the other hand, they are defined as output parameters and mainly used to

create constraints at optimization step. For instance, the total weight of the aircraft is calculated for each different case. When all the design points are determined for these cases, a maximum total weight can be assigned as a constraint to eliminate the heavier ones. In addition to that, an objective may be assigned to these parameters. For example, a minimization of the total weight may be assigned.

Lastly, in MS Excel file there are some parameters which do not affect other calculations. These parameters are pure output and in optimization phase, mainly these parameters are the ones to be optimized.

The MS Excel file can be modified to change the types of parameters according to the purpose. To illustrate, a predetermined payload can be fixed as input and the endurance can be the pure output and the parameter to be optimized; besides that within an endurance range, the payload weight may be the output parameter to be optimized.

The scheme of the MS Excel file is shown by Figure 2.4.

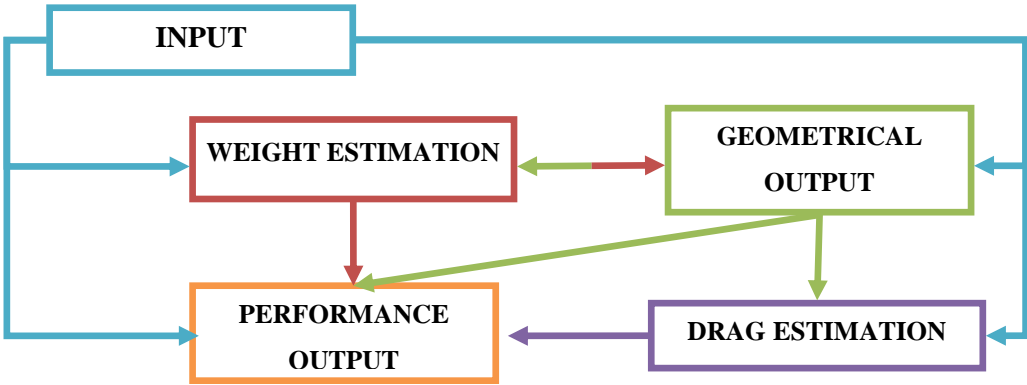


Figure 2.4 Scheme of MS Excel File

**Input Parameters**

There are various groups of input parameters.

Weight Inputs: This group includes the unit weights of the carbon fiber tubes, motors, payload, boom holders and tilt mechanism, avionics, batteries, adhesive and balsa-glass fiber reinforcement plate.

- 20x18 mm Carbon Fiber Tube,  $W_{CFT_{20x18}} = 83.4 \text{ gr/m}$
- 18x16 mm Carbon Fiber Tube,  $W_{CFT_{18x16}} = 82.5 \text{ gr/m}$
- 16x14 mm Carbon Fiber Tube,  $W_{CFT_{16x14}} = 74 \text{ gr/m}$
- 14x12 mm Carbon Fiber Tube,  $W_{CFT_{14x12}} = 64.4 \text{ gr/m}$
- 12x10 mm Carbon Fiber Tube,  $W_{CFT_{12x10}} = 54 \text{ gr/m}$
- 10x8 mm Carbon Fiber Tube,  $W_{CFT_{10x8}} = 51.5 \text{ gr/m}$
- 8x6 mm Carbon Fiber Tube,  $W_{CFT_{8x6}} = 33.4 \text{ gr/m}$
- 6x4 mm Carbon Fiber Tube,  $W_{CFT_{6x4}} = 31.5 \text{ gr/m}$
- 4 mm Carbon Fiber Rod,  $W_{CFR_4} = 29.5 \text{ gr/m}$
- Propulsion Unit (Brushless D/C Motor + ESC),  $W_{Prop\_unit} = 150 \text{ gr}$
- Servo Motor for Tilt Mechanism and Control Surfaces,  $W_{servo} = 16 \text{ gr}$
- Payload,  $W_{payload} = 700 \text{ gr}$  [31]
- Cable,  $W_{cable} = 20 \text{ gr/m}$
- Motor Boom Holder,  $W_{boom\_holder} = 40 \text{ gr}$
- Tilt Mechanism, :  $W_{tilt\_mech} = 81 \text{ gr}$
- Avionic Box (including autopilot, GPS module, data link), OMNI Antenna, AGL Sensor, Video Modem ,  $W_{avionics} = 212 + 36 + 50 + 70 = 368 \text{ gr}$  [33], [34], [35], [36]
- Battery Unit for Propulsion Unit,  $W_{battery_1} = 474 \text{ gr}$  [37]
- Battery Unit for Avionics and Payload ,  $W_{battery_2} = 250 \text{ gr}$  [38]
- Polyurethane Adhesive, the density of the adhesive is  $1.25 \text{ gr/cm}^3$  [39] (If the adhesive is applied using a syringes with 2x2mm depth and width, then
 
$$\rho_{adhesive} = 1.25 \text{ gr/cm}^3 \cdot 2 \text{ mm} \cdot 2 \text{ mm} = 5 \text{ gr/m}$$
- Reinforcement Plate (2.5 mm balsa between two layers of  $49 \text{ gr/m}^2$  e-glass),  $\rho_{plate}=493 \text{ g/m}^2$

Air Properties Inputs: The temperature, density and viscosity values of air at sea level are inputs. The values of them at different altitudes are calculated according to the formulas from Ref. [3]. The altitude is also a direct input.

- Temperature at Sea Level ( $T_0$ ): 288.16 K

- Density of Air at Sea Level ( $\rho_0$ ):  $1.225 \text{ kg/m}^3$

- Altitude (h) : 1000 m

- The temperature of air;

$$T = (1 - 6.875 \cdot 10^{-6} \cdot 3.2808 \cdot h) \cdot T_0$$

- The density of air;

$$\rho = ((1 - 6.875 \cdot 10^{-6} \cdot 3.2808 \cdot h)^{4.2561}) \cdot \rho_0$$

- The viscosity of air;

$$\mu = 1.458 \cdot 10^{-6} \cdot T^{\frac{3}{2}} \cdot \left( \frac{1}{T + 110.4} \right)$$

- Reynolds number of the flow,

$$Re_c = \rho \cdot V \cdot \frac{l_c}{\mu}$$

According to [40], characteristic length,  $l_c$  for fuselage is the full length. For wing and tail it is the mean aerodynamic chord.

- Mach number of the flow,

$$M = V / \sqrt{\gamma \cdot R \cdot T}$$

It is assumed that  $\gamma = 1.4$  and  $R = 287.15 \text{ K}$ ; and they are constant.

Airfoil Parameters: The airfoil of the wing is chosen to be SD7062 due to its good maximum lift coefficient and low moment coefficient. Also its high maximum-lift-angle of attack is thought to be an advantage during the mode transition phase. The necessary parameters of this airfoil are the followings [41]:

- Thickness Ratio,  $\left(\frac{t}{c}\right)_{wing \ airfoil} = 0.14$

- Chord-wise Location of the Aerodynamic Center: 0.25

- Chord-wise Location of the Maximum Thickness: 0.275

- $Cl_{max}$ : 1.589

- $Cl_{\alpha}$ :  $6.1 \text{ rad}^{-1}$

- $\alpha_{@L=0}$ :  $-4.22^\circ$

Table 2.1 Airfoil Comparison @  $Re=200000$  [41]

	WB-135/35	USA 28	SD7062	S3021-095-84	S1223	HQ 3.5/14	GOE 655	GOE 575	FX 63-137	E214
Thickness (%)	13.529	13.16	13.968	9.467	12.067	13.999	13.88	13.348	13.635	11.093
Camber (%)	3.767	3.754	3.981	2.959	8.692	3.527	4.399	3.608	5.988	4.043
Trailing Edge Angle (%)	14.869	20.991	6.301	7.285	7.683	12.018	15.446	35.021	5.675	9.066
Lower Surface Flatness	71.94	81.625	81.518	91.326	17.624	71.535	89.352	85.186	66.522	86.62
Leading Edge Radius (%)	3.458	3.419	2.727	1.779	3.104	2.545	3.999	4.056	2.152	1.891
Maximum Lift ( $C_L$ )	1.41	1.345	1.589	1.122	2.425	1.595	1.646	1.744	2.037	1.549
Maximum Lift Angle-of-Attack (deg)	11	15	15	8	8	11.5	15	10.5	11.5	9
Maximum Lift-to-drag (L/D)	51.679	62.786	52.55	57.274	125.35	63.14	58.202	60.648	97.886	87.641
Lift at Maximum Lift-to-drag	1.2	0.882	0.974	0.821	2.131	1.351	1.098	0.985	1.319	0.973
Angle-of-Attack for Maximum Lift-to-drag (L/D)	7.5	3.5	4.5	4.5	5	6.5	4.5	4	2	2.5

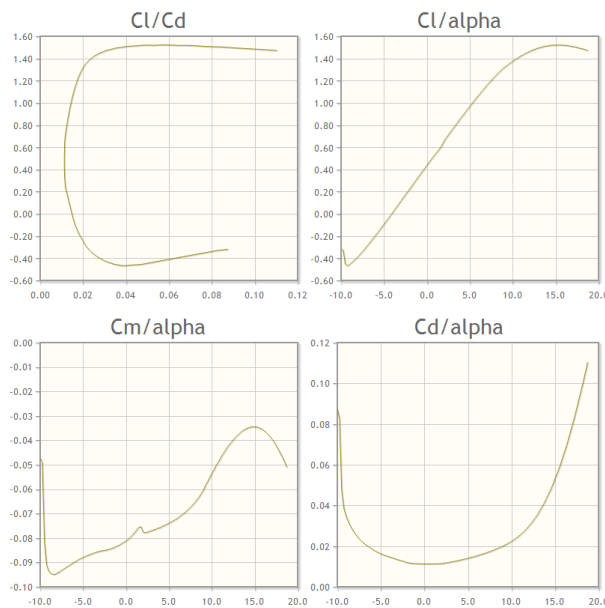


Figure 2.5 Polars of SD7062 @  $Re=200000$  [41]

The airfoil chosen for the horizontal and vertical tail is NACA 0009, and the necessary parameters of this airfoil are the followings:

- Thickness Ratio,  $\left(\frac{t}{c}\right)_{horizontal\ tail\ airfoil} = \left(\frac{t}{c}\right)_{vertical\ tail\ airfoil} = 0.09$
- Chord-wise Location of the Aerodynamic Center: 0.25
- Chord-wise Location of the Maximum Thickness: 0.3
- $Cl_{\alpha}$ :  $5.58\ rad^{-1}$

Power Calculation Inputs: A high energy density lithium-polymer battery is chosen for feeding the propulsion unit. The inputs related to it are the followings [37]:

- Nominal Voltage,  $V_{battery\_1} = 11.1\ V$
- Capacity,  $C_{battery\_1} = 8000mAh$
- Battery Count,  $n_{battery\_1} = 3$
- Vertical Flight Power Consumption: According to the datasheet of the chosen brushless D/C motor (see APPENDIX B), an average value can be approximated for endurance calculations.  $m/P_{vertical} = 4.5gr/W$
- Motor Maximum Continuous Power,  $P_{max} = 550\ W$  [42]

Aerodynamic Inputs:

- Wing Aspect Ratio: The aspect ratio of the wing is a key design parameter, and it is given various values to create different design cases. By the outcome of the literature survey, wing aspect ratio will be in a range between 6 and 13.

$$AR_{wing} = \{6, 13\}$$

- Wing Loading: Another key parameter is the wing loading of the aircraft. It is also given different values to set various design cases. By the outcome of the literature study, the wing loading will be given values in a range between 80 and 200  $N/m^2$

$$W/S = \{80, 200\ N/m^2\}$$

- Velocity: The design velocity parameter is considered as the trim velocity at cruise with no angle of attack. Besides, it is possible to set a range for the velocity parameter for different optimization goals. In optimization phase, velocity is 20 m/s

and constant; but the domain to be analyzed is created to include the variation of the velocity within the range of 20 m/s and 30m/s.

$$V = \{20,30 \text{ m/s}\}$$

○ Horizontal and Vertical Tail Aspect Ratios: Although they might need to be revised after analyzing the prop-wash effects of the propellers by wind tunnel test or numerical methods; for the early phases of the design the aspect ratio of the horizontal and vertical tail is determined from [40] and fixed to those typical values.

$$AR_{HT} = 3.5$$

$$AR_{VT} = 1.6$$

○ Wing Taper Ratio: According to the [40], for most unswept wings a taper ratio of around 0.4 is ideal considering the lift distribution tailoring and weight reduction effects of the taper. In this specific case, in order to increase the clearance between the propellers and the wing; a higher but still a typical value of wing taper ratio is set.

$$\lambda_{wing} = 0.5$$

○ Horizontal and Vertical Tail Taper Ratios: The taper ratios of the horizontal and vertical tails are determined according to the typical values mentioned in [40].

$$\lambda_{HT} = 0.5$$

$$\lambda_{VT} = 0.5$$

○ Volume Ratios of the Horizontal and Vertical Tail: For the initial phases the volume ratios are determined from [40]. On the other hand, according to the stability and maneuverability requirements of a possible controller design, there might be a need of revision.

$$c_{HT} = 0.5$$

$$c_{VT} = 0.04$$

○ Wing Dihedral, Twist and Sweep Angles: Considering the manufacturing easiness and the flight regime of the aircraft, the dihedral and the twist angles of the wing are taken to be zero. In addition to that, for an easier structural integrity, the sweep angle at the quarter chord of the wing, where the main spar is located, is zero.

$$A_{wing@c/4} = 0$$

Motor and Tail Booms Parameters: These parameters are directly imposed and determined at the beginning of the design phase.

○ Motor Booms' Diameters: Four identical propulsion units (Brushless D/C Motor + ESC + Propeller) are used and they are all mounted at the tip of 14x12 mm carbon fiber tubes. The primary consideration in determining the diameter of the tube is the total weight of the aircraft. In vertical flight each boom carries ¼ weights of the aircraft. Based on the weight requirement and an estimated boom length, various carbon fiber tubes with a length of 30 cm is subjected to 1.5 kg load at the tip when the other end is clamped. Consequently, the tip deflection of 14x12 mm carbon fiber is found to be small enough, and it is determined to be the motor boom (see APPENDIX E).

$$d_{motor\ boom} = 0.014\ m$$

○ Tail Boom's Diameter: From past experiences tail boom is determined to be 18x16 mm carbon fiber tube. In need of a reinforcement wall thickness of the tube can be easily increased by inserting a smaller diameter tube.

$$d_{tail\ boom} = 0.018\ m$$

Inputs Related to Payload Geometry: In case of selection of a different payload, related design parameters are calculated accordingly.

$$d_{payload} = 0.1\ m$$

$$l_{payload} = 0.114\ m$$

### **Weight Estimation Parameters**

The weight estimation model is one of the most critical sections in whole design phase. Therefore, a detailed iterative calculation coupled with geometrical parameters is established in MS Excel file.

In this block, first of all, the composite skins' weights are calculated; then the weights of the structural reinforcements, motors, batteries, tilt mechanism, avionic box and the payload are added up.

Skin's Surface Densities: Fuselage, wing, horizontal and vertical tail skin's surface densities are calculated separately as they consist of different composite plies. The composite manufacturing is made by wet lay-up method having a fiber-resin mass ratio of 1. The past experiences showed that for wet lay-up 1:1 mass ratio is good for used resin and all the calculations are made accordingly i.e. fiber mass is equal to the resin mass and total mass is two times the fiber mass. Also from past experiences it is

known that in wet lay-up method, it is very hard to prevent the core material to absorb the resin; and it is a good practice to take the weight of resin used to adhere the core material is equal to the weight of the core material itself. In other words, also the mass fraction of the core material and resin is 1. In addition to that, skins are not isotropic and at some structurally critical zones, reinforcements are applied. Hence, skin surface densities are calculated according to the formula:

$$\rho_{surface} = \sum (Dry\ Laminate\ Surface\ Density) \cdot 2 \cdot \frac{(Area\ of\ the\ reinforced\ zone)}{(Area\ of\ the\ total\ surface)}$$

○ Fuselage Skin Surface Density: The fuselage skin has the plies shown by Figure 2.6. It is determined to reinforce the critical structural junction points with the wing, tail boom and the motor booms. Apart from the inner structure, at these locations, skin has a different laminate shown by the same figure. From the initial CAD drawings it is estimated that 50% of the fuselage surface has reinforcement. Thus, the average surface density is calculated accordingly.

25 gr/m <sup>2</sup> E-glass Fiber	25 gr/m <sup>2</sup> E-glass Fiber
61 gr/m <sup>2</sup> Aramid Fiber	61 gr/m <sup>2</sup> Aramid Fiber
49 gr/m <sup>2</sup> E-glass Fiber	49 gr/m <sup>2</sup> E-glass Fiber
44 gr/m <sup>2</sup> Aramid Honeycomb (1mm)	93 gr/m <sup>2</sup> Carbon Fiber
49 gr/m <sup>2</sup> E-glass Fiber	44 gr/m <sup>2</sup> Aramid Honeycomb (1.5 mm)
	25 gr/m <sup>2</sup> E-glass Fiber
	44 gr/m <sup>2</sup> Aramid Honeycomb (1.5 mm)
	49 gr/m <sup>2</sup> E-glass Fiber

Figure 2.6 Fuselage Skin Plies (without -on the left hand side- and with reinforcement -on the right hand side-)

$$\begin{aligned} \rho_{fuselage\ skin} &= ((25 + 61 + 49 + 44 + 49) \cdot 2) \cdot 0.5 \\ &+ ((25 + 61 + 49 + 93 + 44 + 25 + 44 + 49) \cdot 2) \cdot 0.5 \\ &= 618\ gr/m^2 \end{aligned}$$

- Wing Skin Surface Density: The wing skin is composed of the plies shown by the Figure 2.7. It is determined to reinforce the wing root by adding a carbon fiber ply with area of 20% of the total wing surface.

25 gr/m <sup>2</sup> E-glass Fiber
49 gr/m <sup>2</sup> E-glass Fiber
31 gr/m <sup>2</sup> Rohacell Foam (1 mm)
49 gr/m <sup>2</sup> E-glass Fiber

25 gr/m <sup>2</sup> E-glass Fiber
49 gr/m <sup>2</sup> E-glass Fiber
31 gr/m <sup>2</sup> Rohacell Foam (1 mm)
93 gr/m <sup>2</sup> Carbon Fiber
49 gr/m <sup>2</sup> E-glass Fiber

Figure 2.7 Wing Skin Plies (without -on the left hand side- and with reinforcement -on the right hand side-)

$$\rho_{wing\ skin} = ((25 + 49 + 31 + 49) \cdot 2) \cdot 0.8 + ((25 + 49 + 31 + 93 + 49) \cdot 2) \cdot 0.2 = 345.5\ gr/m^2$$

- Horizontal Tail Skin Surface Density: The horizontal tail skin is composed of the plies shown by the Figure 2.8. It is determined to reinforce the boom connection section of the horizontal tail by adding two carbon fiber plies with area of 25% of the total horizontal tail surface. At that zone, there is no core material.

25 gr/m <sup>2</sup> E-glass Fiber
49 gr/m <sup>2</sup> E-glass Fiber
31 gr/m <sup>2</sup> Rohacell Foam (1 mm)
49 gr/m <sup>2</sup> E-glass Fiber

25 gr/m <sup>2</sup> E-glass Fiber
49 gr/m <sup>2</sup> E-glass Fiber
93 gr/m <sup>2</sup> Carbon Fiber
93 gr/m <sup>2</sup> Carbon Fiber
49 gr/m <sup>2</sup> E-glass Fiber

Figure 2.8 Horizontal and Vertical Tail Skins Plies (without -on the left hand side- and with reinforcement -on the right hand side-)

$$\rho_{ht\ skin} = ((25 + 49 + 31 + 49) \cdot 2) \cdot 0.75 + ((25 + 49 + 93 + 93 + 49) \cdot 2) \cdot 0.25 = 385.5\ gr/m^2$$

- Vertical Tail Skin Surface Density: The vertical tail skin is composed of the plies shown by the Figure 2.8. It is determined to reinforce the boom connection

section of the vertical tail by adding two carbon fiber plies with area of 40% of the total vertical tail surface. At that zone, there is no core material.

$$\begin{aligned}\rho_{vt\ skin} &= ((25 + 49 + 31 + 49) \cdot 2) \cdot 0.6 + ((25 + 49 + 93 + 93 + 49) \cdot 2) \cdot 0.4 \\ &= 432\ gr/m^2\end{aligned}$$

Skin's Wetted Areas: Geometric outputs of the iterative calculations feed this block and from reference area values wetted areas are calculated.

- Fuselage Wetted Area: Fuselage is approximated as a cylinder.

$$S_{wet\ fuselage} = \pi \cdot (l_{fuselage} - l_{payload}) \cdot d_{fuselage}$$

- Wing and Tail Wetted Area: According to [44], note that the second multiplier in the  $S_{wet\ wing}$  formula is the exposed wing area.

$$S_{wet\ wing} = (1.9767 + 0.5333 \cdot \left(\frac{t}{C}\right)_{wing\ airfoil}) \cdot (S_{ref\ wing} - d_{fuselage} \cdot c_{root\ wing})$$

$$S_{wet\ ht} = (1.9767 + 0.5333 \cdot \left(\frac{t}{C}\right)_{tail\ airfoil}) \cdot S_{ref\ ht}$$

$$S_{wet\ vt} = (1.9767 + 0.5333 \cdot \left(\frac{t}{C}\right)_{tail\ airfoil}) \cdot S_{ref\ vt}$$

Composite Part Weights: The composite part weights indicate the weight of the assembled parts with structural reinforcement. In other words, it is the total weight including outer skin and inner structure (ribs, spars, bulkheads etc.) As an important note, the painting is not included in calculations. The reason for this situation is that in a real production case the painting is planned to be done by adding colour pigments into the resin, which is assumed to have very small contribution to the total weight. The painting is not so critical for such an aircraft, and it is unnecessary to make the aircraft heavier with additional putty and painting operations. Otherwise, as deduced from past experiences, painting is a very uncontrollable process for such a small aircraft, and it is not preferable.

- Fuselage Weight: Two separately produced fuselage sides are assembled with polyurethane adhesive. Also, inside the fuselage there are carbon fiber tubes at the

junction points of the wing, tail and motor booms; and these tubes are supported with balsa/e-glass plates.

According to the initial CAD drawings, the total area of the reinforcement plates to be used inside the fuselage is very close to the largest cross section of the fuselage. By formulating the relation in this way, the linkage between fuselage dimensions and the area of the inner structure is kept.

There are booms located centrally to mount the wing spars and the tail boom. The tail boom is assumed to be inserted 10 cm into the fuselage boom in any case.

The adhesive weight is calculated from the lengths of the lines, where adhesive is applied. From the initial CAD drawings, it is found appropriate to approximate the inner structure of the fuselage as “circular bulkheads placed along the fuselage with 10 cm between them”. By this way, the total length of the inner structure parts’ sides is approximated depending on related parameters of fuselage length and diameter.

$$\begin{aligned}
 W_{fuselage} = & \rho_{fuselage\ skin} \cdot S_{wet\ fuselage} + \rho_{plate} \\
 & \cdot \left( (l_{fuselage} - l_{payload}) \cdot d_{fuselage} \right) + W_{boom\ holder} \cdot 4 + d_{fuselage} \\
 & * (W_{CFT_{16x14}} + W_{CFT_{8x6}}) + 0.1 \cdot W_{CFT_{20x18}} \\
 & + \left( 2 \cdot l_{fuselage} + \pi \cdot d_{fuselage} \cdot \left( \frac{l_{fuselage}}{0.1} \right) \right) \cdot \rho_{adhesive}
 \end{aligned}$$

○ Wing Weight: Assembled wing part is composed of composite upper and lower skins, ribs made from the same reinforcement plate used inside the fuselage, carbon fiber tubes with different sizes and the adhesive material.

From past experiences, it is assumed that an average distance of 8 cm between ribs is a good enough for such an aircraft. In addition to that, from the initial CAD drawings it is seen that the total area of the ribs is in order of 10% of the reference area of the wing. This proportion depends on the wing span, thickness ratio of the airfoil and wing taper ratio. Within a small enough range, this proportion is assumed to be more or less applicable.

As the wing is tapered, its thickness is decreasing through the tip; so the diameters of the carbon fiber tubes are decreasing gradually. From the initial CAD drawings, average lengths of the tubes are determined with respect to the wing span. In design aspect, this correlation between wing span and carbon fiber tubes contributes to

proportionality between the aspect ratio and the weight of the wing, which is a demand of the structural side [40].

The length to be applied adhesive is the periphery of the wing added up to the ribs' upper and lower sides. Note that, as assumed before, the ribs are thought to be located with average 8 cm between them.

$$\begin{aligned}
W_{wing} = & \rho_{wing\ skin} \cdot S_{wet_{wing}} + \rho_{plate} \cdot \left( \frac{S_{ref_{wing}}}{10} \right) + 2 \cdot W_{CFT_{16x14}} \cdot (0.1 \cdot b_{wing}) \\
& + 2 \cdot W_{CFT_{14x12}} \cdot (0.1 \cdot b_{wing}) + 2 \cdot W_{CFT_{12x10}} \cdot (0.066 \cdot b_{wing}) \\
& + 2 \cdot W_{CFT_{10x8}} \cdot (0.066 \cdot b_{wing}) + 2 \cdot W_{CFT_{8x6}} \cdot (0.066 \cdot b_{wing}) \\
& + (0.166 \cdot b_{wing}) + 2 \cdot W_{CFT_{6x4}} \cdot (0.066 \cdot b_{wing} + (0.25 \cdot b_{wing})) \\
& + 2 \cdot W_{CFR_4} \cdot (0.066 \cdot b_{wing} + (0.25 \cdot b_{wing})) \\
& + \left\{ 2 \cdot (b_{wing} - d_{fuselage} + \bar{c}_{wing}) + 2 \cdot \left[ \frac{(b_{wing} - d_{fuselage})}{0.08} \right] \right. \\
& \left. \cdot \bar{c}_{wing} \right\} \cdot \rho_{adhesive}
\end{aligned}$$

○ Horizontal and Vertical Tail Weights: Assembled horizontal and vertical tails are composed of upper and lower (or right and left) skins, inner structure made of the reinforcement plate and adhesive material.

The length to be applied adhesive is calculated in a same manner with the wing, and in addition to that tail boom interfaces are added to the formulas. The tail boom goes all below the vertical tail and into the half of the horizontal tail. Note that upper and lower sides of the boom are adhered to the surfaces.

The spar lengths are approximated to be equal to the tail spans; and note that upper and lower sides of the spar are adhered to the surfaces.

$$\begin{aligned}
W_{ht} = & \rho_{ht\ skin} \cdot S_{wet_{ht}} + \rho_{plate} \cdot \left( \frac{S_{ref_{ht}}}{10} \right) \\
& + \left[ 2 \cdot (b_{ht} + c_{tip_{ht}}) + 2 \cdot \frac{b_{ht}}{0.08} \cdot \bar{c}_{ht} + 2 \cdot (2 \cdot b_{ht}) + 2 \cdot \left( \frac{c_{root_{ht}}}{2} \right) \right. \\
& \left. \cdot d_{tail\ boom} \right] \cdot \rho_{adhesive}
\end{aligned}$$

$$W_{vt} = \rho_{vt\ skin} \cdot S_{wet_{vt}} + \rho_{plate} \cdot \left( \frac{S_{ref_{vt}}}{10} \right) + \left[ 2 \cdot (b_{vt} + c_{tip_{vt}}) + 2 \cdot \frac{b_{vt}}{0.08} \cdot \bar{c}_{vt} + 2 \cdot (2 \cdot b_{vt}) + 2 \cdot c_{root_{ht}} \cdot d_{tail\ boom} \right] \cdot \rho_{adhesive}$$

- Boom Weights: The diameters of the booms are determined beforehand and entered as direct inputs as mentioned before. The lengths are calculated according to the other design parameters and assumptions; and they feed these formulas.

$$W_{tail\ boom} = l_{tail\ boom} \cdot W_{CFT_{18x16}}$$

$$W_{motor\ boom} = l_{motor\ boom} \cdot W_{CFT_{14x12}}$$

Empty Weight Calculation: Empty weight is defined as the total weight of the aircraft, including the cables and excluding the weights of the batteries feeding the propulsion unit and the payload.

$$W_e = W_{fuselage} + W_{wing} + W_{ht} + W_{vt} + W_{tail\ boom} + 2 \cdot W_{motor\ boom} + W_{battery\_2} + W_{avionics} + 4 * W_{tilt\_mech} + 4 * W_{Prop\_unit} + 8 * W_{servo} + \rho_{cable} \cdot (2 \cdot l_{motor\ boom} + l_{tail\ boom} + l_{fuselage} + (b_{wing}/3))$$

Design Take-off Gross Weight: The design take-off gross weight is one of the most important parameters in the design phase. It is the total weight of the aircraft, and as it is an electrical powered aircraft, the weight of it does not change during the mission. All the geometrical outputs affect the total weight; and also all of the geometrical outputs somehow are affected by it. It can be considered as the interface parameter of the weight estimation block.

$$W_0 = W_e + n_{battery\_1} \cdot W_{battery\_1} + W_{payload}$$

Quad-rotor Weight: The quad-rotor weight indicates the total weight of the quad-rotor mode of the aircraft. It is an important parameter for the endurance calculation of the quad-rotor mode. It does not include the weights of the wing, tail and tail boom; but it is loaded one extra battery.

$$W_{quad} = (W_{empty} - W_{wing} - W_{ht} - W_{vt} - W_{tail boom}) + (n_{battery_1} + 1) \cdot W_{battery_1} + W_{payload}$$

### Drag Estimation Parameters

Based on geometrical parameters, drag estimation parameters contribute the performance calculations. According to the drag build-up method, each component's parasite drag is found separately, and then the total value is sent to the performance block to calculate the drag coefficient from the drag polar. All the formulas below are taken or derived from [40].

$$c_{D_0} = \frac{\sum(C_{F_c} \cdot FF_c \cdot Q_c \cdot S_{wet_c})}{S_{ref}} + c_{D_{0,motor booms}}$$

Skin friction coefficient for turbulent flows is formulated as,

$$C_{F_c} = \frac{0.455}{(\log_{10} Re_c)^{2.58} (1 + 0.144 M^2)^{0.65}}$$

Form factor for wing and tail is formulated as,

$$FF_c = \left[ 1 + \frac{0.6}{\left(\frac{x}{c}\right)_{\max_c}} \left(\frac{t}{c}\right)_c + 100 \left(\frac{t}{c}\right)_c^4 \right] \cdot [1.34 M^{0.18} \cdot (\cos \lambda_m)_c^{0.28}]$$

For wing and tail surfaces, the sweep angles at maximum thicknesses are calculated considering the fact that the sweep at the quarter chord and the sweep at the trailing edge is zero, respectively. For the tail surfaces, the sweep angle at the trailing edge is zero in order to ease the manufacturing of the control surfaces.

Form factor of the fuselage is formulated as,

$$FF_{fuselage} = \left[ 1 + \frac{60}{f^3} + \frac{f}{400} \right], \text{ and where } f = l_{fuselage} / d_{fuselage}$$

According to [45] the drag coefficient of a cylinder can be taken as roughly 0.5 between  $Re=10^4$ - $10^6$ . If it is normalized according to the reference areas of the motor booms and the wing,

$$\begin{aligned}
c_{D_{0,motor\ booms}} &= 0.5 \cdot \frac{S_{ref\ motor\ booms}}{S_{ref\ wing}} \\
&= 0.5 \cdot \frac{[2 \cdot d_{motor\ boom} \cdot (l_{motor\ boom} - d_{fuselage})]}{S_{ref\ wing}}
\end{aligned}$$

## Geometrical Output Parameters

All of the geometrical outputs are calculated iteratively. When they are found, they feed back the weight and drag estimation parameters. All the lengths and areas are calculated in this block. Generic formulas are taken from [40].

### Basic Lengths:

- Fuselage Length: The main design constraint of the fuselage is the clearance between wing and propellers. So, the wing root chord and the possible propeller diameter are design inputs here. The length of one propeller diameter has to be covered by the fuselage at minimum; so 1.5 half of the propeller diameter is taken as input. In fuselage design that choice is going to be considered. The propeller diameter is chosen to be 12'' (~0.3 m) initially, and as a conservative approach the root chord is used as reference length.

$$l_{fuselage} = c_{root\ wing} + 1.5 \cdot 0.3 + l_{payload}$$

- Fuselage Diameter: The reference value for fuselage diameter depends on the payload (here a gimbal) diameter. There should be enough space to mount the gimbal, which is equal to the payload diameter minimum; and 2 cm of extra length is assumed for lofting of the aerodynamic surface.

$$d_{fuselage} = 2 \cdot 0.02 + d_{payload}$$

- Length of the Motor Booms: As the booms go all along the fuselage, the fuselage diameter is an input and considering the clearance between propellers and fuselage,  $\frac{1}{4}$  length of the propeller diameter is left at each side.

$$l_{motor\ boom} = 1.5 \cdot 0.3 + d_{fuselage}$$

- Length of the Tail Boom: The horizontal and vertical tails are located in sequence on the tail boom (boom ends at the middle of the horizontal tail); so the root chords of them are inputs. Besides, a 15 cm of clearance between fuselage and vertical tail is assumed initially.

$$l_{tail\ boom} = 0.5 \cdot c_{root_{ht}} + c_{root_{vt}} + 0.15$$

- Spans: Wing and tail spans are calculated as follows, (subscript “c” refers to “component”)

$$b_c = \sqrt{AR_c \cdot S_{ref_c}}$$

- Chords: Wing and tail chords are calculated as follows,

$$c_{root_c} = \frac{2}{1 + \lambda_c} \cdot \frac{S_{ref_c}}{b_c}$$

$$\bar{c}_c = \frac{2}{3} \cdot c_{root_c} \cdot \frac{1 + \lambda_c + \lambda_c^2}{1 + \lambda_c}$$

$$c_{tip_c} = c_{root_c} \cdot \lambda_c$$

### Surface Areas:

- Wing Reference Area: It is one of the most important and influential output parameter.

$$S_{ref_{wing}} = \frac{W_0}{(W/S)}$$

- Horizontal Tail Reference Area: The wing quarter chord is assumed to be at the middle of the fuselage; and the tail arm is calculated accordingly.

$$S_{ref_{ht}} = \frac{c_{ht} \cdot \bar{c}_{wing} \cdot S_{ref_{wing}}}{l_{tail\ boom} + \left(\frac{l_{fuselage}}{2}\right)}$$

- Vertical Tail Reference Area: A same logic as the horizontal tail is used here.

$$S_{ref_{vt}} = \frac{c_{vt} \cdot b_{wing} \cdot S_{ref_{wing}}}{\left(l_{tail\ boom} - \frac{c_{root_{ht}}}{2} - \frac{3 \cdot c_{root_{ht}}}{4}\right) + \left(\frac{l_{fuselage}}{2}\right)}$$

Angle of Incidence: According to the necessary  $c_L$  value, a set angle is calculated to give an idea for orienting the wing with respect to the fuselage. The first model is going to be drawn and the prototype is going to be produced according to this set angle.

$$AOI = \frac{c_L}{c_{L\alpha}} + \alpha_{@L=0}$$

## Performance Output Parameters

The outputs of this block do not affect other calculations; so they can be considered as the results. Generic formulas, which are for fixed a wing aircraft, are taken from [40]. Prop-wash effects of the rotors are not included in these calculations.

### Force Coefficients:

- Lift Coefficient: It is directly calculated from the basic inputs without iteration.

$$c_L = \frac{2 \cdot (W/S)}{\rho \cdot V^2}$$

- Drag Coefficient: It is calculated from the drag polar as follows,

$$c_D = C_{D_0} + K \cdot c_L^2$$

Here,

$$K = \frac{1}{AR_{wing} \cdot \pi \cdot e}$$

- The Oswald efficiency factor for a wing with  $\Lambda_{LE} < 30^\circ$  is formulated as,

$$e = 1.78 \cdot (1 - 0.045 \cdot AR_{wing}^{0.68}) - 0.64$$

- Maximum Lift Coefficient: It is calculated as follows,

$$c_{L,max} = 0.9 \cdot c_{l,max} \cdot \cos(\Lambda_{c/4c})$$

Lift Curve Slope: The total lift curve slope From [43]:

$$c_{L\alpha} = c_{L\alpha_{wing-body}} + c_{L\alpha_{ht}} \cdot \eta_H \cdot \frac{S_{refht}}{S_{refwing}} \left( 1 - \left( \frac{d\epsilon}{d\alpha} \right)_{downwash} \right)$$

- Lift curve slope of the wing-body combination:

$$c_{L\alpha_{wing-body}} = c_{L\alpha_{wing}} \cdot \left( 1 - 0.25 \left( \frac{d_{fuselage}}{b_{wing}} \right)^2 + 0.025 \left( \frac{d_{fuselage}}{b_{wing}} \right) \right)$$

- Lift curve slope of the wing and horizontal tail:

$$C_{L\alpha_c} = \frac{2\pi \cdot AR_c}{2 + \sqrt{\frac{(AR_c)^2 \beta^2}{\kappa_c^2} \cdot \left( 1 + \frac{\tan^2 \Lambda_{c/2c}}{\beta^2} \right)} + 4}$$

$$\beta = \sqrt{1 - M^2} \quad \kappa_c = \frac{\beta \cdot C_{l\alpha_c}}{2\pi} \quad \Lambda_{c/2c} = \text{atan}\left(\frac{1}{2} \frac{c_{rootc} - c_{tipc}}{\frac{b_c}{2}}\right)$$

- The downwash factor is calculated as,

$$\left(\frac{d\epsilon}{d\alpha}\right)_{downwash} = \frac{d\epsilon}{d\alpha}\Big|_{M=0} \cdot \frac{C_{L\alpha_{wing}}|_M}{C_{L\alpha_{wing}}|_{M=0}}$$

$$\frac{d\epsilon}{d\alpha}\Big|_{M=0} = 4.44 \left[ K_A \cdot K_\lambda \cdot K_H \sqrt{\cos\Lambda_{c/4}} \right]^{1.19}$$

$$K_A = \frac{1}{AR_{wing}} - \frac{1}{1 + (AR_{wing})^{1.7}} \quad K_\lambda = \frac{10 - 3\lambda_{wing}}{7}$$

$$K_H = \frac{1 - \frac{h_h}{b_{wing}}}{\left( \frac{2(l_{tail\ boom} + \left(\frac{l_{fuselage}}{2}\right))}{b} \right)^{\frac{1}{3}}}$$

From the initial sketches it is assumed that  $h_h = 0.1m$

Thrust and Power Required: For required power calculation typical efficiency factors for propellers and D/C motors are assumed. [46] The ideal power consumption can be thought as the power output; the power required is the input power for the motors and must be drawn from the system. Therefore, the power required is used in all calculations rather than the ideal value.

$$\eta_{propeller} = 0.7 \quad \eta_{motor} = 0.8$$

$$P_{r_{ideal}} = 0.5 \cdot \rho \cdot V^3 \cdot c_D \cdot S_{ref\ wing}$$

$$P_r = \frac{P_{r_{ideal}}}{\eta_{propeller} \cdot \eta_{motor}}$$

$$T_r = 0.5 \cdot \rho \cdot V^2 \cdot c_D \cdot S_{ref\ wing}$$

Power Available: According to [47], about 70% of the maximum thrust should be enough for vertical flight. It means that the 70% of the total maximum static thrust values of the motors must be equal to the total weight of the aircraft. The motor selection is made according to this requirement [47], [11]. So, thrust to weight ratio is happened to be an initial design choice independently from the rate of climb or maximum speed, which are not critical in this aircraft concept. The total power available is the sum of four motors powers' multiplied by motor and propeller efficiencies.

$$P_a = 4 \cdot P_{max} \cdot \eta_{propeller} \cdot \eta_{motor}$$

From the motor propeller data (see Appendix B), it can be deduced that the assumed efficiency values, which are in fact the typical ones, are in a good match with the real cases.

Endurances: In hovering, it is assumed that the aircraft consumes a constant amount of power,  $\frac{W_0}{m/P_{vertical}}$ , determined by vertical flight power consumption value. This constant amount is a function of the total weight, and it is assumed to be linearly increasing with the total weight. The horizontal flight endurances are calculated by dividing the total energy capacity (after subtracting the energy spent during the hovering time) by power required.

- Mission 1 (Horizontal Flight): It is assumed that total time spent for take-off and landing is 30 seconds. ( $t_1 = 30 \text{ s}$ )

$$E_1 = \left[ V_{battery_1} \cdot C_{battery_1} \cdot n_{battery_1} - \frac{W_0}{m/P_{vertical}} \cdot t_1 \right] / P_r$$

- Mission 2 (Vertical Flight in Fixed Wing Mode):

$$E_2 = \left[ V_{battery_1} \cdot C_{battery_1} \cdot n_{battery_1} / \frac{W_0}{m/P_{vertical}} \right]$$

- Mission 3 (Vertical Flight in Quad-rotor Mode):

$$E_3 = \left[ V_{battery_1} \cdot C_{battery_1} \cdot (n_{battery_1} + 1) / \frac{W_{quad}}{m/P_{vertical}} \right]$$

- Mission 4 (Special Mission Flight): It is assumed that total time spent for take-off and landing is 30 seconds. ( $t_4 = 330 \text{ s}$ )

$$E_4 = \left[ V_{battery_1} \cdot C_{battery_1} \cdot n_{battery_1} - \frac{W_0}{m/P_{vertical}} \cdot t_4 \right] / P_r$$

Stall Speed: It is an important parameter in optimization phase in terms of controlling the wing loading; and it is calculated as follows,

$$V_{stall} = \sqrt{\frac{2 \cdot \frac{W}{S}}{\rho \cdot c_{L,max}}}$$

Rate of Climb: As the propulsion unit is chosen for vertical flight capability, the rate of climb values are expected to be higher for a mini class UAV. It is calculated as follows,

$$R/C = \frac{Excess\ Power}{Weight} = \frac{P_A - P_r}{W}$$

Maximum Velocity: Maximum velocity is calculated by finding the point where drag is equal to the available thrust, which is a function of velocity. So, there needs to be an iterative calculation to find the corresponding lift coefficient and available thrust value.

$$V_{max} = \sqrt{2 \cdot \frac{T_{a@V_{max}}}{\rho \cdot S_{ref\ wing} \cdot (C_{D_0} + K \cdot c_{L@V_{max}}^2)}}$$

$$T_{a@V_{max}} = P_a / V_{max} \quad c_{L@V_{max}} = 2 \cdot \frac{W}{S_{ref\ wing} \cdot \rho \cdot V_{max}^2}$$

Maximum Load Factor: The load factor is a function of velocity and it is constraint by available power and maximum lift coefficient. The value of the load factor is calculated according to the limitations of both factors, and the smaller value is accepted as the maximum load factor at that velocity.

$$n_{max} = \frac{1}{2} \cdot \rho \cdot V_{\infty}^2 \cdot \frac{C_{Lmax}}{(W/S)} \quad \text{or}$$

$$n_{max} = \left[ \frac{\frac{1}{2} \cdot \rho \cdot V_{\infty}^2}{K \cdot (W/S)} \left( \frac{1}{V_{\infty}} \cdot \frac{P_a}{W_0} - \frac{1}{2} \cdot \rho \cdot V_{\infty}^2 \cdot \frac{C_{D_0}}{(W/S)} \right) \right]^{1/2}$$

At low velocities, the maximum load factor is limited by the maximum lift coefficient; and at high velocities the available power limits it. The velocity where the limiting factor shifts is called the corner velocity, and it is very important for maneuvering calculations. It can be thought as the best maneuvering velocity.

$$V^* = \sqrt{\frac{2n_{max}}{\rho c_{L_{max}}} \left(\frac{W}{S}\right)}$$

Maximum Turn Rate and Minimum Turn Radius:

$$\omega_{max} = \frac{g\sqrt{n_{max}^2-1}}{V^*} \quad R_{min} = \frac{(V^*)^2}{g\sqrt{n_{max}^2-1}}$$

### 2.3 Determination of Inputs, Outputs and Optimization Criteria

In consideration of the requirements, design criteria are determined; inputs and outputs are defined accordingly. As it is explained in the first chapter, the main purpose of the aircraft is surveillance, and the primary performance goal is endurance, rather than the maximum speed or manoeuvring capabilities. Both horizontal and vertical flight times are considered in the optimization phase by defining constraints and objectives on the necessary parameters.

	A	B	C
1		Input	Output
2	Setup		
3	Book25_design10.xlsx		
4	BATTERY_COUNT	<input type="checkbox"/>	<input type="checkbox"/>
5	ENDURANCE_1	<input type="checkbox"/>	<input checked="" type="checkbox"/>
6	ENDURANCE_2	<input type="checkbox"/>	<input checked="" type="checkbox"/>
7	ENDURANCE_3	<input type="checkbox"/>	<input checked="" type="checkbox"/>
8	ENDURANCE_4	<input type="checkbox"/>	<input checked="" type="checkbox"/>
9	STALL_SPEED	<input type="checkbox"/>	<input checked="" type="checkbox"/>
10	VELOCITY	<input checked="" type="checkbox"/>	<input type="checkbox"/>
11	W_0	<input type="checkbox"/>	<input checked="" type="checkbox"/>
12	W_quad	<input type="checkbox"/>	<input checked="" type="checkbox"/>
13	WING_ASPECT_RATIO	<input checked="" type="checkbox"/>	<input type="checkbox"/>
14	WING_LOADING	<input checked="" type="checkbox"/>	<input type="checkbox"/>
15	WING_SPAN	<input type="checkbox"/>	<input checked="" type="checkbox"/>

Figure 2.9 Defined Parameters in Excel Interface of Ansys Workbench

Wing Loading: The most coupling parameter of the model is the wing loading. It determines the wing reference area, which is the main geometrical output, directly from the total weight. Wing loading is selected to be an input in Ansys Workbench side. The parameter name is assigned as “WING\_LOADING”. A wide range (between 80 and 200 N/m<sup>2</sup>) is determined by the competitor study.

Wing Aspect Ratio: The second important parameter is the aspect ratio of the wing, it affects the wing span and thereby the span efficiency of the wing. So the drag and the endurance calculations are affected. In addition to that the total weight is also slightly affected by the aspect ratio. It is also defined as an input as it can be seen in Figure 2.9, and its name is “WING\_ASPECT\_RATIO”. The range to be analysed of it is between 6 and 13.

Velocity: In fact, the design cruise velocity of the aircraft does not affect the geometry or weight parameters in the mathematical model. Only the possible wing incidence angle is calculated using the velocity. On the other hand, the dominant factor in endurance calculations is the velocity by far. If there is no objective on the design cruise velocity, the optimization phase gives always candidates with the lowest ones. In light of the competitor study, 20 m/s of cruise velocity is determined to be an appropriate value. Considering that the operational range is about 15 km, trading the endurance for velocity is not very sensible. However, it is a good practice to see the effects of the velocity changes on the output parameters, so the design cruise velocity is also defined as input and the response curves are created for velocity variations between 20 m/s and 30 m/s. In optimization phase the velocity is kept constant as 20 m/s. The name of this parameter in Ansys Workbench side is “VELOCITY”.

Stall Speed: For this concept, landing and take-off distance are not applicable and the maximum speed is not a primary requirement. So, the most important performance parameter to constrain the wing loading is the stall speed. It is also important to minimize the stall speed considering the mode transition from vertical flight to

horizontal flight. It is assigned as an output, and its name is “STALL\_SPEED” in Ansys Workbench side. The upper limit for the stall speed is nearly the 2/3 of the cruise velocity, 14 m/s.

Design Take-off Gross Weight: A limit for total weight is determined due to the fact that the whole system including the aircraft, antennas and ground control station is carried by one or almost two operators. The upper limit is determined to be 5000 grams and it is minimized. The total weight is assigned to be an output and its name is “W\_0”.

Endurance for Mission 4: Special mission flight is the default mission profile of the aircraft. It includes 5 minutes of vertical flight during the mission excluding take-off and landing, which gives the opportunity to observe a specific place in detail. It is the parameter to be maximized with higher importance. It is assigned to be “output”; and its name is “ENDURANCE\_4”.

Wing Span: There are two main motivations to define a constraint for wing span. Firstly, considering the aircraft in system level, the modularity and ergonomics are very important issues. The aircraft is going to be carried by a bag; and from past experiences it is deduced that the wing geometry is the primary factor to determine the size of the bag. The smaller wing span means a smaller bag size. It may seem as a detail, but there is chance to implement that factor in mathematical model. Secondly, there are some structural issues that are not implemented in model. When the aircraft lands, as there is no landing equipment, the wing tips may deflect and touch the ground due to the impact, especially in mountainous terrains. The shorter wings are desirable to decrease the deflection. Surface buckling is another possible problem considering the inner structure of the wing; and the longer the wing span the more prone the surface is to buckling. Of course, the whole stiffness cannot be represented by the span only, and a longer wing (if it is stiffer) may deflect less than a shorter wing. However, in the feasible zone of the domain, wing loadings are not expected to vary significantly; and the wing chords –thereby the thicknesses- are expected to be close to each other, i.e. there is little stiffness variation is expected between design

points. Considering all, the wing span is minimized with lower importance. The wing span is an output and its name is “WING\_SPAN” in Ansys Workbench side.

Endurance for Mission 1: The endurance of the horizontal flight in fixed wing mode is not subjected to a design objective, but the lower values of this parameter are not accepted. Therefore a lower boundary of 90 minutes is assigned to it. It is also an output, and its name is “ENDURANCE\_1”.

Endurance for Mission 3: The vertical flight endurance in quad-rotor mode is also maximized. It is directly a result of the quad-rotor weight. In addition to it, there is a loose correlation between the wing aspect ratio as the length of the fuselage is dependent on the wing root chord. It is an output to be maximized in the optimization phase and its name is “ENDURANCE\_3”.

Endurance for Mission 2: The endurance of the vertical flight in fixed wing mode is an exceptional case that might happen in marginal operations. Also, it is a direct function of the total weight of the aircraft only. So it is meaningless to assign a maximizing objective to it. However, it is important to know the endurance limit for vertical flight; as it might be necessary to lengthen the vertical flight at the instant of operation. It is defined as an output to create the response curves, but it does not have any effect in the optimization phase. Its name is “ENDURANCE\_2” in Ansys Workbench side.

Quad-rotor Weight: Like the endurance of the vertical flight in fixed wing mode, the effect of the quad-rotor weight is already included by “ENDURANCE\_3” parameter. So, it is also defined as an output and its response curves are created; but it has no effect in the optimization phase. Its name is “W\_quad”.

Battery Count: In initial optimization studies, the battery count was an input parameter that can have only discrete values. The values of 2, 3 and 4 batteries are tried. As outcome, it was very clear that the candidates with 2 or 4 batteries are always eliminated by the design requirements. The options with four batteries make the aircraft exceed the weight requirement; and the options with two batteries do not

satisfy the endurance requirements. To sum up, battery count is not defined in Ansys Workbench side; its value is 3 and it is constant.

Table 2.2 Defined Parameters in Optimization Toolbox and Optimization Criteria

PARAMETER	OBJECTIVE	OBJECTIVE IMPORTANCE	LOWER BOUND CONSTRAINT	UPPER BOUND CONSTRAINT
WING_LOADING	-	-	-	-
WING_ASPECT_RATIO	-	-	-	-
VELOCITY	-	-	-	-
STALL_SPEED	Minimize	Default	-	14 m/s
W_0	Minimize	Default	-	5000 gr
ENDURANCE_4	Maximize	Higher	-	-
WING_SPAN	Minimize	Lower	-	2 m
ENDURANCE_1	-	-	90 min	-
ENDURANCE_3	Maximize	Default	-	-
ENDURANCE_2	-	-	-	-
W_quad	-	-	-	-

As it can be seen in Table 2.2, “ENDURANCE\_4” has the higher importance. So maximizing objective for it can be seen as the main objective; and the other ones are complementary objective. The objective importances are determined after a long term of optimization runs with different settings. The mechanism of this option is well described in [48].

In a nutshell, the primary objective is to maximize the combined flight endurance; while maximizing the quad-rotor mode’s endurance and minimizing the total weight, stall speed and wing span with lower priorities. No numerical values can be implemented regarding to their “objective importances”, but pre-defined priority options, which are “lower”, “higher” and “default”, can be selected to tune the optimization process. These selections are made according to many trials and [48].

## 2.4 Procedure in Ansys Workbench Design Exploration Toolbox

In Ansys Workbench, inside the Design Exploration toolbox, “Response Surface Optimization” procedure is conducted. This procedure includes three phases. At first, the data is extracted from Excel file in a predetermined method, and then this data is interpolated and used to create a response surface for the model. Lastly, by defining the desired optimization criteria, toolbox chooses the best candidates for the project.

### Design of Experiments

The first step in Response Surface Optimization is the design of experiments. At the beginning of the optimization study, a case domain (domain of different design cases) must be defined. In this defined case domain, all the correlations between parameters are going to be identified and the trends are going to be revealed by the program, i.e. the program learns the relations between parameters. Only after that the optimization phase can decide the best case for the given requirements.

First of all, the limits of the domain are defined by entering ranges for the input parameters. Then according to the selected method, sampling points to be analysed are determined. At that point, Ansys Workbench calls MS Excel and uses it as solver to make all the calculations. The calculations are made according to the formulas embedded in MS Excel file.

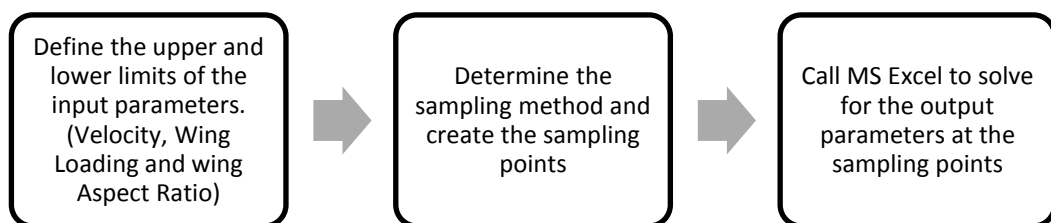


Figure 2.10 The Procedure in Design of Experiments Phase

The ranges for the inputs are stated in the previous section. Here it is determined that the domain is continuous, which means that the input parameters do not have to be integers, but they may have any value.

The method for sampling depends on the type of the design of experiments. The most appropriate option is determined from [48] and numerous trials. “Central Composite

Design” type is selected. “Rotatable” algorithm with “Enhanced” template is selected.

The output of the design of experiments phase is shown below. Note that, the design of experiments table can be filled manually by running MS Excel separately and noting down the output values one by one.

Table 2.3 Output of Design of Experiments

CAS E	V (m/s)	AR	W/S (N/m <sup>2</sup> )	E_1 (min)	E_2 (min)	E_3 (min)	E_4 (min)	V_STALL (m/s)	W_0 (gr)	W_quad (gr)	b (m)
1	25	9.5	140.0	65.0	16.5	27.91	44.70	13.19	4959.8	3909.5	1.82
2	20	9.5	140.0	101.7	16.5	27.91	69.92	13.19	4959.8	3909.5	1.82
3	22.5	9.5	140.0	81.7	16.5	27.91	56.15	13.19	4959.8	3909.5	1.82
4	30	9.5	140.0	41.6	16.5	27.91	28.61	13.19	4959.8	3909.5	1.82
5	27.5	9.5	140.0	51.8	16.5	27.91	35.64	13.19	4959.8	3909.5	1.82
6	25	6	140.0	61.9	16.6	27.74	42.66	13.19	4929.9	3933.7	1.44
7	25	7.75	140.0	63.9	16.553	27.84	43.97	13.19	4943.9	3919.5	1.64
8	25	13	140.0	66.1	16.39	28.01	45.28	13.19	4993	3896.0	2.13
9	25	11.2	140.0	65.7	16.445	27.97	45.09	13.19	4976.3	3901.9	1.98
10	25	9.5	80.0	61.4	14.844	27.65	40.00	9.97	5513	3947.0	2.53
11	25	9.5	110.0	64.2	15.885	27.81	43.36	11.69	5151.7	3923.7	2.09
12	25	9.5	200.0	64.1	17.203	28.03	44.91	15.76	4757.2	3892.3	1.49
13	25	9.5	170.0	64.8	16.909	27.98	45.07	14.53	4839.8	3899.6	1.63
14	22.02	7.41	104.3	83.3	15.806	27.68	56.11	11.38	5177.6	3941.8	1.90
15	23.51	8.45	122.2	73.7	16.203	27.81	50.25	12.32	5050.6	3923.3	1.85
16	27.97	7.41	104.3	47.9	15.806	27.68	32.28	11.38	5177.6	3941.8	1.90
17	26.48	8.45	122.2	56.0	16.203	27.81	38.19	12.32	5050.6	3923.3	1.85
18	22.02	11.5	104.3	86.7	15.654	27.86	58.06	11.38	5227.8	3916.8	2.39
19	23.51	10.5	122.2	75.0	16.134	27.89	51.03	12.32	5072.5	3912.1	2.07
20	27.97	11.5	104.3	48.3	15.654	27.86	32.34	11.38	5227.8	3916.8	2.39
21	26.48	10.5	122.2	56.5	16.134	27.89	38.45	12.32	5072.5	3912.1	2.07
22	22.02	7.41	175.7	79.4	17.027	27.92	55.39	14.77	4806.3	3909.0	1.41
23	23.51	8.45	157.8	73.1	16.791	27.92	50.64	14.00	4873.9	3908.5	1.60
24	27.97	7.41	175.7	49.1	17.027	27.92	34.27	14.77	4806.3	3909.0	1.41
25	26.48	8.45	157.8	56.5	16.791	27.92	39.13	14.00	4873.9	3908.5	1.60
26	22.02	11.5	175.7	85.6	16.915	28.05	59.53	14.77	4838.3	3890.3	1.77
27	23.51	10.5	157.8	74.9	16.731	27.99	51.85	14.00	4891.5	3898.8	1.79
28	27.97	11.5	175.7	50.6	16.915	28.05	35.16	14.77	4838.3	3890.3	1.77
29	26.48	10.5	157.8	57.3	16.731	27.99	39.65	14.00	4891.5	3898.8	1.79

## Response Surface

The second step is creating a response surface. The output of the design of experiments is taken in Response Surface section. The trends are determined from the design of experiments data and necessary interpolations and extrapolations are performed. So, the whole domain is covered. For rather complicated studies or in case of insufficient data these interpolations and extrapolations may result inaccurate results. So the fitting should be checked.

The type of response surface is very critical. Inappropriate selections may result in completely misleading results. From [48] and numerous trials, it is deduced that “Standard Response Surface-Full 2<sup>nd</sup> Order Polynomials” option is suitable for this case.

Table 2.4 Goodness of Fit Table

Name	E_1	E_2	E_3	E_4	V_STALL	W_0	W_quad	b
Coefficient of Determination (Best Value = 1)	1.000	0.998	0.999	1.000	1.000	0.998	0.999	1.000
Adjusted Coeff. of Determination (Best Value = 1)	1.000	0.998	0.999	1.000	1.000	0.998	0.999	1.000
Maximum Relative Residual (Best Value = 0%)	0.096	0.353	0.026	0.128	0.031	0.296	0.026	0.460
Root Mean Square Error (Best Value = 0)	0.032	0.021	0.003	0.030	0.001	6.623	0.415	0.004
Relative Root Mean Square Error (Best Value = 0%)	0.047	0.134	0.011	0.067	0.000	0.130	0.011	0.200
Relative Maximum Absolute Error (Best Value = 0%)	0.492	10.06 7	6.859	0.579	0.232	9.978	6.962	3.072
Relative Average Absolute Error (Best Value = 0%)	0.189	3.272	2.192	0.272	0.045	3.150	2.212	0.998

For this specific case, the correlations are well defined and there are enough sampling points; so the accuracy of the response surface is good. For the design studies involving FEM or CFD outputs as parameters, sampling may be very costly, and creating a satisfying design of experiments output may be hard. On the other hand, MS Excel calculations are very quick and enough sampling for a good fitting is easier to obtain. In Table 2.4 and Figure 2.11, the validity of the response surface can be checked. [48]

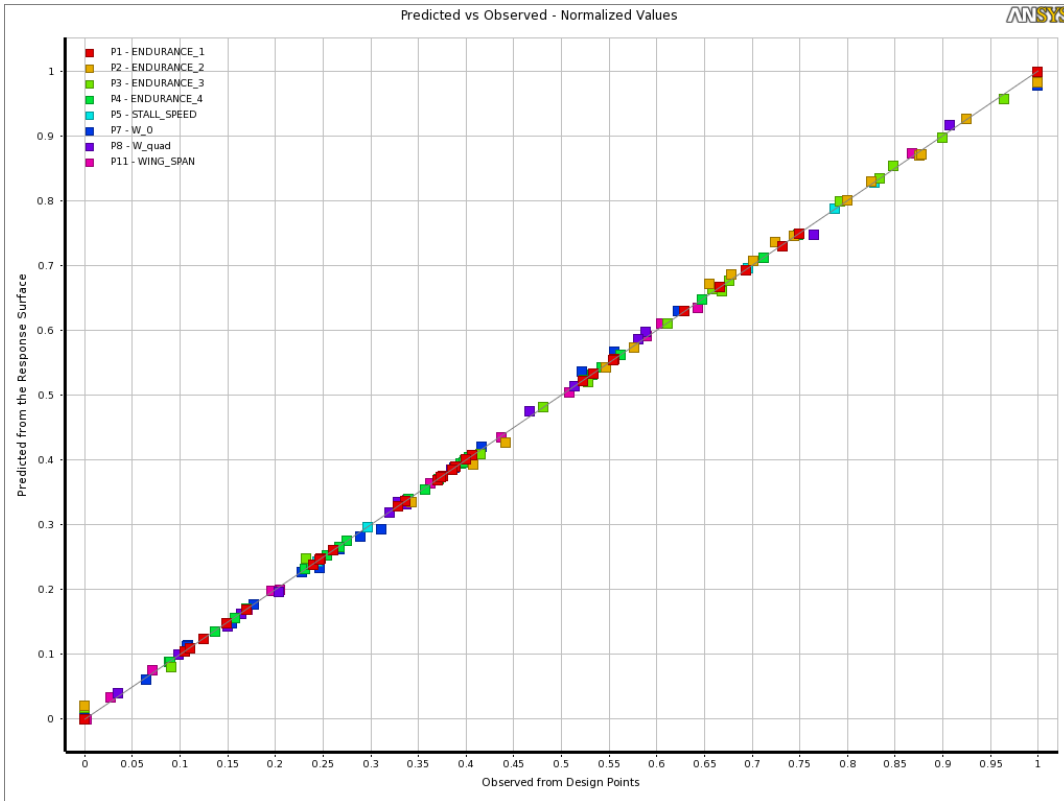


Figure 2.11 Accuracy of Response Surface

## Optimization

Lastly, in optimization phase, the desired criteria are defined; and let the toolbox choose the best candidates for requirements. As the optimization method, “Multi Objective Genetic Algorithm (MOGA)” is used. This method is suitable for finding the global optimum in the presences of multiple objectives and constraints. [48] In literature, there are many recent studies using this algorithm with similar methodology [62], [63], [64], [65]. The best eight candidates are requested in this study. The assignments shown in Table 2.1 are entered one by one exactly as they are.

## CHAPTER 3

### OUTCOME OF THE OPTIMIZATION AND DECISION OF THE FINAL CONFIGURATION

#### 3.1 Important Correlations and Graphs

The results of the local sensitivities and response surfaces show the validity of the design model prepared in MS Excel. Therefore, they need to be examined in detail. A better modelling of the real case brings more realistic and successful design. The important correlations are going to be explained one by one.

##### Local Sensitivities

Local sensitivity bars show how much an output parameter depends on defined inputs. As is evident from its name, local sensitivity bars are local and varies from case to case. For the chosen design point, where wing loading is  $140 \text{ N/m}^2$ , wing aspect ratio is 9.5 and the cruise velocity is 20 m/s, the sensitivities are shown in Figure 3.1. This point is at somewhere near the center of the case domain, and it exhibits the general characteristics of the model well. A direct deduction on optimization from this chart only is inefficient for this study. Examining response curves are more meaningful for this purpose, but it gives better idea about how mathematical model works; so comments on the sensitivity curves are important.

Endurances: “The horizontal flight involving” (1 and 4) endurances mainly depend on velocity as expected. In addition to that weight factor and aerodynamic efficiency is also effective. On the other hand, for “the only vertical” flight endurances (2-3), the horizontal velocity is not a factor. They only depend on the weight based factors. Moreover, ENDURANCE\_3, which is the quad mode endurance, is almost independent of defined inputs. For ENDURANCE\_2, as the wing is still mounted, wing loading remains as a factor for controlling the wing weight.

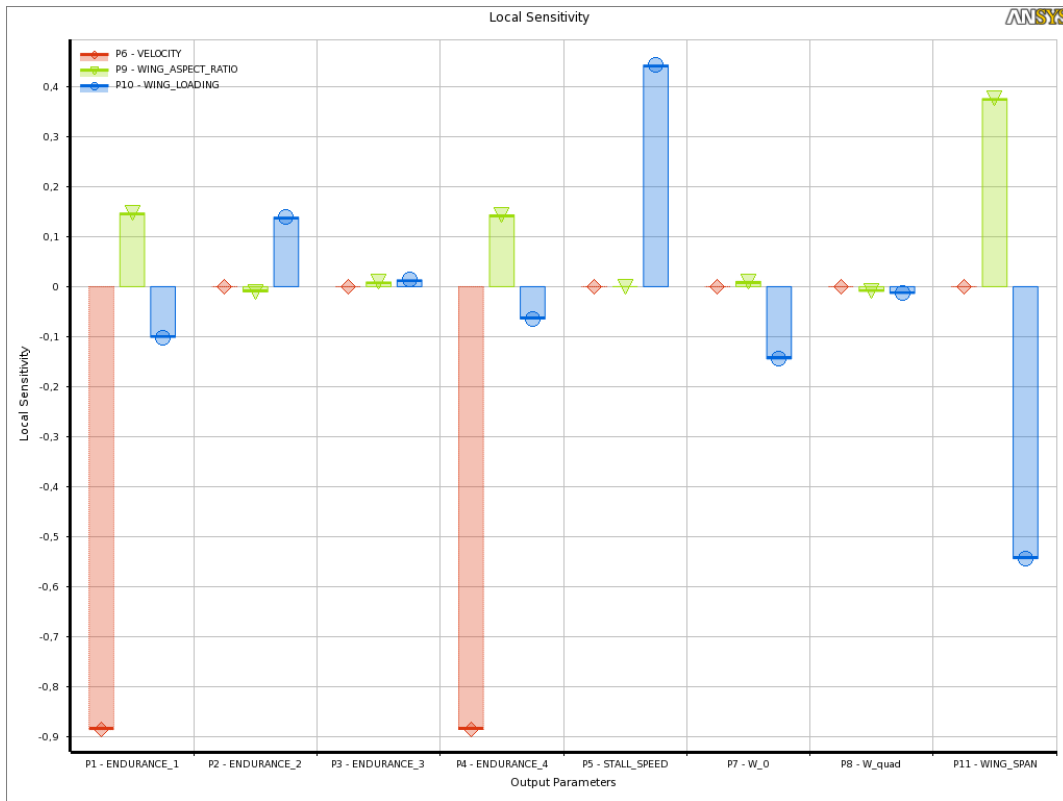


Figure 3.1 Local Sensitivity Bars @  $W/S=140$ ,  $AR_{wing}=9.5$ ,  $V=20m/s$

Stall Speed: As expected, the stall speed is directly dependent to the wing loading and it is one of the primary constraints to limit it.

Design Take-off Gross Weight: There is an iterative formulation between the wing and tail sizes and  $W_0$  established over the wing loading. So, it is influenced by the wing loading. In addition to that, increasing the aspect ratio increases the total weight. It is especially taken care in the establishment of the model, as it creates a structural limitation for aerodynamic efficiency.

Quad-rotor Weight:  $W_{quad}$  is only affected due to the side effects of the input parameters on fuselage sizing.

Wing Span: Two major inputs are almost equally effective on the wing span.

## Response Curves

All the necessary response curves are going to be explained in order of importance.

Responses of  $E_4$ : The primary goal of this design study is to maximize the special mission flight time ( $E_4$ ) by satisfying the other requirements with adjusting the values of the wing aspect ratio and the wing loading. So, Figure 3.2 and Figure 3.3 are two of the most important outcomes of the design study.

Firstly, the wing loading itself establishes a tradeoff between weight and drag. When the wing loading is increased, not only the wing size but also the sizes of tails and fuselage are also decreased due to the inductive effect of reducing wing size. To illustrate, the decrement of the necessary clearance between the wing and the propellers shortens the fuselage and for a constant volume ratio, a smaller wing means smaller tails.

On the other hand, when the velocity is constant a smaller wing requires higher lift coefficient. The lift comes with induced drag and the power required is also increased. Thus, after a point the increment of the wing loading is no longer useful. As it can be seen in Figure 3.2, the wing loading has an optimum value for given aspect ratio consequently. Besides that it is obvious that increasing aspect ratio postpones the saddle point. It is simply because of the fact that increasing aspect ratio increases the aerodynamic efficiency. The induced drag is decreased; so the optimum wing loading can have higher values without making the drag so high. Again, as explained above this aerodynamic benefit is not structurally free. Increment in aspect ratio also increases the weight in small amounts.

At the off design velocity of 25m/s, first of all, the endurance ranges are decreased dramatically. Secondly, the optimum values of the wing loading are higher. It is even out of range after the wing aspect ratio of 11. It is because of the fact that the drag coefficient is more sensitive to the wing loading at lower velocities. When velocity is higher, the lift coefficient is lower; so the drag coefficient increases more slowly with the increasing wing loading. Therefore, it remains beneficial for a wider range to increase the wing loading to reduce the total weight, despite of increasing the induced drag.

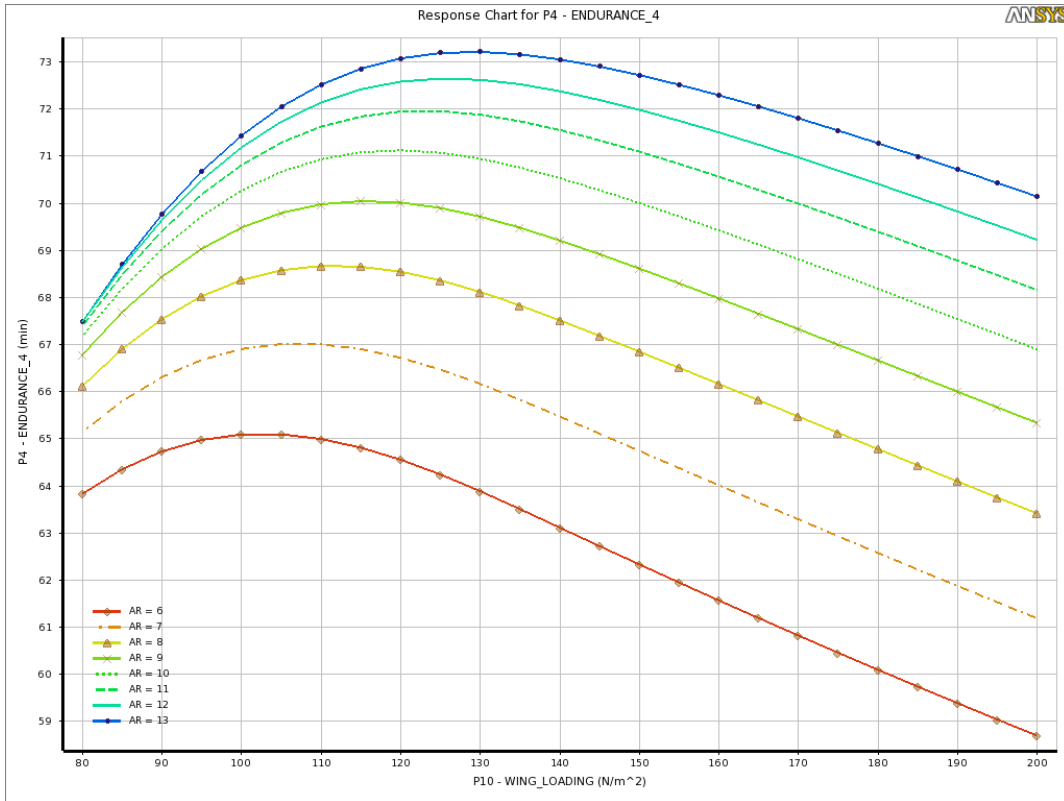


Figure 3.2 W/S and AR\_wing Response of ENDURANCE\_4 @ V=20 m/s

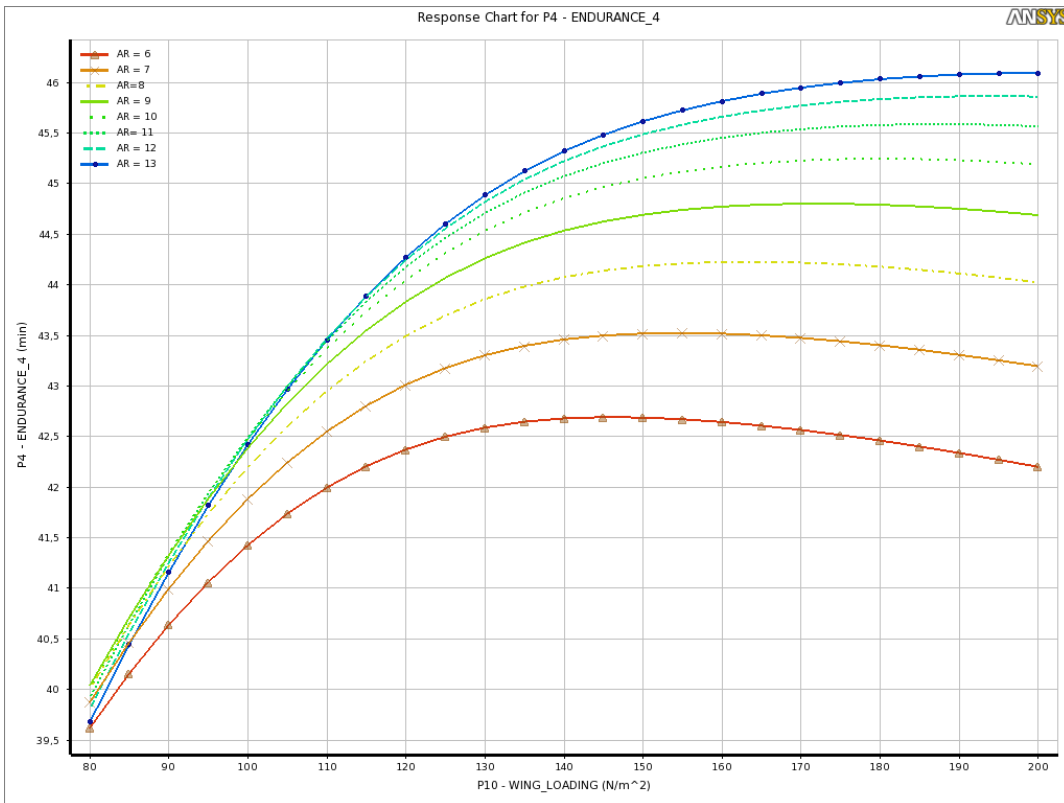


Figure 3.3 Wing Loading and Wing Aspect Ratio Responses of ENDURANCE\_4 @ V=25 m/s

Independent from the wing loading and the wing aspect ratio, the velocity affects  $E_4$  dramatically. The variations of  $W/S$  and  $AR_{wing}$  do not change the trend; they only have small effects on inclinations of the curves. A 50% increase in velocity, decreases the endurance below its half.

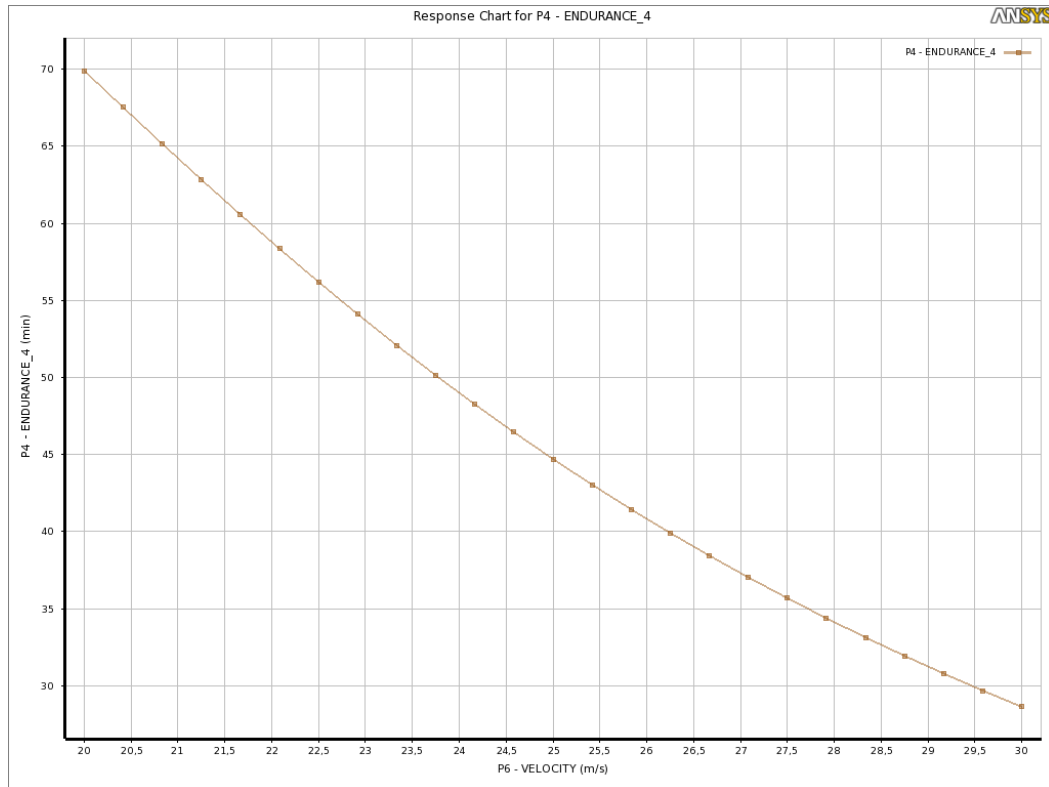


Figure 3.4 Velocity Response of ENDURANCE\_4 @  $W/S=140 N/m^2$ ,  $AR_{wing}=9,5$

Response of  $W_0$ : The structural inputs like the weights of the skin material, carbon fiber booms, tilt mechanism, batteries and other avionic equipment dominantly determine the total weight. The wing loading has a substantial effect due to the sizing of the components, but the influence of the aspect ratio becomes very small comparing to those structural inputs.

Increasing wing aspect ratio raises the total weight. This is due to the fact that the moment arm of the pressure center on the wing is longer in a high aspect ratio wing; so they must be stronger, thereby heavier. This effect is established by linking the amount of used material to the wing span according to the initial CAD drawings. In Figure 3.5, at first an inverse proportionality is seen due to the effect of wing aspect

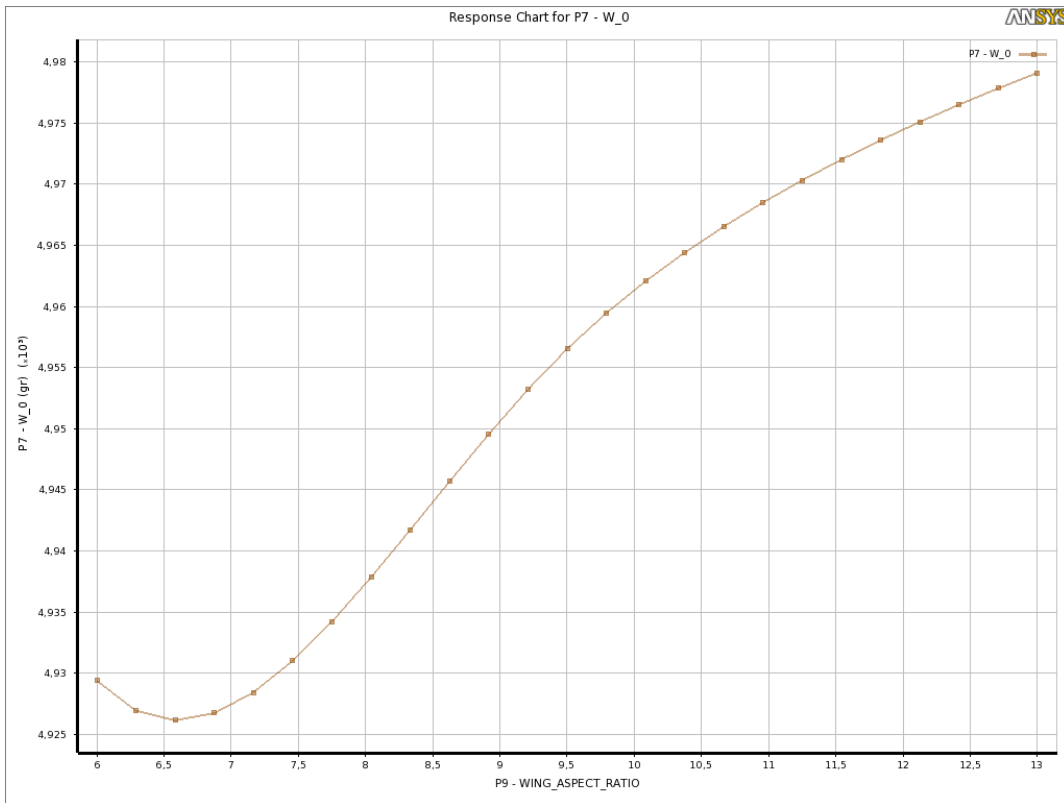


Figure 3.5 Wing Aspect Ratio Response of Design Take-off Weight @  $W/S=140 \text{ N/m}^2$ ,  $V=20$

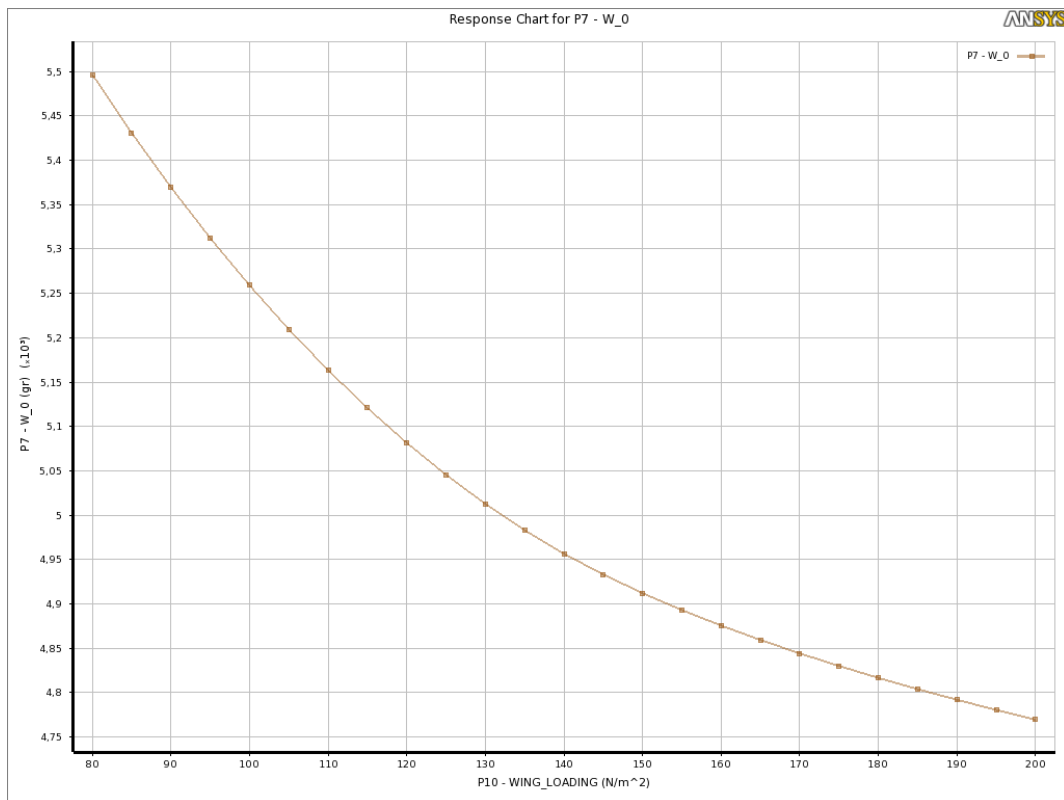


Figure 3.6 Wing Loading Response of Design Takeoff Weight @  $AR_{wing}=9.5$ ,  $V=20\text{m/s}$

ratio on fuselage sizing. As explained before it is related to the propeller clearance. As the wing aspect ratio increases the fuselage length and weight decreases a bit. On the other hand, the wing weight is affected more seriously than the fuselage. So, the general trend of the response curve is generated accordingly.

The effect of the wing loading is clear. As the wing loading is increased and the size of the wing is reduced, it is like a chain reaction: The tail gets smaller directly by the constant volume ratio, and the fuselage gets shorter by obtaining constant clearance between propellers and the wing.

Response of Stall Speed: The stall speed is directly dependent to the wing loading. It almost linearly increases with increasing wing loading. So it is the limiting parameter for the wing loading.

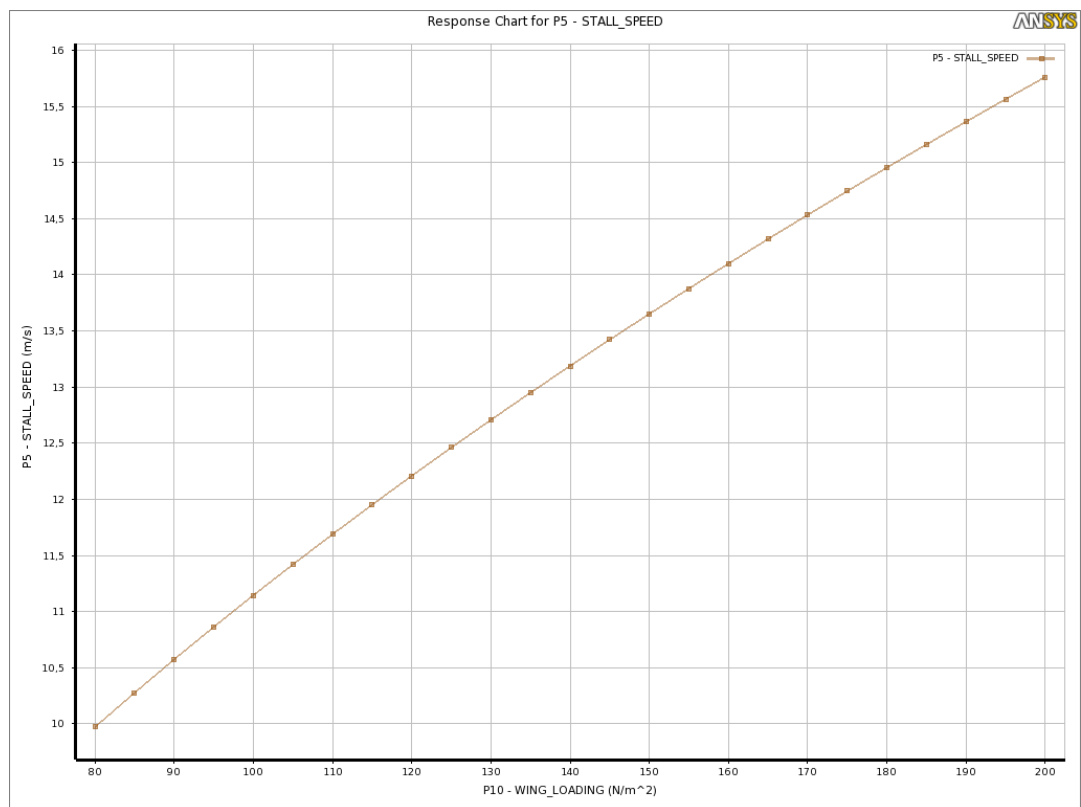


Figure 3.7 Wing Loading Response of Stall Speed @AR\_wing=9.5, V=20m/s

Responses of  $E_1$ : The trend of the horizontal flight endurance resembles the special mission one. However, there are two important differences to mention. The first one

is obvious that the endurance values are 1.5 times higher. It means that 5 minutes of vertical flight consumes 30 min of horizontal flight. Average numbers in MS EXCEL file shows that the power consumed during the vertical flight is almost 6 times higher than the one during the horizontal flight. The second noticeable point is that the saddle point is shifted to the left. The reason is that the time for vertical flight for this mission is limited to 30 seconds for take-off and landing. So, the need for reducing the weight is less critical with respect to the special mission. Then the optimum value of the wing loading is a value which is less intended to reduce the weight but, more intended to decrease the drag coefficient with respect to the special mission flight.

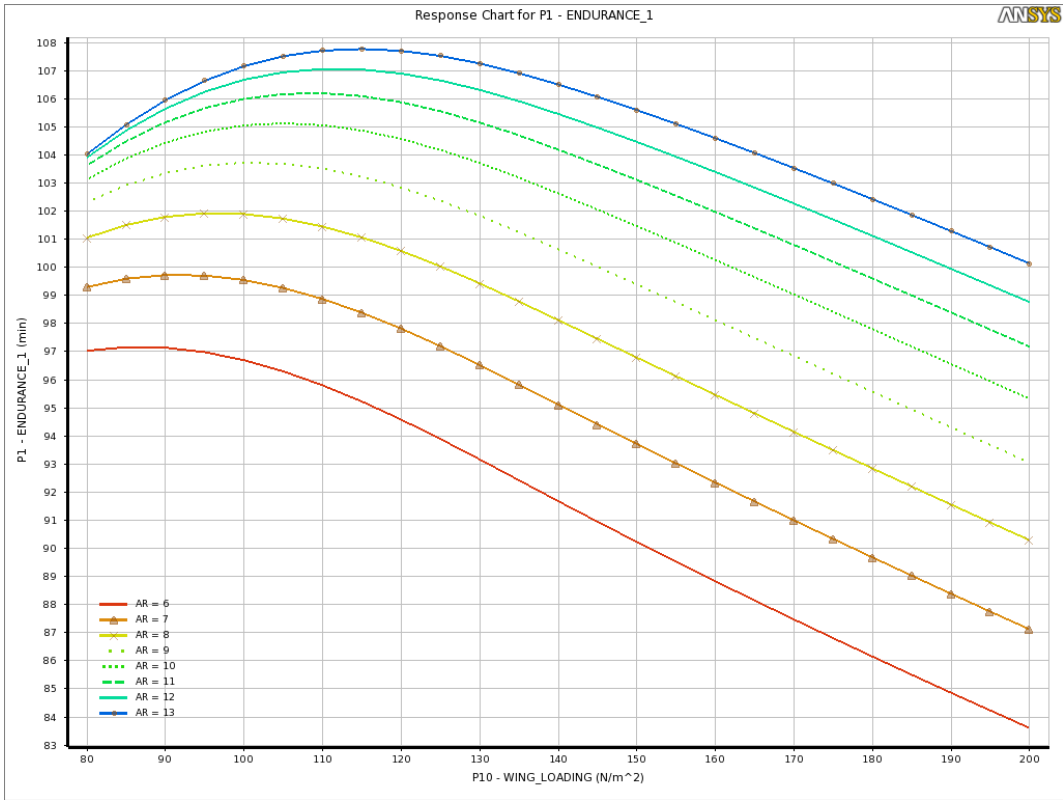


Figure 3.8 Wing Loading and Wing Aspect Ratio Responses of ENDURANCE\_1 @V=20m/s

The velocity response of the horizontal flight time is shown in Figure 3.9. The reason for keeping the design cruise velocity as low as possible can be clearer here. Increasing the velocity from 20 m/s to 25 m/s results in 35% less endurance; while increasing it to 30 m/s decreases the endurance by 60%.

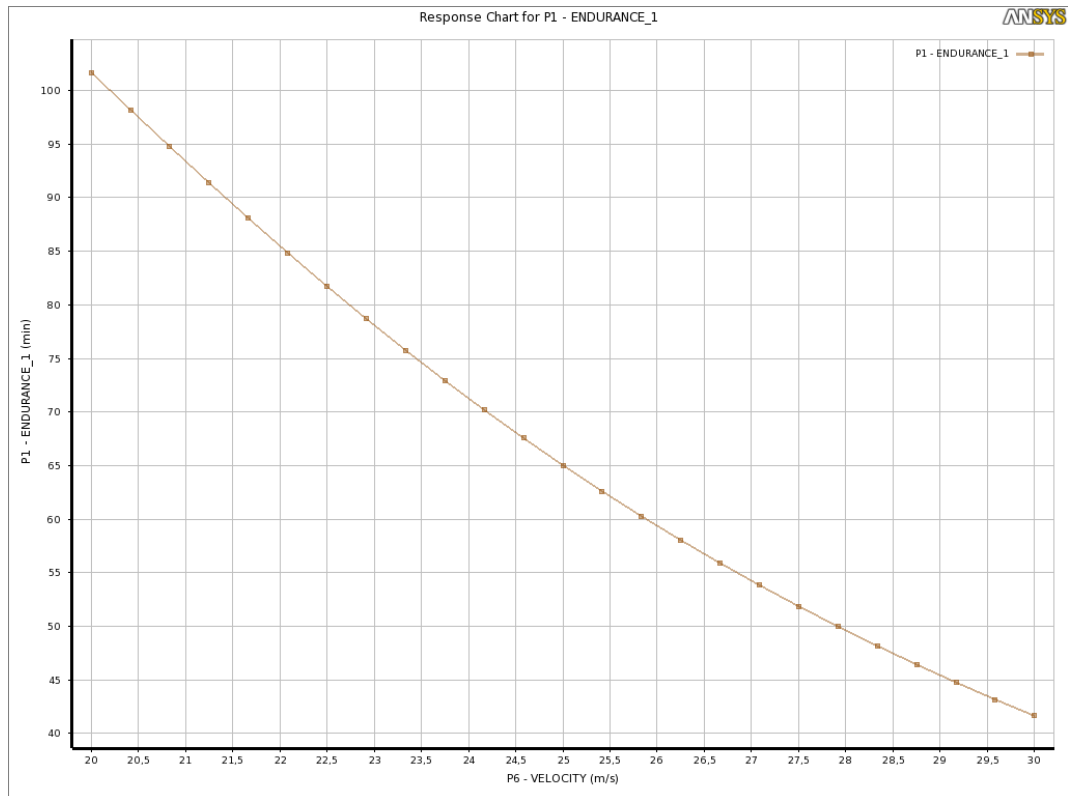


Figure 3.9 Velocity Response of ENDURANCE\_1 @  $W/S=140 \text{ N/m}^2$ ,  $AR_{\text{wing}}=9.5$

Responses of  $E_2$  and  $E_3$ : The vertical flight endurances do not change with the design cruise velocity parameter. They slightly change with wing loading and the wing aspect ratio. The weight reducing effects of these inputs slightly increases these endurances as shown in Figure 3.10 and Figure 3.11. For both cases, as wing loading is inversely proportional to the weight, their endurances increase with wing loading. On the other hand,  $E_2$  decreases with the aspect ratio due to the heavier wing; while  $E_3$  increases with the aspect ratio very slightly due to the shorter fuselage. Also, Figure 3.11 can be considered as just the opposite of the “ $W_{\text{quad}}$  vs.  $W/S$  and  $AR_{\text{wing}}$ ” curve.

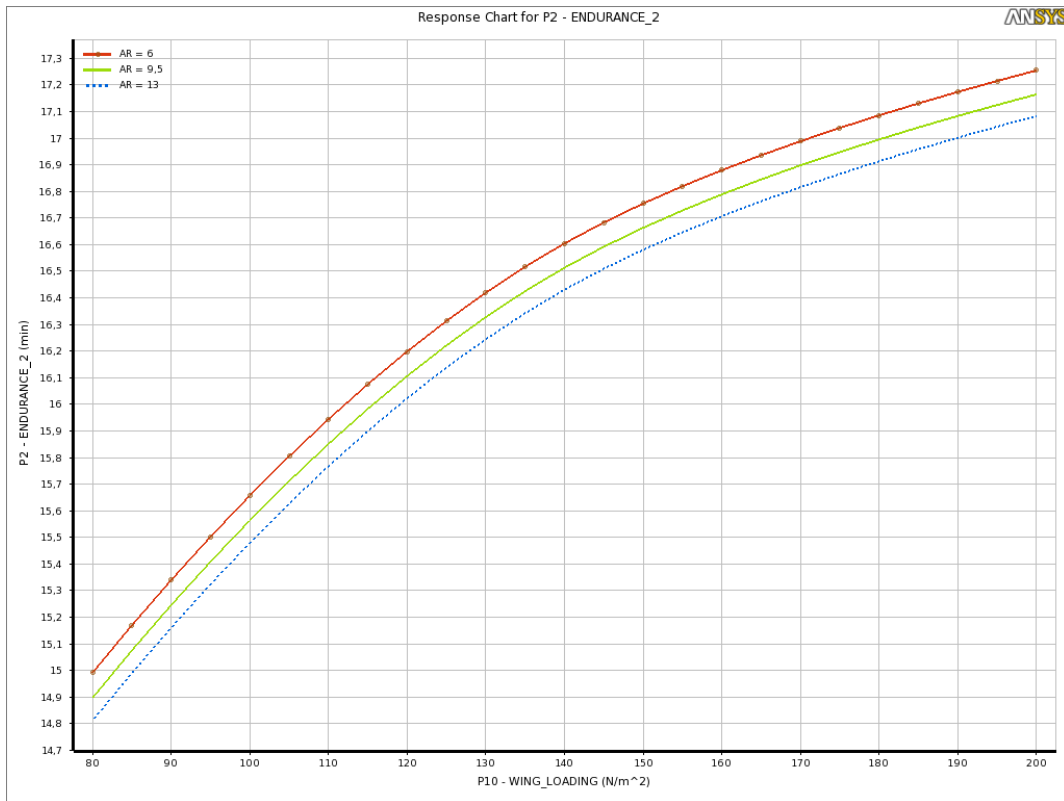


Figure 3.10 Wing Loading and Wing Aspect Ratio Response of ENDURANCE\_2

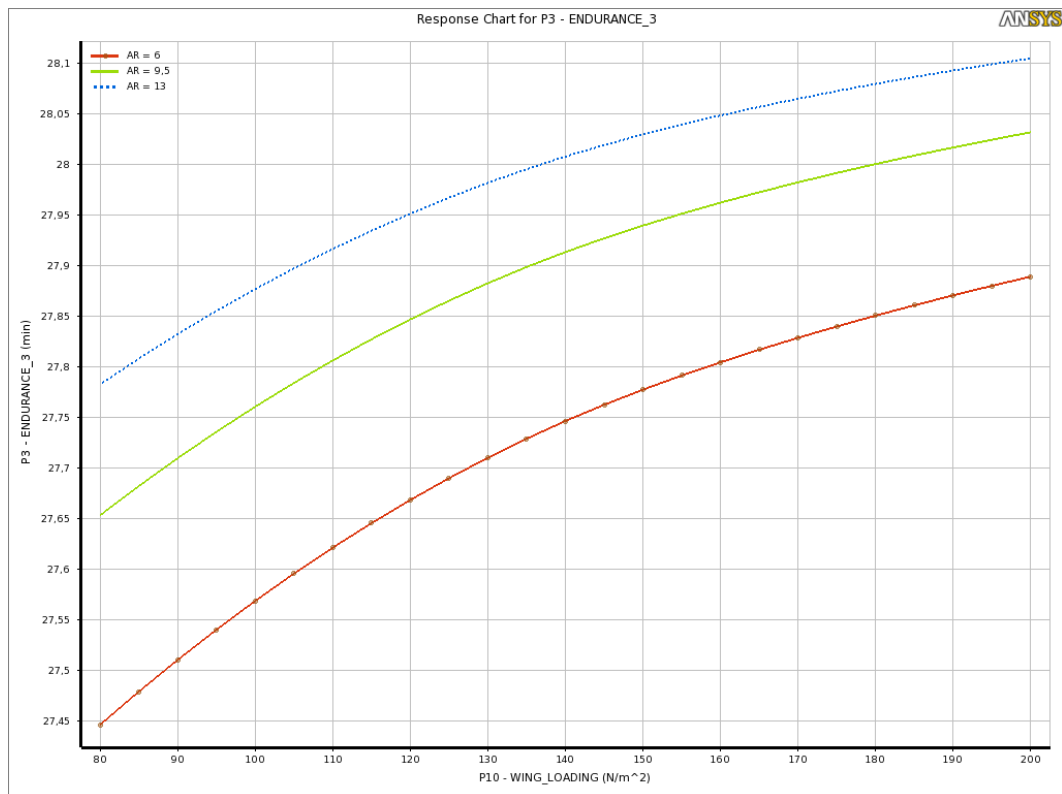


Figure 3.11 Wing Loading and Wing Aspect Ratio Response of ENDURANCE\_3

Response of Wing Span: The last one is obvious. The increasing wing loading reduces the area, and thereby the span and the increasing aspect ratio increase the span itself as it is shown in Figure 3.12.

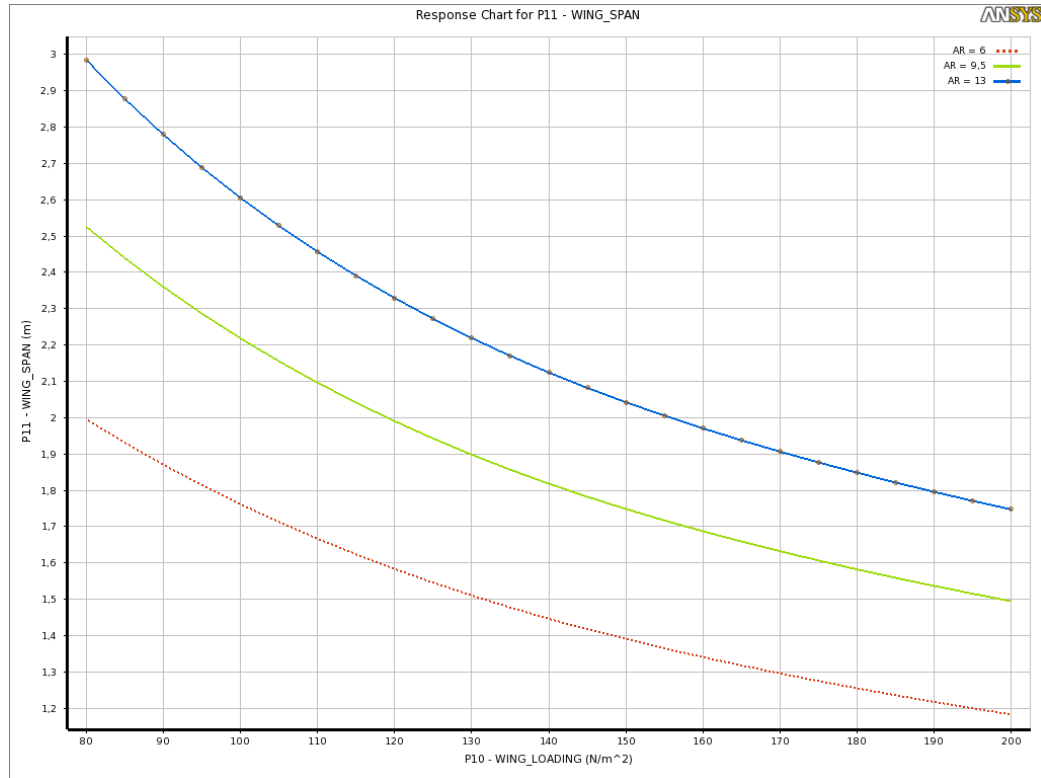


Figure 3.12 Wing Loading and Wing Aspect Ratio Response of Wing Span

### Trade off Charts

After this point, defined criteria are used by the toolbox. According to the criteria defined in the optimization phase, feasible points are determined. The best candidates are among these feasible points. The important trade-offs between parameters are going to be discussed. The points that satisfy the constraints are considered as feasible points [48].

AR<sub>wing</sub> and W/S: All the feasible points of the design study lie within the band shown in Figure 3.13. Here, there is one thing to be observed that the wing loading range is chosen appropriately for the design study. It is because the feasible range is between two infeasible regions. If it was otherwise, there would be a possibly feasible zone that is not considered in the study.

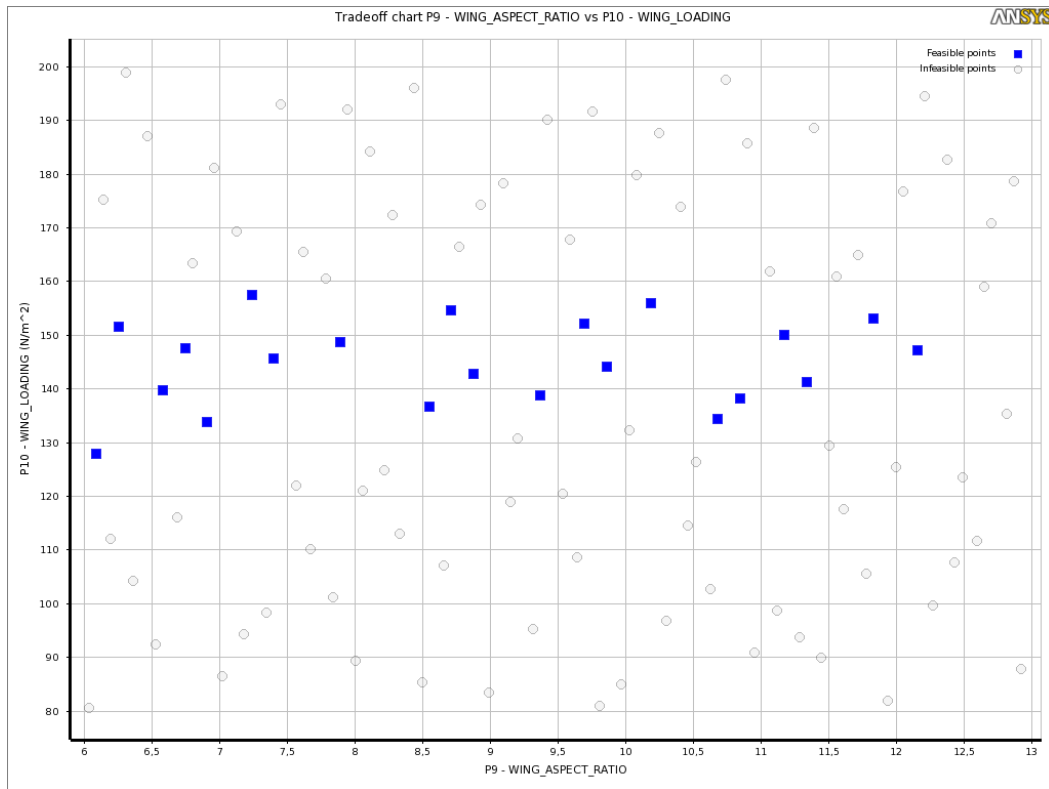


Figure 3.13 Trade-off Between W/S and AR\_wing

W<sub>0</sub> vs. E<sub>4</sub>: As shown in Figure 3.14, points with a total weight of above 5000 gr are marked as infeasible. So, not all the points with high special mission endurance are feasible due to the other requirements.

Stall Speed vs. E<sub>4</sub>: A narrow band is feasible for stall speed. Below 12.5 m/s, wing loading is so low that the total weight requirement cannot be obtained. The points having a stall speed higher than 14 m/s are also dismissed directly.

Stall Speed vs. W<sub>0</sub>: Together with Figure 3.14 and Figure 3.15, Figure 3.16 explains the design limits very well. Above 14 m/s and the right side of 5000 gr are marked as infeasible. In fact, these points are out of defined margins and not acceptable.

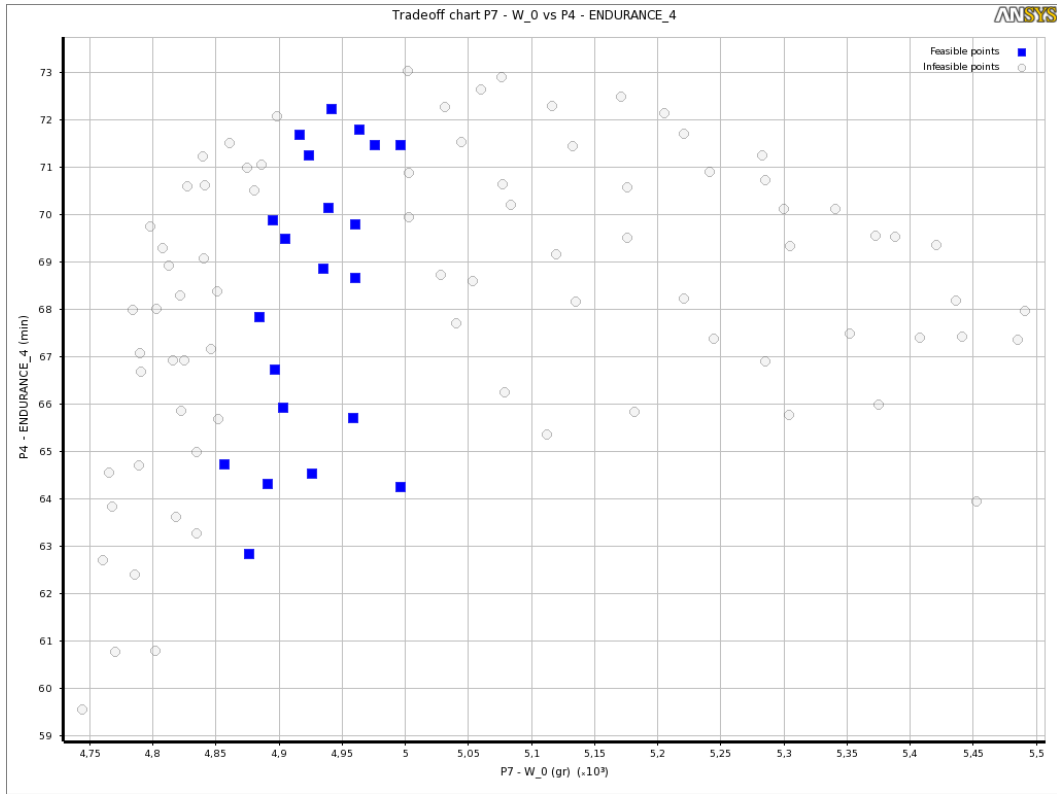


Figure 3.14 Trade-off between W\_0 and ENDURANCE\_4

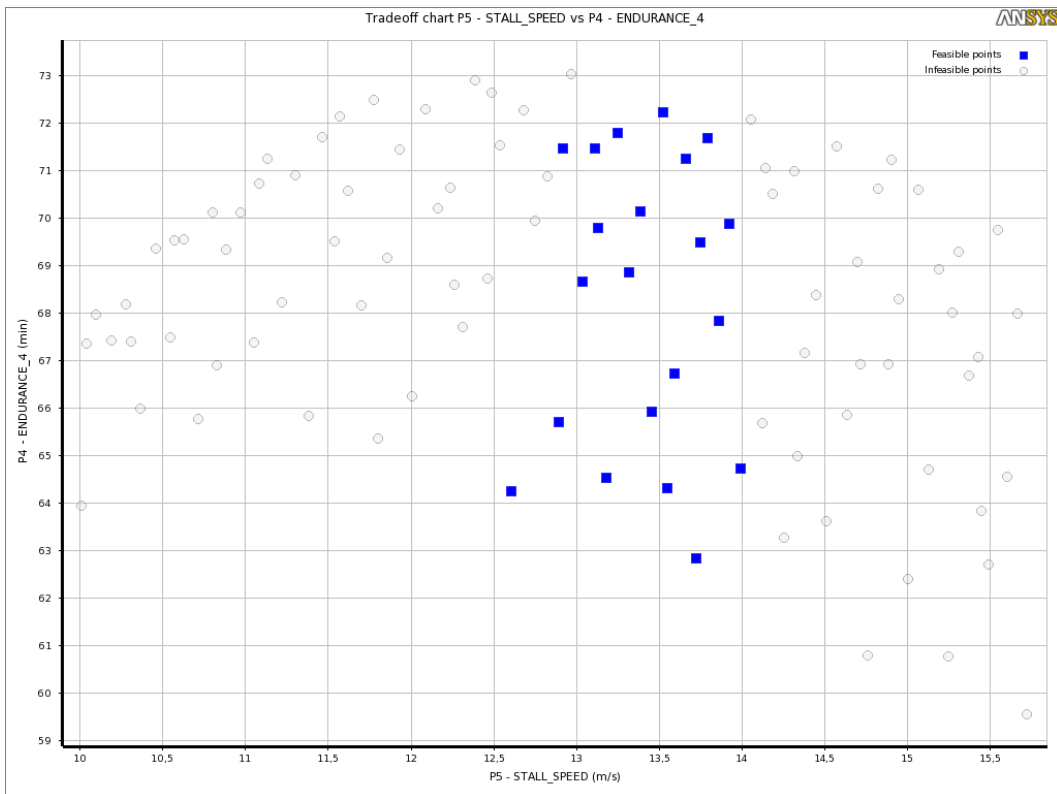


Figure 3.15 Trade-off Between Stall Speed and ENDURANCE\_4

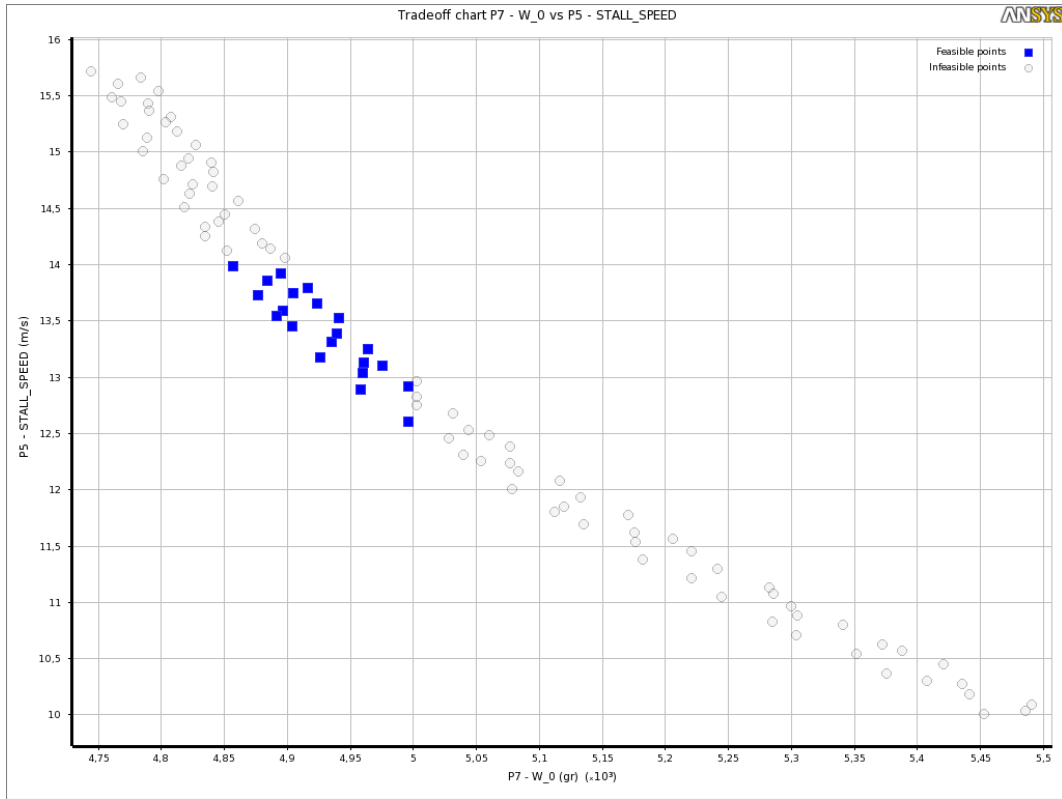


Figure 3.16 Trade-off Between Stall Speed and W\_0

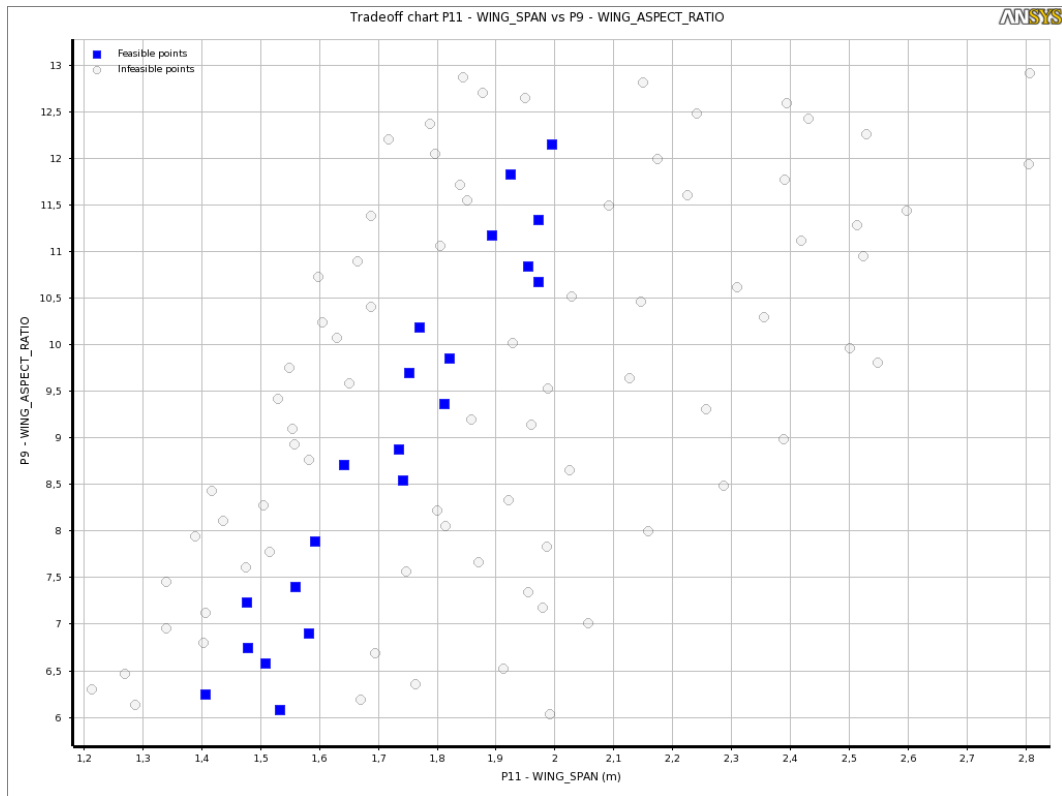


Figure 3.17 Trade-off Between The Wing Span and Aspect Ratio

Wing Span and Aspect Ratio: For each aspect ratio, there is a feasible wing span zone. In fact this figure implies the same relationship with Figure 3.13, but from a different point of view.

### 3.2 The Decision of the Final Design

In the light of all those charts and correlations, the final design is determined among the candidates offered by the toolbox.

	Candidate Point 1	Candidate Point 2	Candidate Point 3	Candidate Point 4	Candidate Point 5	Candidate Point 6	Candidate Point 7	Candidate Point 8
P6 - VELOCITY	20	20	20	20	20	20	20	20
P9 - WING_ASPECT_RATIO	11,832	12,16	11,176	10,191	11,34	9,6991	10,848	9,8631
P10 - WING_LOADING	153,19	147,27	150,23	156,16	141,34	152,2	138,38	144,3
P1 - ENDURANCE_1	★★ 103,91	★★ 104,93	★★ 103,34	★★ 101,08	★★ 104,51	★★ 100,63	★★ 104,14	★★ 101,89
P3 - ENDURANCE_3	★★ 28,012	★★ 28,007	★★ 27,99	★★ 27,976	★★ 27,973	★★ 27,951	★★ 27,952	★★ 27,937
P4 - ENDURANCE_4	★★ 71,695	★★ 72,225	★★ 71,251	★★ 69,885	★★ 71,8	★★ 69,496	★★ 71,479	★★ 70,15
P5 - STALL_SPEED	== 13,796	== 13,526	== 13,662	== 13,929	★ 13,251	== 13,751	★ 13,111	== 13,389
P7 - W_0	★ 4916,3	★ 4941,7	★ 4924,2	★ 4895,1	== 4964,2	★ 4905,5	== 4976,1	★ 4939,8
P11 - WING_SPAN	== 1,9257	== 1,9955	== 1,8931	★ 1,7711	== 1,9735	★ 1,7527	== 1,9548	★ 1,8211

Figure 3.18 The candidate Points

The stars next to the values show the goodness of the point in domain according to the defined objectives. All the candidates have the best  $E_4$  values in domain as expected.  $E_1$  has a similar requirement, so the same candidates also have the best  $E_1$  values in domain. On the other hand, it is understood that there are some candidates have better  $E_3$  in domain but, they are not selected due to the priorities. In terms of the total weight parameter, the candidates with moderate weights are found feasible. The same observation is valid for the stall speed and the wing span.

For final decision, one of the candidates (the first one) is chosen to be the reference and the variations of output parameters from the reference are examined.

Reference	Name	P4 - ENDURANCE_4	
		Parameter Value	Variation from Reference
<input checked="" type="radio"/>	Candidate Point 1	★★★ 71,695	%0,00
<input type="radio"/>	Candidate Point 2	★★★ 72,225	%0,74
<input type="radio"/>	Candidate Point 3	★★★ 71,251	-%0,62
<input type="radio"/>	Candidate Point 4	★★★ 69,885	-%2,52
<input type="radio"/>	Candidate Point 5	★★★ 71,8	%0,15
<input type="radio"/>	Candidate Point 6	★★★ 69,496	-%3,07
<input type="radio"/>	Candidate Point 7	★★★ 71,479	-%0,30
<input type="radio"/>	Candidate Point 8	★★★ 70,15	-%2,16

Figure 3.19 ENDURANCE\_4 Values of the Candidates (units are in minutes)

As the primary consideration, the values of  $E_4$  are crucial. In Figure 3.19, only the candidates 4 and 6 seem a bit lower than the reference.

Reference	Name	P7 - W_0	
		Parameter Value	Variation from Reference
<input checked="" type="radio"/>	Candidate Point 1	★ 4916,3	%0,00
<input type="radio"/>	Candidate Point 2	★ 4941,7	%0,52
<input type="radio"/>	Candidate Point 3	★ 4924,2	%0,16
<input type="radio"/>	Candidate Point 4	★ 4895,1	-%0,43
<input type="radio"/>	Candidate Point 5	— 4964,2	%0,97
<input type="radio"/>	Candidate Point 6	★ 4905,5	-%0,22
<input type="radio"/>	Candidate Point 7	— 4976,1	%1,22
<input type="radio"/>	Candidate Point 8	★ 4939,8	%0,48

Figure 3.20 Design Take-off Weight Values of the Candidates (units are in grams)

For the design take-off weight, there is not an indicative difference between the candidates. For stall speeds, Candidates 5, 7 and 8 seem better.

Reference	Name	P5 - STALL_SPEED	
		Parameter Value	Variation from Reference
<input checked="" type="radio"/>	Candidate Point 1	13,796	%0,00
<input type="radio"/>	Candidate Point 2	13,526	-%1,96
<input type="radio"/>	Candidate Point 3	13,662	-%0,97
<input type="radio"/>	Candidate Point 4	13,929	%0,96
<input type="radio"/>	Candidate Point 5	★ 13,251	-%3,95
<input type="radio"/>	Candidate Point 6	13,751	-%0,32
<input type="radio"/>	Candidate Point 7	★ 13,111	-%4,96
<input type="radio"/>	Candidate Point 8	13,389	-%2,95

Figure 3.21 Stall Speed Values of the Candidates (units are in m/s)

For the wing span, the values vary significantly. The candidates 4, 6 and 8 have shorter wings, which could be advantageous for the final decision.

Reference	Name	P11 - WING_SPAN	
		Parameter Value	Variation from Reference
<input checked="" type="radio"/>	Candidate Point 1	1,9257	%0,00
<input type="radio"/>	Candidate Point 2	1,9955	%3,62
<input type="radio"/>	Candidate Point 3	1,8931	-%1,69
<input type="radio"/>	Candidate Point 4	★ 1,7711	-%8,03
<input type="radio"/>	Candidate Point 5	1,9735	%2,48
<input type="radio"/>	Candidate Point 6	★ 1,7527	-%8,99
<input type="radio"/>	Candidate Point 7	1,9548	%1,51
<input type="radio"/>	Candidate Point 8	★ 1,8211	-%5,43

Figure 3.22 Wing Span Values of the Candidates (units are in meters)

The quad-rotor mode endurance is almost the same for all candidates.

Reference	Name	P3 - ENDURANCE_3	
		Parameter Value	Variation from Reference
<input checked="" type="radio"/>	Candidate Point 1	★★ 28,012	%0,00
<input type="radio"/>	Candidate Point 2	★★ 28,007	-%0,02
<input type="radio"/>	Candidate Point 3	★★ 27,99	-%0,08
<input type="radio"/>	Candidate Point 4	★★ 27,976	-%0,13
<input type="radio"/>	Candidate Point 5	★★ 27,973	-%0,14
<input type="radio"/>	Candidate Point 6	★★ 27,951	-%0,22
<input type="radio"/>	Candidate Point 7	★★ 27,952	-%0,21
<input type="radio"/>	Candidate Point 8	★★ 27,937	-%0,27

Figure 3.23 ENDURANCE\_3 Values of the Candidates (units are in minutes)

The horizontal flight endurance,  $E_1$ , are well above the requirement, and they do not vary significantly.

To sum up, all the candidates are well suited for the design requirements, so any of them may be the final design choice. In overall, it is seen that the endurance values do not vary significantly. In addition to that the stall speed and the total weight values are very close to each other. The only indicative parameter remains is the wing span. As explained before a relatively shorter wing is a reason for preference. Additionally, considering the variations of the other parameters the final design point is determined to be “Candidate Point 8”.

Reference	Name	P1 - ENDURANCE_1	
		Parameter Value	Variation from Reference
<input checked="" type="radio"/>	Candidate Point 1	★★★ 103,91	%0,00
<input type="radio"/>	Candidate Point 2	★★★ 104,93	%0,98
<input type="radio"/>	Candidate Point 3	★★★ 103,34	-%0,55
<input type="radio"/>	Candidate Point 4	★★★ 101,08	-%2,73
<input type="radio"/>	Candidate Point 5	★★★ 104,51	%0,58
<input type="radio"/>	Candidate Point 6	★★★ 100,63	-%3,16
<input type="radio"/>	Candidate Point 7	★★★ 104,14	%0,22
<input type="radio"/>	Candidate Point 8	★★★ 101,89	-%1,95

Figure 3.24 ENDURANCE\_1 Values of the Candidates (units are in minutes)

### 3.3 The Numerical Outputs

All the numerical values are calculated in MS Excel file by the embedded formulas, which are given in the section, “Construction of the MS Excel File”.

#### Geometrical Outputs

Table 3.1 Geometrical Outputs

Fuselage Length ( $l_{\text{fuselage}}$ )	0.82 m
Fuselage Diameter ( $d_{\text{fuselage}}$ )	0.14 m
Length of Motor Booms ( $l_{\text{motor boom}}$ )	0.6 m
Length of Tail Boom ( $l_{\text{tail boom}}$ )	0.43 m
Wing Span ( $b_{\text{wing}}$ )	1.821 m
Horizontal Tail Span ( $b_{\text{ht}}$ )	0.365 m
Vertical Tail Span ( $b_{\text{vt}}$ )	0.252 m
Wing Root Chord ( $c_{\text{r\_wing}}$ )	0.245 m
Wing Mean Chord ( $\bar{c}_{\text{wing}}$ )	0.191 m
Wing Tip Chord ( $c_{\text{t\_wing}}$ )	0.123 m
Horizontal Tail Root Chord ( $c_{\text{r\_ht}}$ )	0.139 m
Horizontal Tail Mean Chord ( $\bar{c}_{\text{hg}}$ )	0.108 m
Horizontal Tail Tip Chord ( $c_{\text{t\_ht}}$ )	0.0695 m
Vertical Tail Root Chord ( $c_{\text{r\_vt}}$ )	0.210 m
Vertical Tail Mean Chord ( $\bar{c}_{\text{vt}}$ )	0.163 m
Vertical Tail Tip Chord ( $c_{\text{t\_vt}}$ )	0.105 m
Wing Reference Area ( $S_{\text{ref\_wing}}$ )	0.334 m <sup>2</sup>
Horizontal Tail Reference Area ( $S_{\text{ref\_ht}}$ )	0.0380 m <sup>2</sup>
Vertical Tail Reference Area ( $S_{\text{ref\_vt}}$ )	0.0400 m <sup>2</sup>
Angle of Incidence (AOI)	3.27°

## Weight Outputs

Table 3.2 Weight Outputs

Fuselage Weight ( $W_{\text{fuselage}}$ )	448.9 gr
Fuselage Weight Including Motor Booms	526.2 gr
Wing Weight ( $W_{\text{wing}}$ )	476.3 gr
Horizontal Tail Weight ( $W_{\text{ht}}$ )	48.1 gr
Vertical Tail Weight ( $W_{\text{vt}}$ )	50.8 gr
Empty Weight ( $W_e$ )	2464.2 gr
Design Take-off Gross Weight ( $W_0$ )	4939.8 gr
Quad-rotor Weight ( $W_{\text{quad}}$ )	3886.6 gr

## Aerodynamic and Performance Outputs

Table 3.3 Aerodynamic and Performance Outputs

Fuselage Parasite Drag Coefficient ( $c_{d_{0\text{fus}}}$ )	0.00539
Wing Parasite Drag Coefficient ( $c_{d_{0\text{wing}}}$ )	0.00541
Horizontal Tail Parasite Drag Coefficient ( $c_{d_{0\text{ht}}}$ )	0.000787
Vertical Parasite Drag Coefficient ( $c_{d_{0\text{vt}}}$ )	0.000661
Motor Booms Normalized Drag Coefficient( $c_{d_{0\text{motorbooms}}}$ )	0.0252
Parasite Drag Coefficient ( $c_{d_0}$ )	0.0393
Design Lift Coefficient ( $c_L$ )	0.655
Design Drag Coefficient at Cruise ( $c_D$ )	0.0576

Table 3.3 (continued)

Maximum Lift Coefficient ( $C_{L_{max}}$ )	1.46
Oswald Span Efficiency (e)	0.760
K	0.0425
Lift Curve Slope ( $C_{L_{\alpha}}$ )	5.014 rad <sup>-1</sup>
Power Required at Cruise ( $P_r$ )	152.1 W
Thrust Required at Cruise ( $T_r$ )	434.0 gf
Power Available ( $P_a$ )	1232 W
Mission 1 Endurance ( $E_1$ )	101.9 min
Mission 2 Endurance ( $E_2$ )	16.6 min
Mission 3 Endurance ( $E_3$ )	27.9 min
Mission 4 Endurance ( $E_4$ )	70.1 min
Stall Speed ( $V_{stall}$ )	13.4 m/s
Maximum Rate of Climb ( $R/C_{max}$ )	24.2 m/s
Maximum Speed ( $V_{max}$ )	55.2 m/s
Maximum Load Factor ( $n_{max}$ )	7.65
Corner Velocity ( $V^*$ )	37.1 m/s
Maximum Turn Rate ( $\omega_{max}$ )	2.01 s <sup>-1</sup>
Minimum Turn Radius ( $R_{min}$ )	18.4 m

Maximum Load Factor Variation with Velocity:  $n_{max}$  varying with velocity generates the typical shape of the flight envelope as shown in Figure 3.25. The corner velocity is the corresponding velocity where two limiting curves intersect.

Power Required and Power Available Variation with Velocity: The available power is constant with velocity; and the required power increases exponentially after a minimum. The maximum velocity is the corresponding velocity where two curves intersect in Figure 3.26.

As the power unit is selected for vertical flight capability, the power available is very high for such an aircraft. So, power available is not the limiting factor until very high velocities.

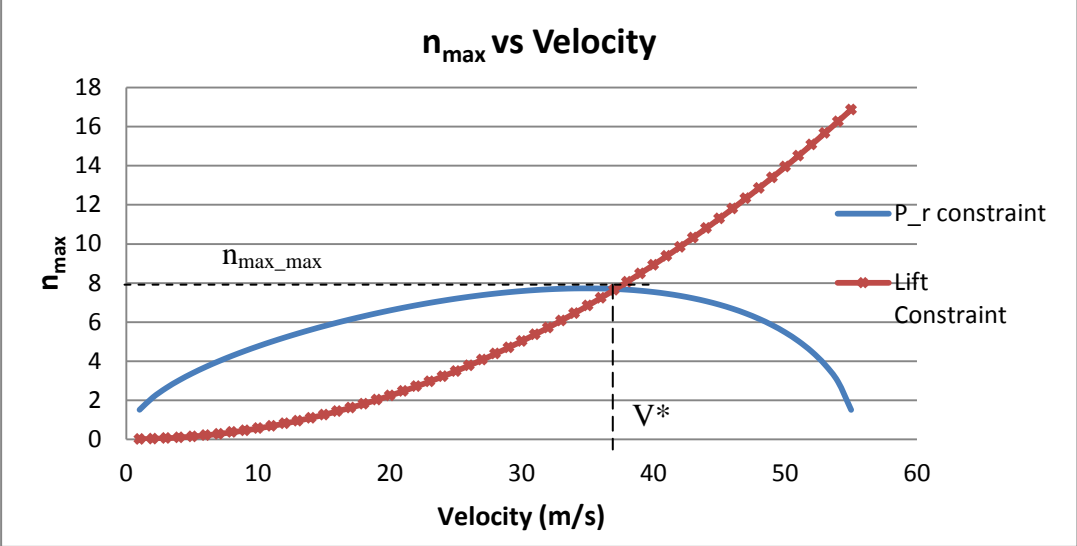


Figure 3.25 Variation of Maximum Load Factor with Velocity

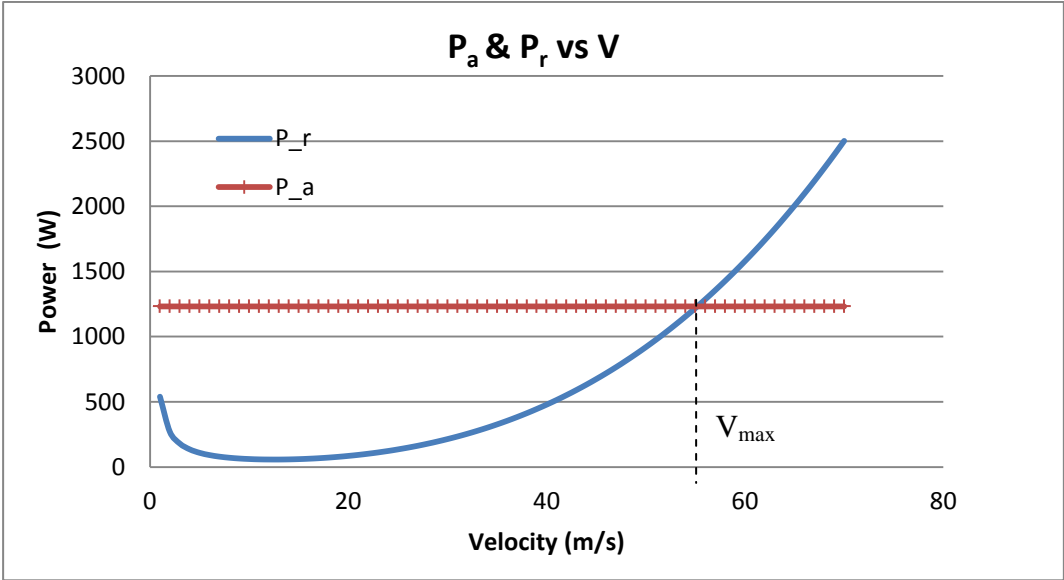
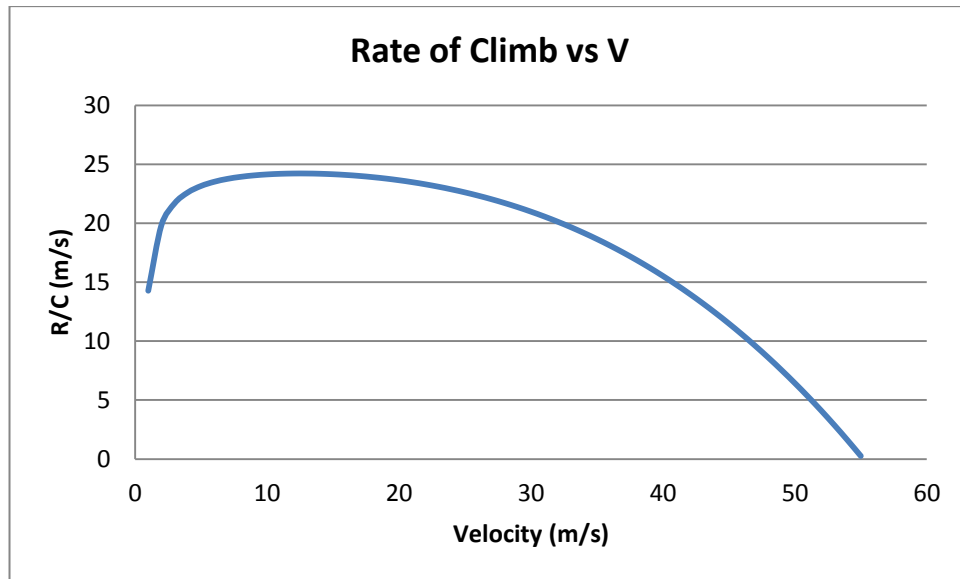


Figure 3.26 Variation of Power Required and Power Available with Velocity

Rate of Climb Variation with Velocity: Best rate of climb speed is close to the stall speed since thrust-to-weight ratio is high.



3.27 Rate of Climb Variation with Velocity

### 3.4 Constructing the Outer Geometry

Many non-generic formulas shaping the outer geometry of the aircraft are generated and modified according to the initial CAD drafts while constructing the mathematical model. Therefore geometry outputs of the MS Excel file defines almost everything regarding to the outer geometry. A basic methodology is followed in constructing the outer geometry. The logical steps generating the geometry are the followings:

#### Fuselage

- i. A cylindrical gimbal with known diameter is located on the front.
- ii. A circular boom with known diameter is inserted at the back.
- iii. The distance between them is known (output of the model).
- iv. Between head and tip, two motor booms and one wing are located.
- v. Considering the propeller clearances, their locations are more or less definite.
- vi. A modular high wing, composed of right and left parts, is placed in its position, so the curvature of the upside of the fuselage continues smoothly between two parts in span-wise direction.
- vii. The lofting of the fuselage surface is tangent to the wing's airfoil's upper surface in chord-wise direction.
- viii. Underside of the fuselage should be appropriate for landing on it.

- ix. Sides are relatively flat especially the zones for the motor booms' inserts.

### **Wing**

- i. After very rough static margin estimation the position of the wing is ensured not to be too bad and fixed, and fuselage is modified accordingly.
- ii. Airfoil is drawn at the symmetry axis, set the incidence angle with respect to the fuselage, and swept through a straight line, which is perpendicular to the symmetry axis, at the quarter chord until the wing tip with a known taper.
- iii. The control surfaces are determined to have width of 30% of the local chord and length of 70% of the span.

### **Booms**

- i. Ensure the locations of the motor booms.
- ii. Draw the tail boom according to the predetermined length.

### **Tails**

- i. For vertical tail, the airfoil is drawn at the centric axis of the tail boom. Sweep the profile from the trailing edge vertically up to the tail tip, which is at a known distance. (As explained before due to the ease of manufacturing, the sweeps at the trailing edges are zero for both tails.)
- ii. Trim the vertical tail and generate a smooth surface transition for boom junction.
- iii. For horizontal tail, is drawn at the centric axis of the tail boom. Sweep the profile in a same manner with the vertical tail. Trim the portion that the boom is inserted and generate a smooth surface transition at the junction.
- iv. The control surfaces are determined to have width of 25% of the mean chord and length of 90% of the span.

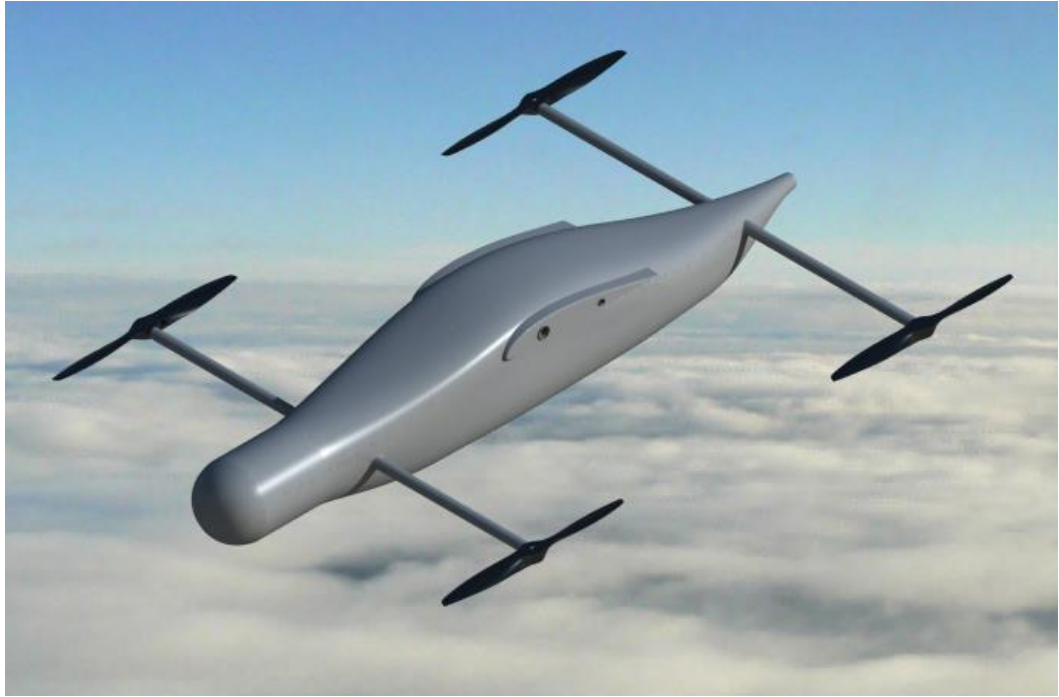


*Figure 3.28 Isometric View of the Quad-rotor Mode of the Aircraft*

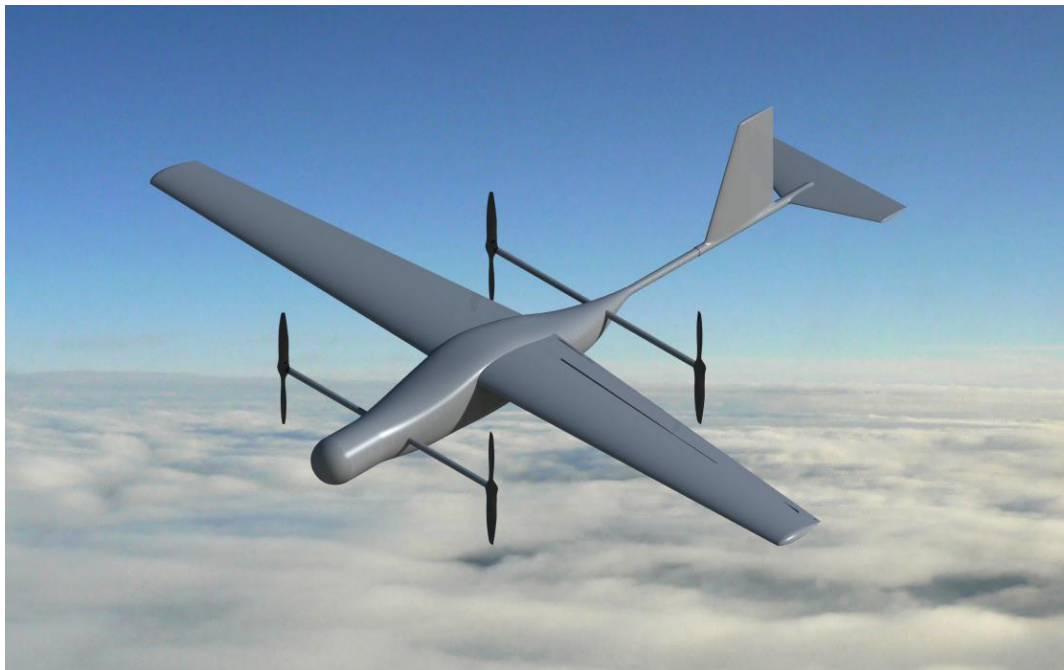


*Figure 3.29 Isometric View of the Fixed Wing Mode of the Aircraft (Horizontal Flight Mode)*

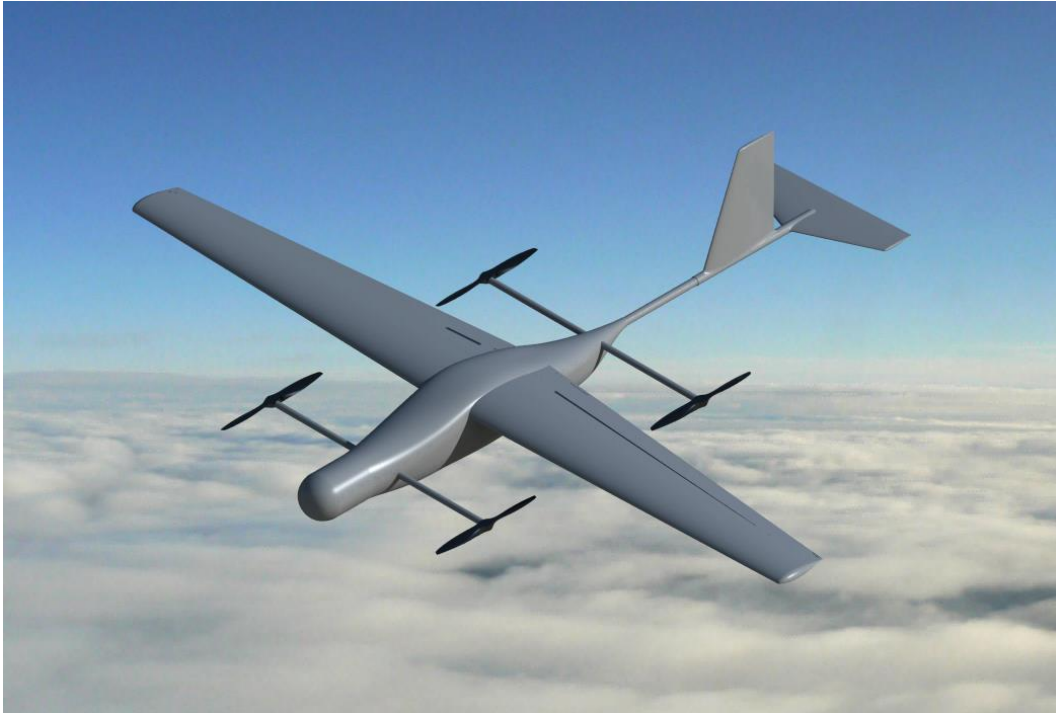


*Figure 3.30 Isometric View of the Fixed Wing Mode of the Aircraft (Vertical Flight Mode)*

In Figure 3.29 and Figure 3.30, isometric views of the aircraft, in horizontal and vertical flight respectively, can be seen. This is the final outer geometry drawn according to the logic written above; and this is the prototype to be manufactured. In Figure 3.31, three views of the aircraft are shown. The curvatures of the aircraft can be seen clearly there.

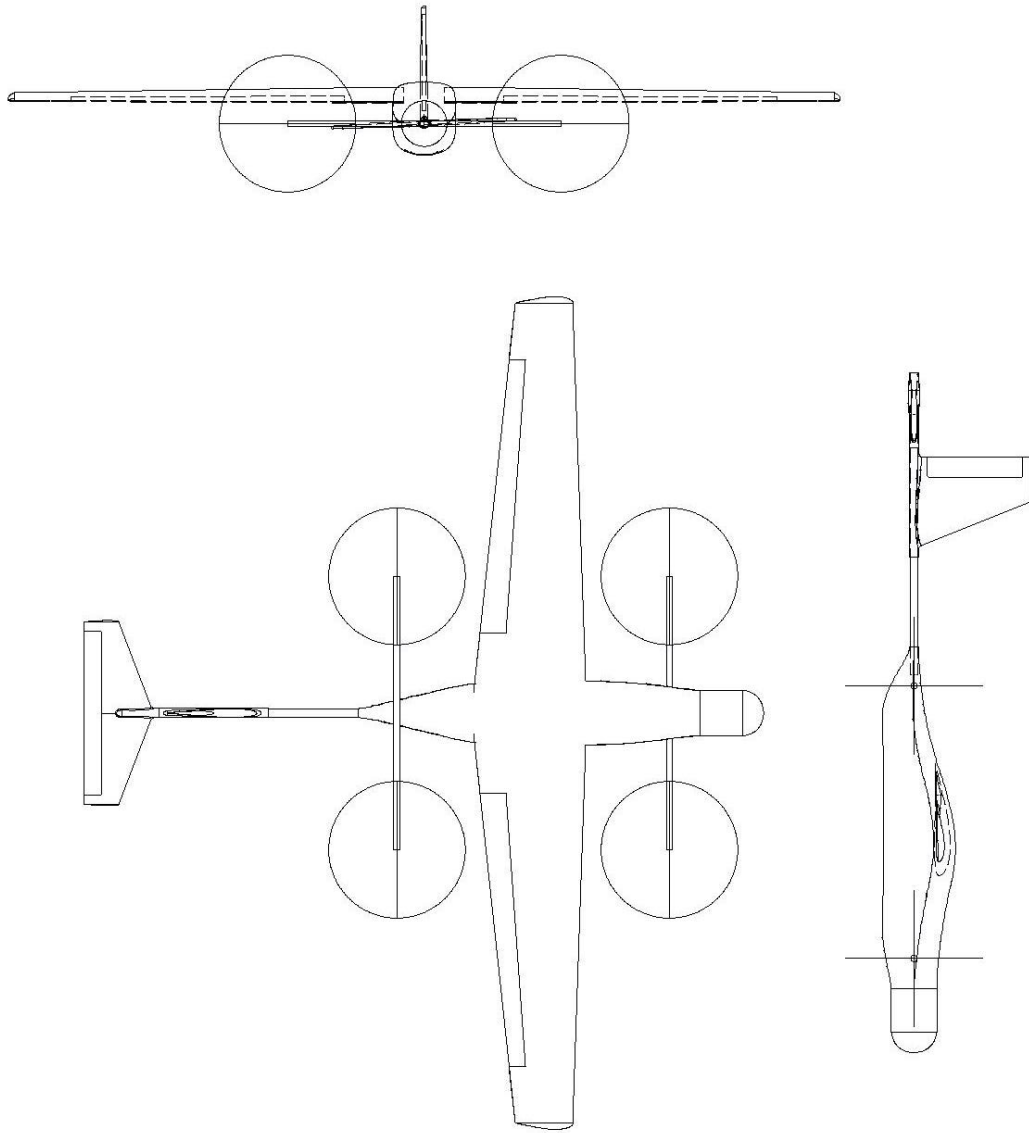


Figure 3.31 The Front, Top and Right Views of the Fixed Wing Mode of the Aircraft

### 3.5 Structure of the Components and Inner Placement

In general, balsa wood covered with one layer of  $49 \text{ gr/m}^2$  e-glass fiber is used to reinforce the composite skin of the aircraft. There are also carbon fiber booms as the primary load carrying components in wings and fuselage.

#### Fuselage

The most important issue in structural design of the fuselage is the junction points. As it is seen in Figure 3.32, there is gimbal mount at the front end wall. At the back, tail boom insert is placed and the back motor boom is just in front of it. These two

booms are structurally integrated by using the balsa bulkheads. The front motor boom is reinforced in similar fashion. Lastly the wing junction zone is supported with balsa plates.

The main strategy here is to distribute the stress at that junction points. As it is explained in the manufacturing chapter, extra honeycomb and carbon fiber layers are added at that junction zones.

## Wing

The inner structure of the wing is composed of the balsa ribs and carbon fiber tube spars. At the root the ribs are more frequent and the tubes have larger diameter. As shown in Figure 3.33, the front spar is composed of centric carbon fiber tubes with decreasing diameter from root to tip. On the other hand, due to the geometry of the wing, the rear spar cannot be a centric combination and split into three separate parts again decreasing diameter from root to tip.

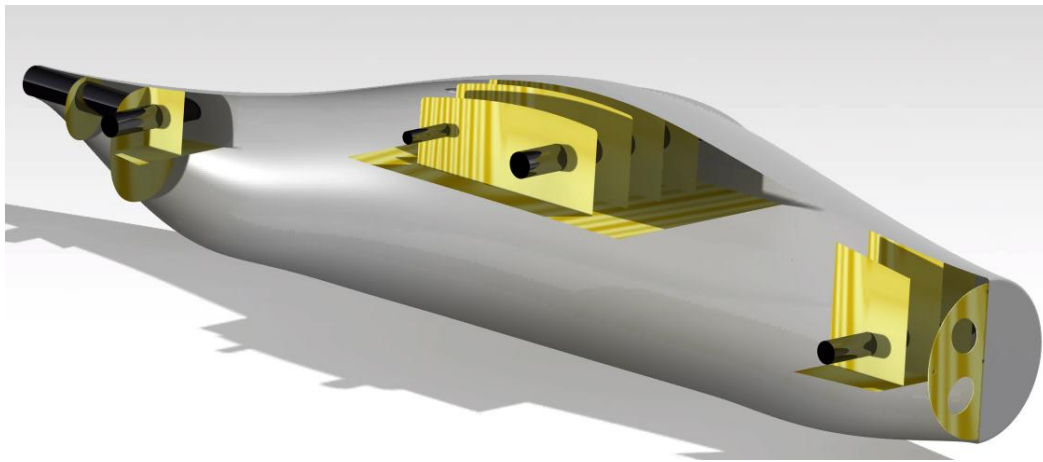


*Figure 3.32 Inner Structure of the Fuselage*

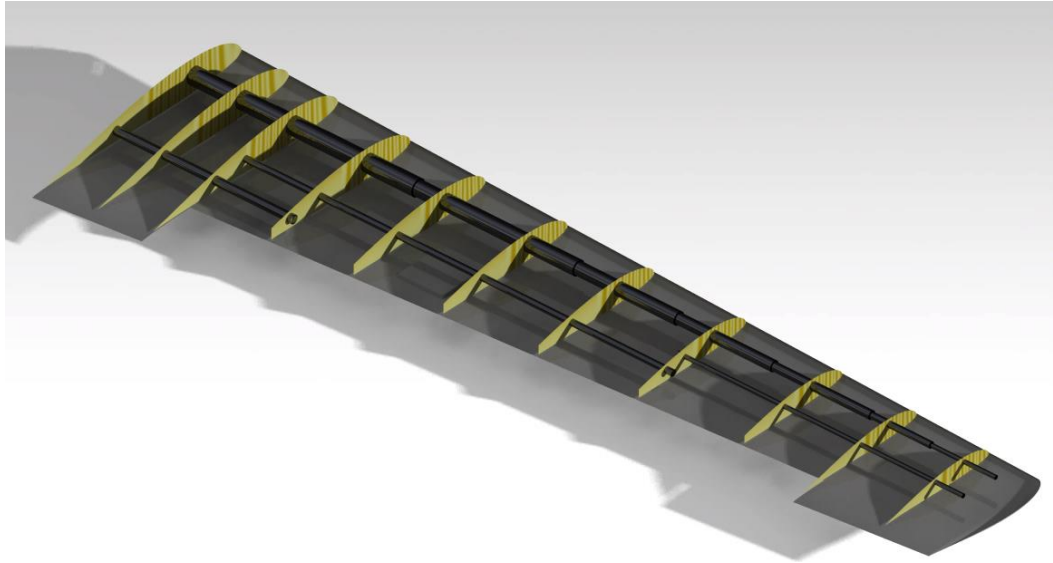


*Figure 3.33 Inner Structure of the Wing*

### **Horizontal and Vertical Tails**

As shown in Figure 3.34 and Figure 3.35, e-glass coated balsa ribs and spars are used in horizontal and vertical tails. There is no extra carbon tube in tail parts; but the tail boom supports them. The spars are adhered to the tail boom in both tails.

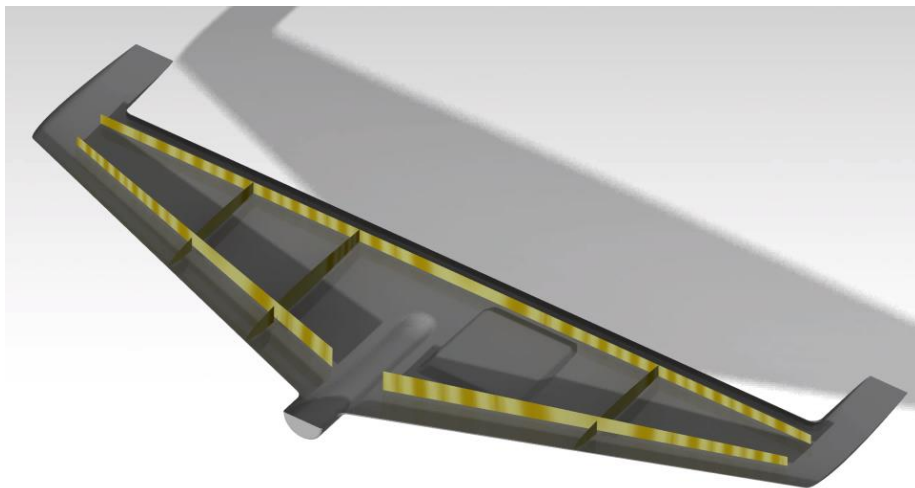


*Figure 3.34 Inner Structure of the Horizontal Tail*

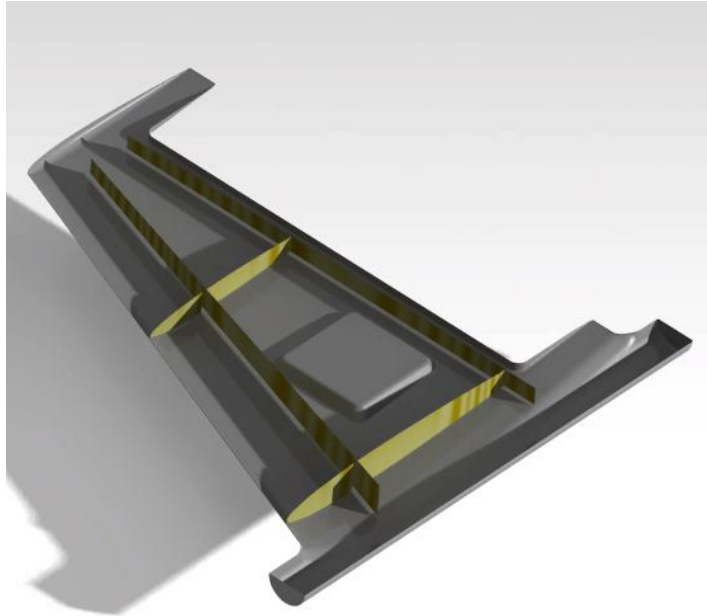


Figure 3.35 Inner Structure of the Vertical Tail

### **Placement inside the Fuselage**

The placement of the wing is dependent on many other parameters and more or less determined by the outputs of the optimization phase. So the placement of the inner components are done in such a way that the center of gravity is in an appropriate place with respect to the wing aerodynamic center. The center of gravity and the static margin are calculated roughly in MS Excel file automatically by using the parametric values of all variables like other geometric and performance outputs; and an approximate value is found. This calculation is used in the wing geometry construction step, which is mentioned above: *“After very rough static margin estimation the position of the wing is ensured not to be too bad and fixed, and fuselage is modified accordingly.”*

In the end, all the weights are defined in CAD program and the center of gravity is checked accordingly.

For quad-rotor mode, center of gravity is aimed to be located at the middle of the motor booms to balance the motors. Therefore, the extra battery is placed at the very back of the fuselage.

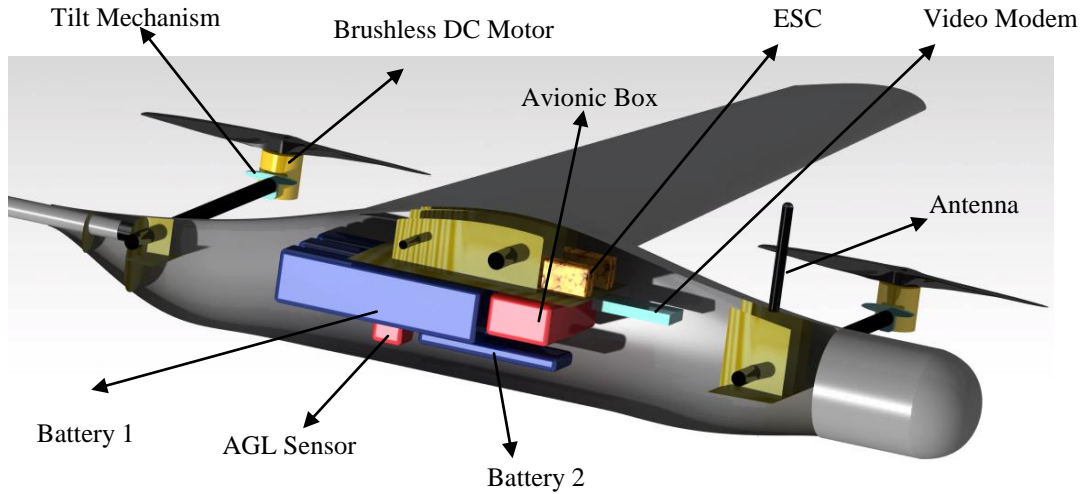


Figure 3.36 Placement of the Components (Fixed Wing Mode)

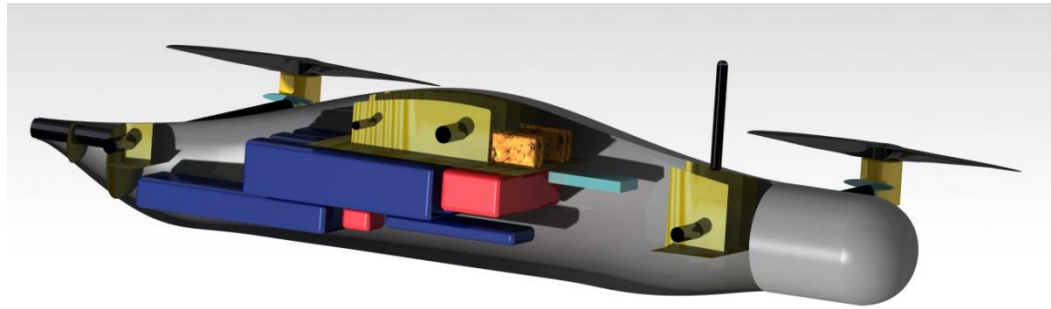


Figure 3.37 Placement of the Components (Quad-rotor Mode)

### 3.6 Static Margin Calculation

For fixed wing mode, the static margin calculation is very crucial in terms of understanding the characteristics of the longitudinal stability of the aircraft. According to the final placement and CAD drawings, the weight distribution is finalized. The static margin calculations are done according to [49].

$$\text{Static Margin} = \overline{X_{NP}} - \overline{X_{CG}}$$

The parameter  $\overline{X_{CG}}$  is the normalized (by wing mean chord) value of the location of the center of gravity of the aircraft on body-x axis in stability coordinate system. It is found by simply adding up all the components in Table 3.4.

Table 3.4 Weight Distribution of the Fixed Wing Mode

Component	Weight (gr)	X (mm)
Fuselage	448.9	351.7
Wing	476.3	458.7
Horizontal Tail	48.1	1.291
Vertical Tail	50.8	1084
Tail Boom	35.5	1033
Motor Booms	77.3	491.6
Motors	520	491.6
ESC'S	144	389.7
Avionic Box	212	450.1
Tilt Mechanisms	324	491.6
Battery 1's	1422	545.8
Battery 2	250	450.8
Payload	700	70*
Antenna	36	180.8
Video Modem	70	310.5
AGL Sensor	50	458.7
Cables	74.9	520.6
<b>TOTAL (gr) / X<sub>cg</sub> (mm)</b>	<b>4939.8</b>	<b>437.7</b>

$$\overline{X_{CG}} = X_{CG}/\overline{c_{wing}} = 2.287$$

$$\overline{X_{NP}} = \frac{c_{L\alpha} \cdot \overline{X_{acwing}} - c_{M_{fuselage}} + \eta_h \cdot S_{ht}/S_{wing} \cdot c_{L\alpha_{ht}} \cdot (\delta\alpha_{ht}/\delta\alpha) \cdot \overline{X_{ac_{ht}}}}{c_{L\alpha} + \eta_h \cdot S_{ht}/S_{wing} \cdot c_{L\alpha_{ht}}}$$

According to the final placement,

$$\overline{X_{acwing}} = 2.246 \text{ and } \overline{X_{ac_{ht}}} = 6.660$$

The contribution of the fuselage to the pitching moment is as follows,

$$C_{m_{fuselage}} = \frac{K_{fuselage} \cdot d_{fuselage}^2 \cdot l_{fuselage}}{\bar{c}_{wing} \cdot S_{wing}}$$

$K_{fuselage} = 0.03$  , according to the figure in [REF 49].

The tail dynamic pressure ratio,  $\eta_{ht} = \frac{c_{l_{\alpha_{ht}}} \cdot \beta}{2 \cdot \pi}$  , where  $\beta = \sqrt{1 - M^2}$

Downwash:  $\frac{\delta \alpha_{ht}}{\delta \alpha} = 1 - \frac{\delta \varepsilon_{ht}}{\delta \alpha}$

$$\frac{\delta \varepsilon_{ht}}{\delta \alpha} = \frac{\delta \varepsilon_{ht}}{\delta \alpha}_{@M=0} \cdot \frac{C_{L_{\alpha_{wing}}}}{C_{L_{\alpha_{wing}@M=0}}}$$

$$\frac{\delta \varepsilon_{ht}}{\delta \alpha}_{@M=0} = 4.44 \cdot \left[ K_A \cdot K_\lambda \cdot K_H \cdot \sqrt{\cos(\Lambda_{wing@c/4})} \right]^{1.19}$$

The value of the static margin is 7.58 % , and it is between the margins of 5-10% , which is typical for that kind of a plane [40].



## CHAPTER 4

### MANUFACTURING

Manufacturing of the prototype is long and demanding work. It is a process from drawing the spline of the airfoil to painting of the body. The steps of the manufacturing are shown in Figure 4.2.

#### 4.1 Constructing a Manufacturable Geometry

##### Carrying the Numerical Values of the Design Output to the CAD

The drawing of the outer geometry of the aircraft starts with the coordinates of the wing airfoil. The spline of SD7062 airfoil is discretized by 100 points. The coordinates of the points are scaled according to the root chord length of the aircraft. After that the wing geometry is drawn according to the span, taper and sweep values. The same methodology is applied for the tail surfaces. In Figure 4.1, the root and tip chord, quarter-chord-line that has no sweep and the root chord line tilted according to the set angle of the wing can be seen. The wing surface is generated by sweeping the tapered airfoil spline between root and chord.

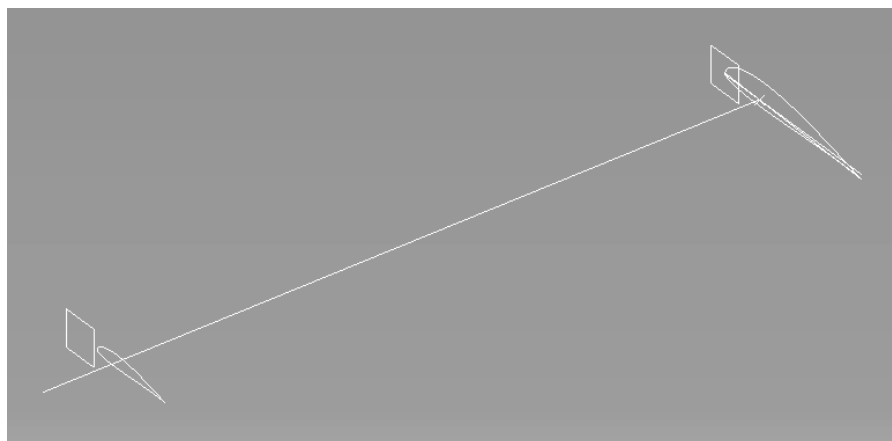


*Figure 4.1 Construction of the Wing Surface*

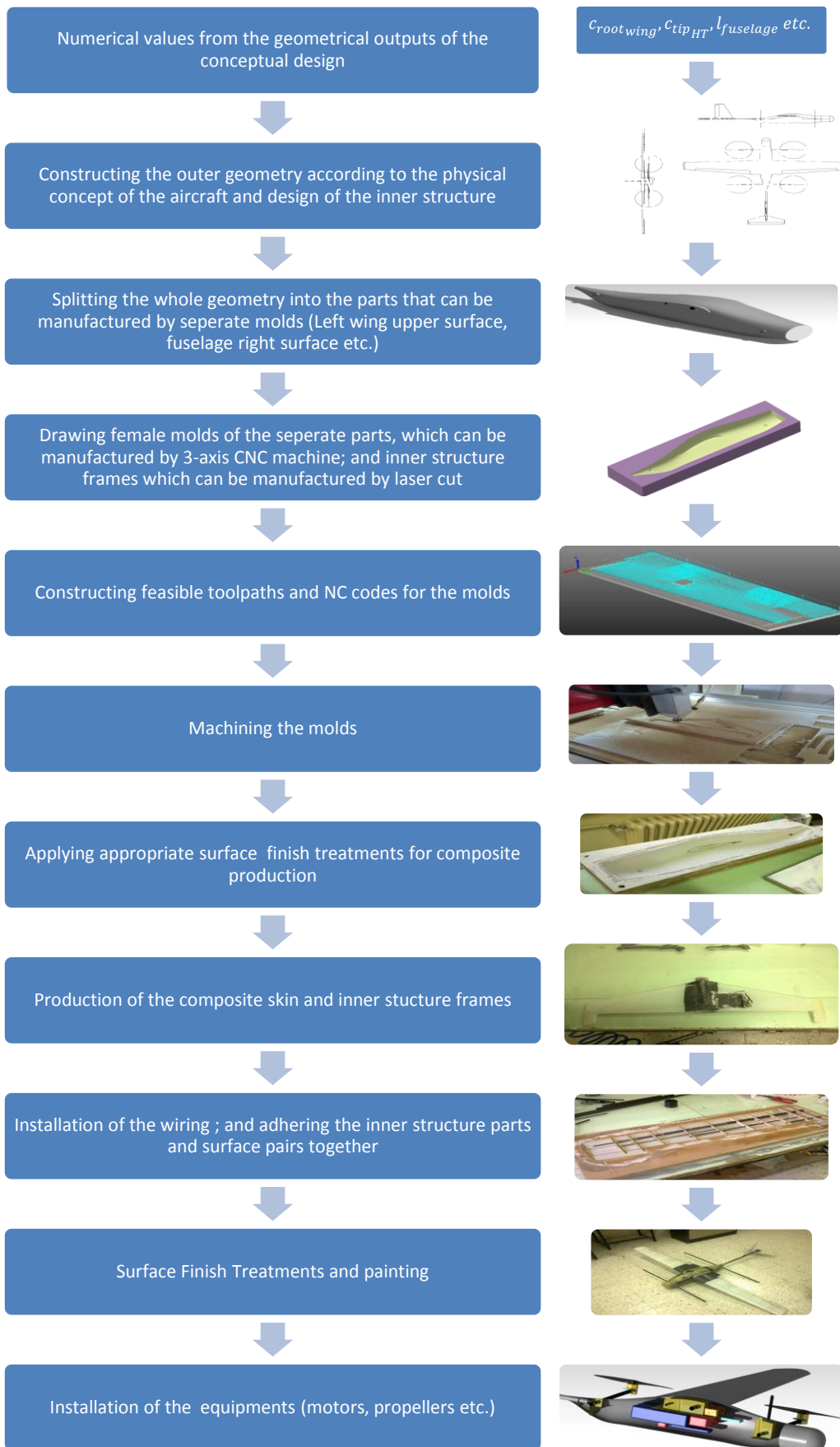
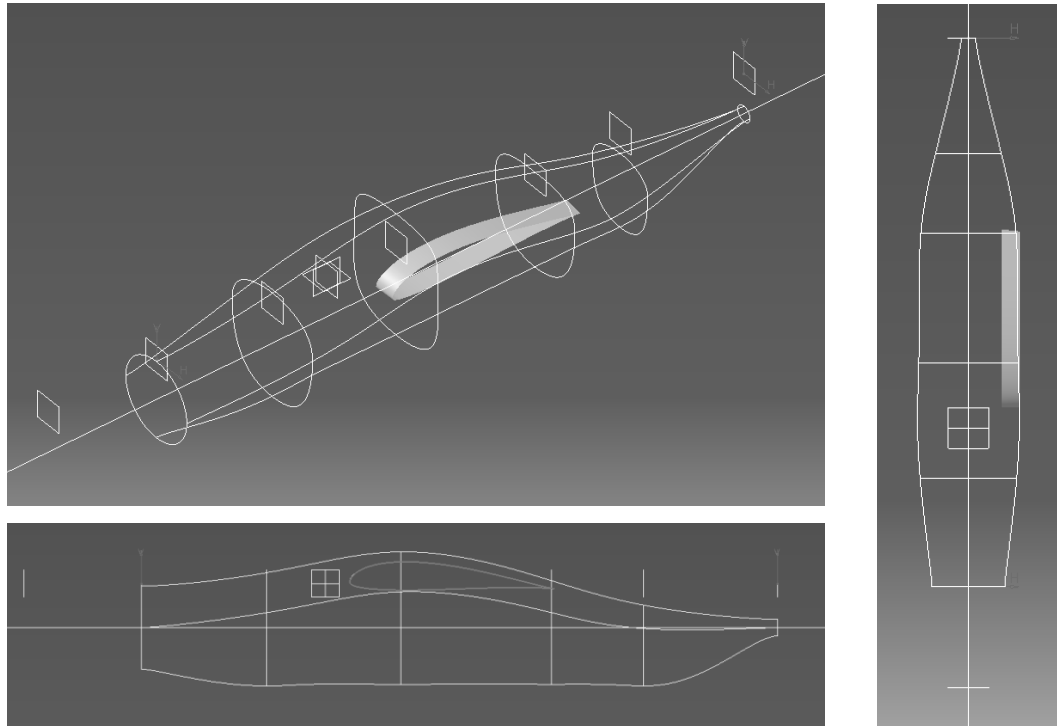


Figure 4.2 Manufacturing Steps

For the fuselage, the locations of the wing and motor booms are critical. The length and diameters are directly taken from the design outputs. The upper surface of the wing airfoil is used to shape the upper part of the fuselage. The bottom line of the fuselage is drawn considering that there is not landing equipment and the aircraft directly lands on its fuselage. The side of the fuselage is drawn considering that the wing is mounted on the sides. In general, guiding lines and the reference cross-sections have smooth transitions to obtain an aerodynamically efficient body.



*Figure 4.3 Guiding Curves and Reference Cross-Sections of the Fuselage*

### **Splitting the Geometry and Drawing the Female Molds**

Because this is an aircraft and the outside of the surfaces are interacted with air; the outside of the skin parts are supposed to be smooth and shiny considering the surface roughness and drag issues. The side that is faced to the mold becomes shiny in composite manufacturing; therefore, female molds are used.

The molds are machined by a 3-axis CNC machine. The knife of the machine is perpendicular to the log; and it machines the log from one direction only. Therefore, adverse slopes in the mold geometries cannot be machined and they are not allowed.

To illustrate, in Figure 4.4, the portion above the dashed line has an adverse slope and that zone cannot be machined. Primary thing to consider when splitting the geometry is not to have adverse slope. So the outer geometry is split from the extremum points. And when the outer geometry is crated, it is taken into account not to have more than one local extremum lines on surfaces anyway.

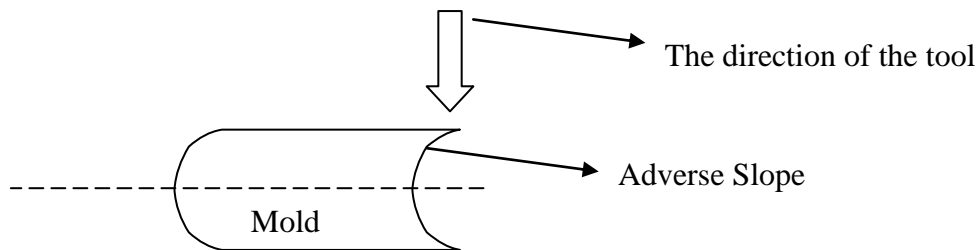


*Figure 4.4 An Example of Adverse Slope on Molds*

The mounting points of the wing parts and the motor booms are determined on the fuselage to ease the orientation and to avoid asymmetry problems as seen in

Figure 4.5. On the lower surfaces of the wing parts and horizontal tail, and on the right side of the vertical tail, there are servo motor mounting zones fixed on the molds.

There are ten molds produced:

- 2 for right and left fuselage surfaces
- 4 for upper and lower surfaces of the left and right wings
- 2 for upper and lower horizontal tail surfaces
- 2 for right and left vertical tail surfaces

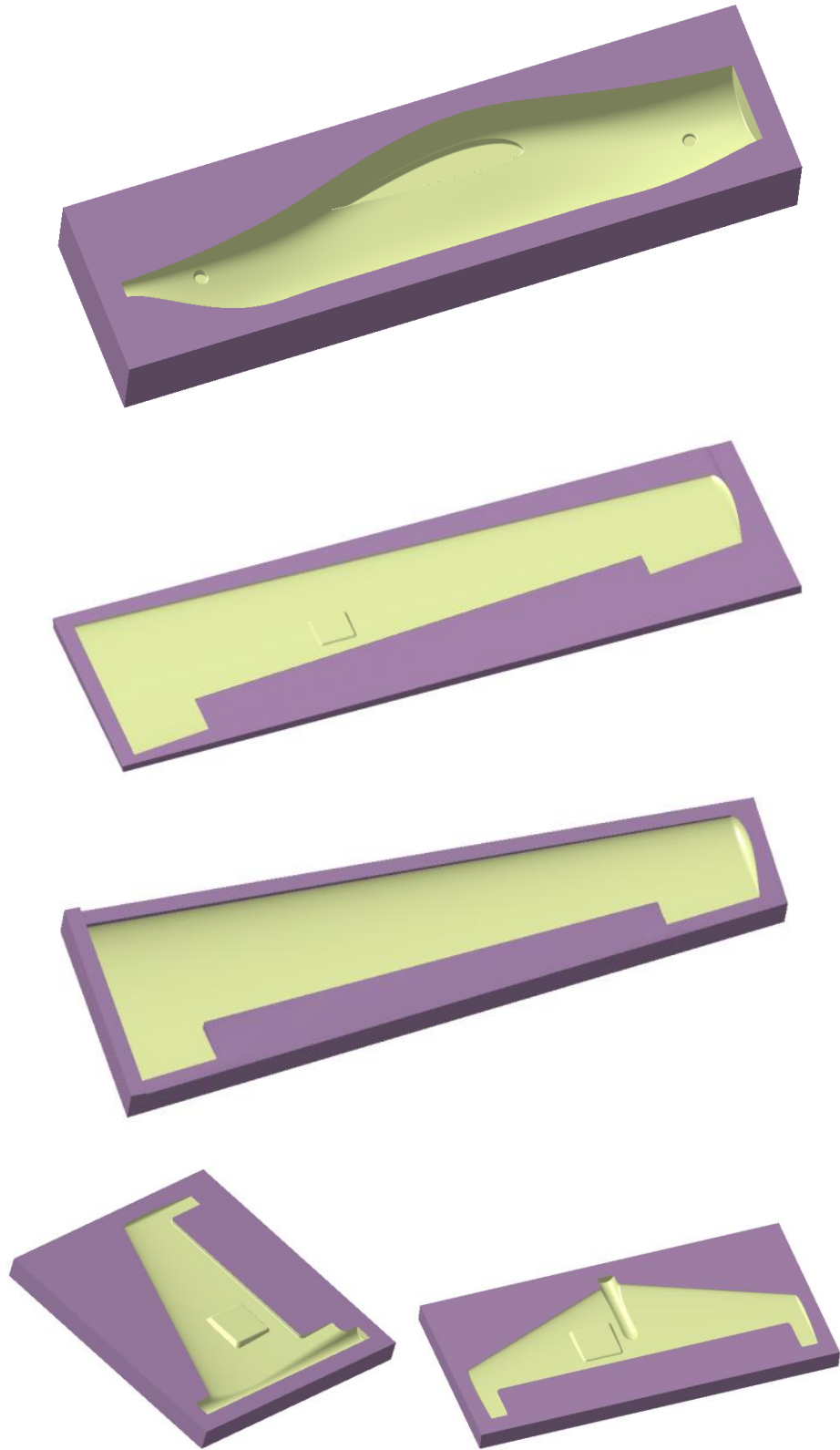


*Figure 4.5 CAD Drawing of the Molds (one side only)*

## 4.2 Manufacturing of the Molds

### Defining the Tool-paths and Generating the Numerical Code

The geometries of the molds are exported to the commercial program ALPHACAM. The tools on hand are defined in the program. Appropriate tool-paths are created and numerical codes that are compatible with the CNC machine are generated.

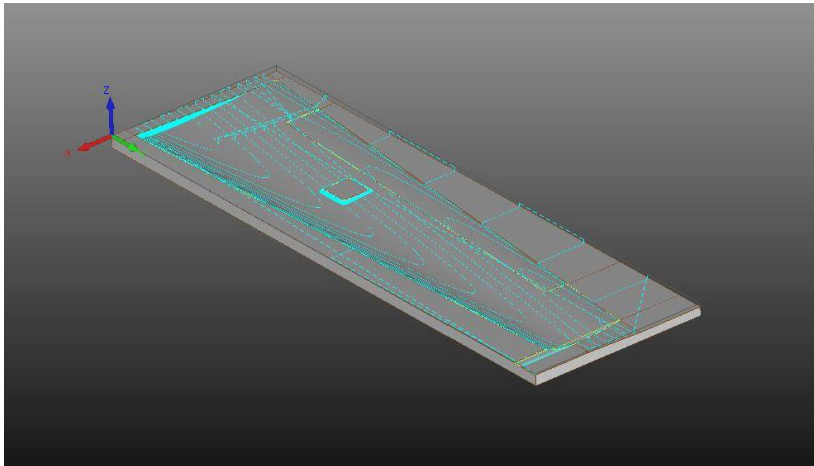


*Figure 4.6 An Example of Tool-Paths (Left Wing Lower Surface Finishing Tool-Path)*

### Machining the Molds

The material of the molds is MDF. First of all, it is cheap and easy to machine. Machining time is significantly reduced by using MDF. On the other hand, it is not durable. In total, it is appropriate for prototype manufacturing. Another disadvantage is that MDF requires extra surface finish treatments for composite manufacturing.

The knife is not long enough to machine the most below points of the fuselage mold. Therefore the fuselage mold is machined section by section. After that, sections are glued together. The reference holes are used for orientation. This application decreased the machining time dramatically, also.

The other molds are machined directly at one time.



*Figure 4.7 Machining the Fuselage Mold*



*Figure 4.8 Scenes from Machining of the Molds (Finishing of the wing and horizontal tail; roughening of the vertical tail)*

## Surface Finish Treatments

MDF soaks liquids if there is no coating on surface. So, it is not possible to apply epoxy for manufacturing; and carrying on the procedure without sealing the surface simply sticks the composite laminate to the mold. There are possible alternatives for coating surface. For fuselage molds, at first, polyester putty is applied to surface. After that, one layer of surfacing primer is used. Finally, two layers of varnish are applied. Sanding is applied between all layers in a fining fashion. For other molds polyester putty is not applied, and the rest is the same. Both brush and spray gun are used in coating process.



*Figure 4.9 Scenes from Surface Finishing Treatments (Polyester putty on fuselage mold, applying primer on wing molds and varnished molds)*

### **4.3 Manufacturing of the Composite Skins and Inner Structural Frames**

#### **Methodology**

In composite manufacturing, vacuum bagging wet lay-up method is used. This is a typical procedure for homemade composite applications. MOMENTIVE (HEXION) MGS L285 two component epoxy [50] is used as the resin, which is typical for small scale aviation applications.

In wet lay-up, the operator simply drapes the plies onto the waxed molds and make sure that the fabrics are impregnated well. The mixture of the resin, the amount of used resin and the checking of the impregnation are directly dependent to the skill of the operator. After draping, to hold the laminate in its position on the molds, it is bagged and applied vacuum. The bagging is very crucial in terms of obtaining good geometry. It is a simple composite manufacturing procedure with its pros and cons. No heat treatment while curing is applied due to the lack of equipment.

The laminates of the composite skins are as shown in Figure 2.6, Figure 2.8 and Figure 2.7.

Procedure of lay-up is as follows:

- Mold release agent is applied properly to the mold.
- Laminate is laid on the mold. At necessary zones, where the mold has corners and other complexities; glass bubble or yarns of fabric are placed to hold the resin at those points.
- Peel-ply film is not used due to the weight considerations; also the thicknesses of the skins are very small, and the skin may be harmed while releasing the peel-ply film. The surfaces to be adhered somewhere is going to be sanded
- Release film is laid and the bleeder is put onto it.
- All of them are put into the vacuum bag, sealant is checked; and vacuum is applied.
- Wait for at least eight hours for curing.

After curing, parts are trimmed according to the contours on the molds.

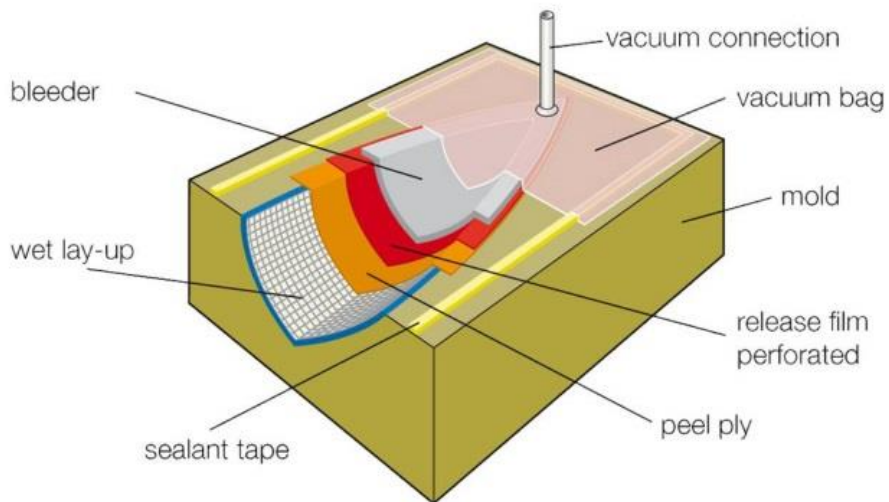


*Figure 4.10 Vacuum Bagging Wet Lay-up Method (from [51])*

## **Fuselage**

The fuselage is produced in three phases. Firstly, the plies before the honeycomb are vacuumed and cured. After that the core is adhered to the laminate with the same epoxy. Here vacuum is used again to position the core. At this point, it is important to put at least one layer of fabric between two honeycomb layers, otherwise the adhesion between honeycomb layers is weak. Lastly, the final layer of e-glass is laid up, vacuumed and cured.

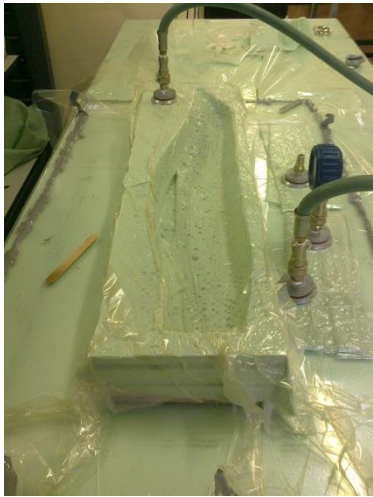


Figure 4.11 Manufacturing of the Fuselage Skins

**Wing and Tail**

The wing and tail surfaces are produced at one vacuum.



*Figure 4.12 Manufacturing of the Wing Skins*



*Figure 4.13 All of the Composite Skins Parts of the Aircraft*

### **Inner Structural Frames**

Inner structural frames are made of 2.5 mm coated with 49 gr/m<sup>2</sup> e-glass fiber. A plate is produced and the parts are obtained from it by laser cut.



*Figure 4.14 Manufacturing of the Inner Structural Frames*

## Weights of the Produced Parts

After trimming the parts are weighed and compared with the weight estimation outputs of the mathematical model.

$$Error (\%) = \frac{\text{Measured Weight of the Produced Part} - \text{Calculated Output of the MS EXCEL}}{\text{Measured Weight of the Produced Part}} \times 100$$

Table 4.1 Comparison of the Calculated and Measured Weights of the Composite Skin Parts

Parts	Calculated Output of the MS EXCEL (gr)	Measured Weight of the Produced Part (gr)		Error (%)
Left Fuselage Surface	197.9	100	199	0.55
Right Fuselage Surface		99		
Left Wing Upper Surface	236.1	58	222	-6.35
Left Wing Lower Surface		57		
Right Wing Upper Surface		53		
Right Wing Lower Surface		54		
Horizontal Tail Upper Surface	35.2	19	38	7.37
Horizontal Tail Lower Surface		19		
Vertical Tail Left Surface	37.9	17	38	0.26
Vertical Tail Right Surface		21		

## 4.4 Assemblage

### Fuselage

The inner structural frames and booms are adhered according to the CAD drawings by using polyurethane and epoxy adhesives.



*Figure 4.15 Assemblage Steps of the Fuselage*

Lastly two sides of the fuselage are brought together and adhered with a polyurethane adhesive. This step is very critical as the symmetry of the aircraft is crucial in terms of flight stability.



*Figure 4.16 Assembled Fuselage*

## **Wing**

Firstly, the carbon fiber tubes serving as front spar are assembled. As the wing is tapered, the diameters of the tubes reduce step by step. These tubes are adhered together.



*Figure 4.17 Front Spar of the Wing*

All the ribs and spars are adhered together inside the mold, and then the assembled inner structure is adhered to the upper surface of the wing. After that balsa laths are adhered between ribs along the wing periphery to obtain a better adhesion surface between upper and lower wing surfaces.

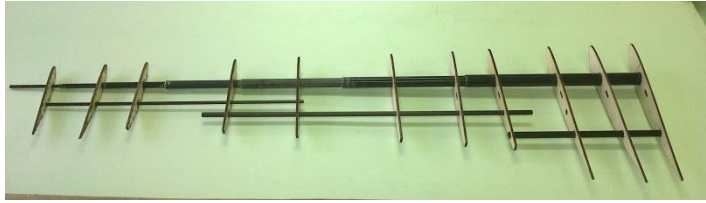


*Figure 4.18 Preparing the Upper Wing Surface*

After that, lower surface adhered to the upper surface.



*Figure 4.19 Assembled Wings*

## Tails

Again, the inner structural frames are placed on one side of the tail surfaces. The spars are fixed such that they are in contact with the tail boom.



*Figure 4.20 Inner Structure of the Tail Surfaces*

At first, lower surface of the horizontal tail is adhered to the end of the tail boom, and then the upper surface is placed on to the boom and the lower surface.



*Figure 4.21 Horizontal Tail Adhered to the End of the Tail Boom*

After that, one surface of the vertical tail is adhered to the tail boom. At this step, it is crucial to position the vertical tail perpendicular to the horizontal tail.



*Figure 4.22 Positioning and Adhering the Vertical Tail*

Finally, the other side of the vertical tail is fixed and the tail boom is trimmed to desired length.



*Figure 4.23 Assembled Horizontal and Vertical Tails*

## **Weights of the Assembled Parts**

Overall production procedure highly depends on craftsmanship, so it is very difficult to estimate the weights of the produced parts. Many components like wooden frames or metal parts have certain weights. On the other hand, the weights of the composite skins may change significantly due to the wrong mass ratio of fiber and resin. In wet lay-up method, this ratio is completely dependent to the skill of the operator. In addition to that, the amount of adhesive to be used is more ambiguous. In mathematical weight model, the adhesive to be used is tried to be estimated parametrically by taking every possible details into account. Despite that, the amount of used adhesive creates a considerable difference between the calculated and measured weight values.

In fuselage, all the internal frames are adhered to the skin and the amount of adhesive to be used is calculated by an empiric formula depending on initial CAD drawings. An allowable error is seen due to the fact that the shapes of the internal frames are not determined beforehand and correlation between the fuselage dimensions and the amount of adhesive to be used is not very strong.

In wings, the geometry is fairly determined and the regions to apply adhesive are clear. The weights of the ribs and spars are calculated parametrically from the unit weights. Therefore, the weight estimation seems more successful.

In tail parts, it is seen that the amount of adhesive needed to fix the tail boom to the tail surfaces is much more than estimated. Also a more careful workmanship is required at that phase comparing the other parts. As a result, the tail is produced a bit heavier.

In overall, the estimated and calculated weight values are close enough to carry on system development procedure. Approaching the problem in system level, it is important to be aware that the requirements of the air vehicle may slightly change during the development procedure, because of the external factors like a vibration issue for the payload or shadowing problem for data-link antenna. These kinds of troubles may result in additional weights to be loaded on the aircraft. After all, system development is always an iterative procedure. So the weight of the prototype is hardly possible to be the same with the final product. Here the important thing is to

show that it is possible to produce a useable prototype satisfying the basic requirements like aerodynamical efficiency, structural integrity and physical space for payloads.

*Table 4.2 Comparison of the Calculated and Measured Weights of the Assembled Parts*

<b>Parts</b>	<b>Calculated Output of the MS EXCEL (gr)</b>	<b>Measured Weight of the Produced Part (gr)</b>	<b>Error (%)</b>
Fuselage (with motor booms)	526.2	486	-8.27
Wing	476.3	470	-1.34
Tail (with tail boom)	134.4	163	17.5
<b>TOTAL</b>	<b>1136.9</b>	<b>1119</b>	<b>-1.60</b>

$$Error (\%) = \frac{\text{Measured Weight of the Produced Part} - \text{Calculated Output of the MS EXCEL}}{\text{Measured Weight of the Produced Part}} \times 100$$

As explained in “Weight Estimation Parameters” part of Chapter 2, for standard production of such an aircraft, the painting is planned to be done by injecting color pigments into the resin. So, when the weight comparisons are made, unpainted state of the prototype is used by considering that adding pigments have little contribution to the total weight.

After the assemblage of the parts, the aircraft is ready to be installed other equipment after the manufacturing process.

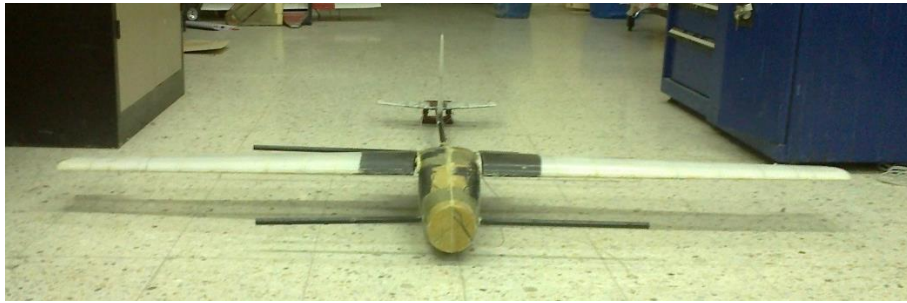


*Figure 4.24 Views of the Assembled Aircraft*



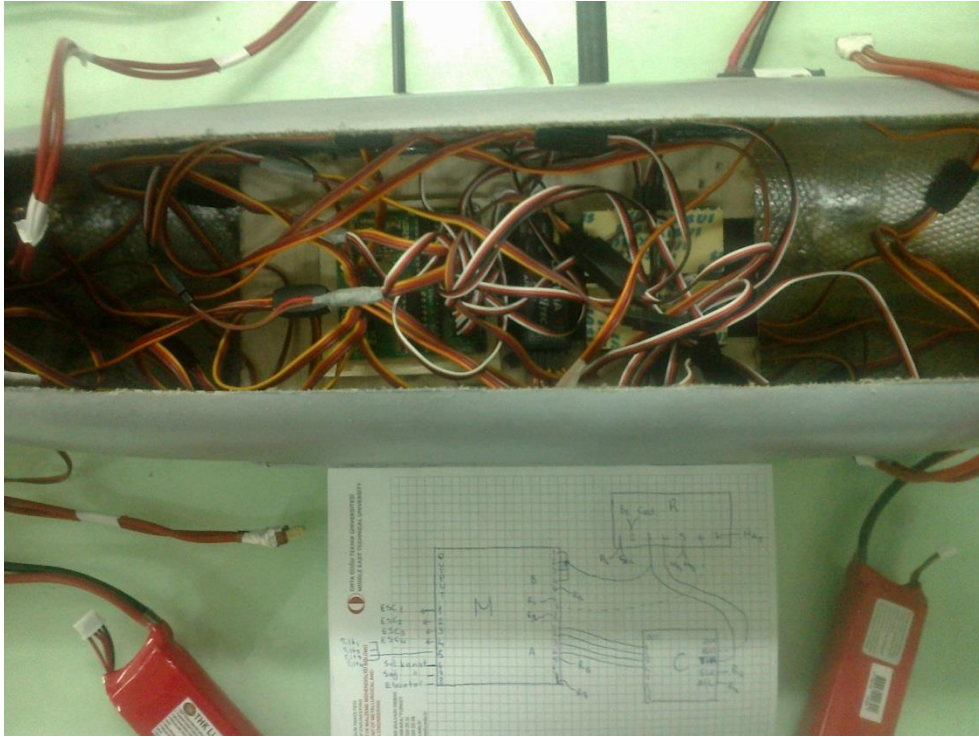


*Figure 4.26 Radio Receiver, Flight Controller, Servo Multiplexer Card and Cabling Installed on the Aircraft*

A ready-to-use tilt mechanism is installed on the aircraft for the initial tests, but it is seen that a more reliable mechanism should be replace it.



*Figure 4.27 Tilt Mechanism Installed on the Aircraft*



*Figure 4.28 View of the Equipped Aircraft (Fixed Wing Mode) for R/C Flight*



*Figure 4.29 View of the Equipped Aircraft (in Quad-rotor mode) for R/C Flight*



*Figure 4.30 A Scene From Vertical Flight in Quad-rotor Mode*

As it is stated some flight tests are conducted only to get an idea about the future work on mechanical side (tilt mechanism, vibration etc.), and no data is collected during these tests.

## **CHAPTER 5**

### **CONCLUSION**

In this thesis study, optimal design and prototype manufacturing procedures of a miniature class convertible quad tilt rotor (QTR) unmanned air vehicle (UAV) are explained. The aircraft carries its four motors on its motor booms separately from the wing. These four motors can be tilted to change the flight mode of the aircraft from horizontal to vertical flight, and vice versa. This design choice gives the aircraft the capability of operating as a fixed wing aircraft and a quad-rotor optionally. The modular design of the aircraft enables the operator to demount the wing and tail parts to use the aircraft as a highly manoeuvrable quad-rotor with tilting rotors. The fixed wing mode of the aircraft has VTOL capabilities, and a combined flight endurance of about 70 minutes. The combined flight refers to total 5 minutes of hovering, excluding vertical take-off and landing, besides horizontal flight. This ability of flight mode transition gives aircraft mission flexibility in many areas. The quad-rotor mode has almost 30 minutes of hovering time. In quad-rotor mode, an extra battery module can be installed instead of the removed wing and tail parts to extend the flight time. The motivation behind the optional quad-rotor mode is to obtain stealth and longer hovering time for some special mission objectives. The payload of the aircraft is a gyro stabilised gimbal with electro-optical day light and infrared sensors, which weighs about 700 grams.

Inherently, the primary objectives of the aircraft are accomplishing intelligence, surveillance and reconnaissance missions. Therefore the design procedure is conducted such that the primary consideration is maximizing the endurances of the determined mission profiles. Besides, the introduced conceptual design methodology can be used to maximize the payload weight or maximum velocity of the aircraft as well. Almost no modification in mathematical model is required to accomplish completely different optimization cases.

The main claim of this thesis study is to show the applicability of MS Excel-Ansys Workbench Design Optimization Toolbox coupled design methodology for such an aircraft design study. In this optimal design procedure, firstly a numerical model, in which all the weight estimation, outer geometry and performance parameters are calculated iteratively by embedded generic and non-generic formulas, is constructed in MS Excel. Then this model is introduced to Ansys Workbench's Design Optimization Toolbox. All the characteristics of the mathematical model are examined in detail by local sensitivity curves, response curves and trade-off charts. According to the requirements of the aircraft, the best candidates are determined by the toolbox from the pool of design cases that are created by using the mathematical model. Multi-objective genetic algorithm (MOGA) is used in the optimization phase, which is found to be most appropriate for this design study. For instance, MOGA allows multiple objectives like maximizing the combined flight endurance, limiting the total weight and minimizing stall speed at the same time according to the tuned priorities.

After the optimization procedure, a set of design parameters, including all geometrical and performance outputs, is obtained. According to these outputs, the outer geometry and inner structure of the aircraft is drawn. The molds for manufacturing the aircraft are designed. Tool-paths and numerical codes to machine the molds are constructed, and 10 parts of molds are machined by a 3-axis CNC machine. Surface finishing treatments are applied to the molds, so that they are prepared for wet lay-up composite production. The skin of the aircraft is made of composite materials, namely e-glass fiber, carbon fiber, aramid (Kevlar) fiber, Rohacell® foam, aramid honeycomb and epoxy resin. The measured weights of the manufactured composite skins and calculated values of them are compared; and it is seen that the estimation of the mathematical model is satisfactory. In inner structure of the aircraft, e-glass coated balsa frames and carbon fiber tubes are used. In assembly phase, the inner components and composite skins are adhered. Assembled parts' values are also measured and compared with the calculated values; and the errors are found to be acceptable. Considering that all the other electronic components of the aircraft are ready-to-use equipment, whose weights are well known; the weight estimation of the mathematical model is proven to be functional.

Consequently, it is seen that by coupling MS Excel and Ansys Workbench's Design Optimization Toolbox, an optimal output can be obtained for defined set of requirements. In addition to that, the estimations of the mathematical model are accurate enough such that the weight of the manufactured prototype is very close to the calculated value. The prototype is ready to be installed payload, mechanisms, motors, and electronic equipment.

Justifications of the aerodynamic and structural designs are made. It is possible and straightforward to implement the result of CFD runs to the optimization procedure, but it increases calculation costs enormously. So, CFD analyses are used to check the design. CFD analyses are conducted to calculate the critical aerodynamic properties of the aircraft. The outcomes of the CFD runs are compared with the results of the analytical calculations made by the mathematical model used in the design study. Static loading tests are applied to the wing and the motor booms of the aircraft. Elliptical wing loading is assumed for wing loading and 1g and 3g loading cases are tested. No sign of fracture or surface buckling is observed.

Possible solutions for drag problem of the motor booms in horizontal flight are discussed. This is the fundamental problem of the concept. Due to the circular cylinder shape of the motor booms, form drag of them in horizontal flight is very high. There are very obvious improvements for this issue, but finding an optimal solution is very hard and complicated work considering all the dynamics of the system. So for this thesis study, CFD solutions are used to comment on the issue and the possible solutions are discussed; but the base (reference) case -booms with circular cylinder shape- is kept in design phase.

As future work, the suggested items are the followings:

- The mode transition of the aircraft should be studied in detail. Thrust data of the propulsion unit should be collected at different angles and speeds of the heading wind. The test should be employed statically, and, if possible, dynamically by using a tilt mechanism. The best way for mode transition in terms of propulsion should be investigated.

- A mathematical flight model should be constructed by using motor tests' and CFD data. Guidance algorithms for efficient flight and mode transition should be generated by using this model.
- By employing an inertial measurement unit (IMU), flight test should be conducted and sets of data should be collected for validating the mathematical flight model.
- A genuine autopilot system specific for this aircraft should be developed by integrating attitude control, guidance and navigation algorithms.
- Data-link and video-link tests should be conducted and verified.
- Vibration analysis for the aircraft and refinement for tilt mechanism should be performed.
- For motor booms, drag reduction studies should be conducted.
- Stability and performance of the tailless version of this aircraft concept in horizontal flight should be investigated by using the mathematical models. By driving the tilting servos and propulsive motors separately, the need for tail can be eliminated. So a significant decreasing in total weight can be obtained.

## REFERENCES

- [1]. Bell X-22, Retrieved in July 2014, “[http://en.wikipedia.org/wiki/Bell\\_X-22](http://en.wikipedia.org/wiki/Bell_X-22)”.
- [2]. Bell Boeing Quad Tilt Rotor, Retrieved in July 2014, “[http://en.wikipedia.org/wiki/Bell\\_Boeing\\_Quad\\_TiltRotor](http://en.wikipedia.org/wiki/Bell_Boeing_Quad_TiltRotor)”.
- [3]. Gupta, V., “Quad Tilt Rotor Simulations in Helicopter Mode using Computational Fluid Dynamics” Ph.D. Thesis, University of Maryland, College Park, 2005.
- [4]. Armutçuoğlu, Ö., “The Conceptual Design Of a Tilt-Duct VTOL UAV” M.Sc. Thesis, Middle East Technical University, December 2000.
- [5]. Bell Boeing V-22 Osprey, Retrieved in July 2014, “<http://www.boeing.com/boeing/rotorcraft/military/v22>”.
- [6]. Agusta Westland AW609, Retrieved in July 2014, “<http://www.agustawestland.com/product/aw609>”.
- [7]. Boeing Phantom Swift, Retrieved in July 2014, “[http://www.boeing.com/boeing/Features/2013/09/bds\\_phantom\\_swift\\_09\\_11\\_13.page](http://www.boeing.com/boeing/Features/2013/09/bds_phantom_swift_09_11_13.page)”.
- [8]. Bell Eagle Eye, Retrieved in July 2014, “[http://en.wikipedia.org/wiki/Bell\\_Eagle\\_Eye](http://en.wikipedia.org/wiki/Bell_Eagle_Eye)”.
- [9]. IAI Panther, Retrieved in July 2014, “<http://www.iai.co.il/2013/35673-41636-en/IAI.aspx>”.
- [10]. KARI Smart UAV, Retrieved in July 2014, “<http://www.uasvision.com/2011/12/01/south-korea-tilt-rotor-uas>”.
- [11]. Ozdemir, U. et al, “Design of a Commercial Hybrid VTOL UAV System” , Journal of Intelligent and Robotic Systems, Volume 74, Issue 1-2, Pages 371-393, April 2014.
- [12]. Koker 1, Retrieved in July 2014, “<http://theaviationist.com/2012/11/08/koker>”.
- [13]. IAI Mini Panther, Retrieved in July 2014, “<http://www.iai.co.il/2013/35673-41637-en/IAI.aspx>”.
- [14]. Cetinsoy, E. et al, “Design and construction of a novel quad tilt-wing UAV”, Mechatronics, Volume 22, Issue 6, Pages 723–745, September 2012.

- [15]. Flores, G., Escareño, J., Lozano, R., Salazar, S., “Four Tilting Rotor Convertible MAV: Modeling, Control and Real-time Hover Flight Control”, *Journal of Intelligent & Robotic Systems*, Volume 65, Issue 1-4, Pages 457-471, January 2012.
- [16]. Aerovironment Shrike VTOL, Retrieved in July 2014, “<https://www.avinc.com/uas/adc/shrikevtol>”.
- [17]. IAI Ghost, Retrieved in July 2014, “[http://www.iai.co.il/36079-43473-en/BusinessAreas\\_UnmannedAirSystems.aspx](http://www.iai.co.il/36079-43473-en/BusinessAreas_UnmannedAirSystems.aspx)”.
- [18]. IAI Bird Eye 500, Retrieved in July 2014, “<http://www.unmanned.co.uk/autonomous-unmanned-vehicles/uav-data-specifications-fact-sheets/bird-eye-500-unmanned-vehicle-uav-specifications-data-sheet>”.
- [19]. Aerovironment RQ-11B Raven, Retrieved in July 2014, “[http://www.avinc.com/uas/small\\_uas/raven](http://www.avinc.com/uas/small_uas/raven)”.
- [20]. Aerovironment RQ-20A Puma, Retrieved in July 2014, “[http://www.avinc.com/uas/small\\_uas/puma](http://www.avinc.com/uas/small_uas/puma)”.
- [21]. EMT Aladin, Retrieved in July 2014, “[http://en.wikipedia.org/wiki/EMT\\_Aladin](http://en.wikipedia.org/wiki/EMT_Aladin)”.
- [22]. Aeronautics Orbiter, Retrieved in July 2014, “[http://www.aeronautics-sys.com/orbiter\\_mini\\_uav\\_muas](http://www.aeronautics-sys.com/orbiter_mini_uav_muas)”.
- [23]. Rafael Skylite B, Retrieved in July 2014, “<http://www.rafael.co.il/Marketing/334-919-en/Marketing.aspx>”.
- [24]. IAI Bird Eye 400, Retrieved in July 2014, “[http://www.iai.co.il/35098-34720-en/Groups\\_Military\\_Aircraft\\_MALAT\\_Products\\_Bird\\_Eye\\_Family.aspx](http://www.iai.co.il/35098-34720-en/Groups_Military_Aircraft_MALAT_Products_Bird_Eye_Family.aspx)”.
- [25]. Topivision Casper 200, Retrieved in July 2014, “<http://defense-update.com/products/c/casper200.htm>”.
- [26]. DP-6 Whisperer, Retrieved in July 2014, “[http://dragonflypictures.com/index.php?option=com\\_content&task=view&id=15](http://dragonflypictures.com/index.php?option=com_content&task=view&id=15)”.
- [27]. Heli Spy II, Retrieved in July 2014, “<http://www.unmanned.co.uk/autonomous-unmanned-vehicles/uav-data-specifications-fact-sheets/helispay-ii-unmanned-vehicle-uav-specifications-data-sheet>”.

- [28]. Datron Scout, Retrieved in July 2014, “<http://www.dtwc.com/products/aerial-recon/scout-suas>”.
- [29]. Honeywell RQ-16 T-Hawk, Retrieved in July 2014, “[http://en.wikipedia.org/wiki/Honeywell\\_RQ-16\\_T-Hawk](http://en.wikipedia.org/wiki/Honeywell_RQ-16_T-Hawk)”.
- [30]. Oviwun, Retrieved in July 2014, “[http://www.trekaero.com/Trek\\_VTOL\\_OVIWUN\\_Specifications.htm](http://www.trekaero.com/Trek_VTOL_OVIWUN_Specifications.htm)”.
- [31]. Uavvision Gyro-Stabilized Multi-Sensor CM100 Gimbal, Retrieved in July 2014, “<http://www.uavvision.com/product/cm100.html>”.
- [32]. City Center Altitudes in Turkey, Retrieved in July 2014, “[http://tr.wikipedia.org/wiki/T%C3%BCrkiye\\_il\\_merkez\\_rak%C4%B1mlar%C4%B1](http://tr.wikipedia.org/wiki/T%C3%BCrkiye_il_merkez_rak%C4%B1mlar%C4%B1)”
- [33]. Cloud Cap Piccolo Nano Autopilot, Retrieved in July 2014, “<http://www.uasvision.com/2013/03/22/cloud-cap-technology-launches-piccolo-nano-autopilot-for-small-uas>”.
- [34]. TP-Link Omni Antenna, Retrieved in July 2014, “<http://www.tp-link.com/en/products/details/?model=TL-ANT2415D>”.
- [35]. UTC Aerospace Systems AGL Sensor, Retrieved in July 2014, “[www.cloudcaptech.com/Sales%20and%20Marketing%20Documents/AGL%20Sensors%20Data%20Sheet.pdf](http://www.cloudcaptech.com/Sales%20and%20Marketing%20Documents/AGL%20Sensors%20Data%20Sheet.pdf)”
- [36]. TP-Link Video-link, Retrieved in July 2014, “<http://www.tp-link.com/lk/products/details/?model=TL-WA5210G>”
- [37]. Thunder Power Lithium Polymer Battery 8000mAh 3-CELL/3S4P 11.1V PRO LITE MS LIPO, Retrieved in July 2014, “[http://www.thunderpowerrc.com/Products/8000-mAh\\_2/TP8000-3S4PL](http://www.thunderpowerrc.com/Products/8000-mAh_2/TP8000-3S4PL)”.
- [38]. Thunder Power Lithium Polymer Battery 3300mAh 3-Cell/3S 11.1V G8 Pro Lite+ 25C LiPo, Retrieved in July 2014, “[http://www.thunderpowerrc.com/Products/3300-mAh\\_3/TP3300-3SPP25](http://www.thunderpowerrc.com/Products/3300-mAh_3/TP3300-3SPP25)”.
- [39]. PT-326 Polyurethane Structural Adhesive, Retrieved in July 2014, “[www.easycomposites.co.uk/downloads/TDS/EC-TDS-PT326.pdf](http://www.easycomposites.co.uk/downloads/TDS/EC-TDS-PT326.pdf)”
- [40]. Raymer, Daniel P., Aircraft Design: A conceptual Approach, AIAA, 1992.
- [41]. Airfoil Database, Retrieved in July 2014, “<http://airfoiltools.com>”

- [42]. Scorpion SII-3014-830KV (V2), Retrieved in July 2014, “[http://www.scorpionsystem.com/catalog/motors/s30\\_series\\_v2/SII-3014-830KV](http://www.scorpionsystem.com/catalog/motors/s30_series_v2/SII-3014-830KV)”.
- [43]. Roskam, Jan , Airplane Flight Dynamics And Automatic Flight Controls, Roskam Aviation and Engineering Corporation, 1979.
- [44]. Roskam, Jan , Tau Edward Lan, Dr. Chuan, Airplane Aerodynamics and Performance, DarCorporation, 1997.
- [45]. Hoerner, S. F., Fluid-Dynamic Drag, Hoerner Fluid Dynamics, 1965.
- [46]. Anderson, John D., Aircraft Performance and Design, McGraw-Hill, 1999
- [47]. Kacar, A., Üç Dönerkanatlı ve Döner-Rotorlu İnsansız Hava Aracının Tasarımı, EMO, Cilt 3, Sayı 6, 2014.
- [48]. Ansys Workbench User’s Guide Release 15.0, Nov 2013
- [49]. Roskam, Jan, Methods for Estimating Stability and Control Derivatives of Conventional Subsonic Airplanes, 1971.
- [50]. MGS Epoxy L285/H285, Retrieved in July 2014, “<http://www.kompozit.net>”.
- [51]. Vacuum Bagging Wet Lay-up Method, Retrieved in July 2014, “<http://www.kutec.at/vakuum.html>”.
- [52]. R. H. Stone, “Control Architecture for a Tail-sitter Unmanned Air Vehicle”, 5th Asian Control Conference, Melbourne, Australia, July 23-25, 2004.
- [53]. D. Snyder, “The Quad Tiltrotor: Its Beginning and Evolution”, Proceedings of the 56th Annual Forum, American Helicopter Society, Virginia Beach, Virginia, May 2000
- [54]. W. E. Green and P. Y. Oh, “Autonomous Hovering of a Fixed-Wing Micro Air Vehicle”, International Conference on Robotics and Automation, Orlando, Florida, USA, May, 2006
- [55]. Radhakrishnan, A., Schmitz, F., “Quad Tilt Rotor Download and Power Measurements in Ground Effect,” Proceedings of the 24th Applied Aerodynamics Conference, AIAA, San Francisco, CA, June 2006.
- [56]. Etkin, Bernard, Dynamics of Atmospheric Flight, 1972.
- [57]. Science Fair Projects, Retrieved in August 2014, “[http://www.sciencebuddies.org/science-fair-projects/project\\_ideas/Sports\\_p012.shtml](http://www.sciencebuddies.org/science-fair-projects/project_ideas/Sports_p012.shtml)”.

- [58]. Choi J, Jeon WP, Choia H. “Mechanism of Drag Reduction by Dimples on a Sphere.” *Physics of Fluids*. Vol.18 4 041702. 2006.
- [59]. Tsutsui, T., Igarashi, T., “Drag Reduction of a Circular Cylinder in an Air-stream”, *Journal of Wind Engineering and Industrial Aerodynamics*, 90, 527-541, 2002.
- [60]. Roshko, A., 1954b. On the drag and shedding frequency of two-dimensional blunt bodies. Technical Report TN 3169, NACA, US Government Printing O4ce, Washington, DC, 1954.
- [61]. Lienhard, J., H., *Synopsis of Lift, Drag and Vortex Frequency Data for Rigid Circular Cylinders*, 1966.
- [62]. Alatan, B., Shakib, H., “Parametric Design and Optimization of Steel Car Deck Panel Structures”, M.Sc. Thesis, Department of Shipping and Marine Technology Division of Marine Design, CHALMERS UNIVERSITY OF TECHNOLOGY, Gothenburg, Sweden, 2012.
- [63]. W. Chen et al., “Optimization Of Processing Parameters For Beam Blank Continuous Casting Using Moga Combined With Fem”, *Rev. Adv. Mater. Sci.* 33, 337-341, 2013.
- [64]. Mandloi, P., Gunjan V., *Design Optimization of An In-Cylinder Engine Intake Port*, Nafems World Congress, Greece, 2009.
- [65]. Sánchez-Caballero, S. et al., *Weight Reduction In Structures Using Finite Elements And Multi-objective Genetic Algorithms*, Fascicle of Management and Technological Engineering, Volume X (XX), 2011, NR2.



## APPENDIX A

### COST ANALYSIS

Estimated costs of the components are as follows:

*Table A.1 Costs of the Components*

PART	UNIT PRICE	AMOUNT	TOTAL (TL)
Raw Mold Material (MDF)	35 TL/m <sup>2</sup>	3.8 m <sup>2</sup>	133
CNC Machining	150 TL/hr	50	7500
Surface Finish Materials (total)	-	-	80
Workmanship (Mold Manufacturing)	6.5 TL/hr/man	30 man.hr	195
Molds Total			<b>7908</b>
63 gr/m <sup>2</sup> Kevlar Fabric	150 TL/m <sup>2</sup>	0.36 m <sup>2</sup>	54
25 gr/m <sup>2</sup> E-glass Fabric	28 TL/m <sup>2</sup>	1.3 m <sup>2</sup>	36.4
49 gr/m <sup>2</sup> E-glass Fabric	26 TL/m <sup>2</sup>	2.6 m <sup>2</sup>	67.6
93 gr/m <sup>2</sup> Carbon-fiber Fabric	288 TL/m <sup>2</sup>	0.5 m <sup>2</sup>	144
1 mm Fine Grid Rohacell	183 TL/layer	1 layer	183
1.5 mm Kevlar Honeycomb	171 TL/m <sup>2</sup>	0.4 m <sup>2</sup>	684
Epoxy&Hardener Set	157 TL/set	1 set	157
Consumables (gloves, vacuum bags, etc.)	-	-	400
Carbon-fiber tubes (total)		-	350
2.5 mm balsa wood	3.25 TL/plate	4 plate	13
Laser Cutting	-	-	20
Workmanship (Manufacturing)	6.5 TL/hr/man	80 man.hr	520
Structure Total (without painting)			<b>2629</b>
Brushless DC Motors	200 TL/unit	4 unit	800
Tilting Servo Motors	50 TL/unit	4 unit	200
Control Surface Servo Motors	50 TL/unit	4 unit	200
Propellers	25 TL/unit	4 unit	100
Tilt Mechanism	40 TL/unit	4 unit	160
Electronic Speed Controllers	100 TL/unit	4 unit	400
Wiring	50 TL/set	1 set	50
Battery (for propulsion)	570 TL/unit	3 unit	1710
Workmanship (Assemblage)	6.5 TL/hr/man	10 man.hr	65
Ready for radio controlled flight (excluding receiver and transmitter)			<b>6314</b>

Avionic Box (including data-link)	16,000 TL/unit	1 unit	16000
AGL Sensor	500 TL/unit	1 unit	500
Video Modem	170 TL/unit	1 unit	170
Antenna	80 TL/unit	1 unit	80
Battery (for avionics)	140 TL/unit	1 unit	140
Gimbal Camera	40,000 TL/unit	1unit	40000
<b>Aircraft Total</b>			<b>63204</b>

## APPENDIX B

### MOTOR DATASHEET

From [42],

*Table B.1 Performance of the Motor with Different Propellers*

Prop Manf	Prop Size	Input Voltage	Motor Amps	Watts Input	Prop RPM	Pitch Speed	Thrust (Grams)	Thrust (Ounces)	Thrust Eff. (Gr/W)
APC	8x6-E	11.1	12	133.2	9,070	51.5	693.5	24.46	5.21
APC	8x6-SF	11.1	16.56	183.9	8,759	49.8	806	28.43	4.38
APC	8x8-E	11.1	16.48	182.9	8,725	66.1	662.7	23.38	3.62
APC	9x4.5-E	11.1	11.37	126.2	9,127	38.9	821.7	28.98	6.51
APC	9x4.7-SF	11.1	12.48	138.5	9,063	40.3	892.1	31.47	6.44
APC	9x6-E	11.1	13.72	152.3	8,923	50.7	843.3	29.75	5.54
APC	9x6-SF	11.1	24.21	268.8	8,128	46.2	1125.7	39.71	4.19
APC	9x7.5-E	11.1	20.21	224.3	8,426	59.8	918	32.38	4.09
APC	9x7.5 -SF	11.1	27.41	304.2	7,870	55.9	1081.7	38.16	3.56
APC	9x9-E	11.1	23.95	265.9	8,137	69.3	899.7	31.74	3.38
APC	10x3.8 -SF	11.1	21.39	237.4	8,387	30.2	1344.6	47.43	5.66
APC	10x4.7 -SF	11.1	22.51	249.8	8,284	36.9	1361	48.01	5.45
APC	10x5-E	11.1	16.12	178.9	8,769	41.5	1079.7	38.08	6.03
APC	10x6-E	11.1	18.37	203.9	8,593	48.8	1153.2	40.68	5.66
APC	10x7-E	11.1	21.49	238.5	8,349	55.3	1170.1	41.27	4.91
APC	10x7-SF	11.1	31.47	349.3	7,552	50.1	1451.1	51.19	4.15
APC	10x10-E	11.1	30.7	340.8	7,596	71.9	1006.1	35.49	2.95
APC	11x3.8 -SF	11.1	23.9	265.2	8,162	29.4	1522	53.69	5.74
APC	11x4.7-SF	11.1	27.85	309.1	7,832	34.9	1661.9	58.62	5.38
APC	11x7-E	11.1	26.64	295.7	7,951	52.7	1518.6	53.57	5.14
APC	11x8-E	11.1	28.41	315.4	7,790	59	1482.5	52.29	4.7
APC	11x8.5-E	11.1	30.49	338.4	7,613	61.3	1467	51.75	4.34
APC	12x6-E	11.1	28.8	319.7	8,593	48.8	1153.2	40.68	3.61
APC	12x8-E	11.1	34.84	386.7	7,219	54.7	1507.3	53.17	3.9
APC	13x4-E	11.1	25.74	285.7	8,019	30.4	1783.2	62.9	6.24
GEM	9x4.7-C	11.1	12.65	140.4	8,660	38.5	883.6	31.17	6.29
GEM	10x4.5-C	11.1	19	210.9	8,176	34.8	1221.7	43.09	5.79
GEM	11x4.7-C	11.1	25.15	279.2	7,700	34.3	1579.2	55.7	5.66

<b>GEM</b>	12x4.5-C	11.1	29.4	326.3	7,372	31.4	1648.1	58.13	5.05
<b>GWS</b>	9x5-DD	11.1	10.99	122	9,185	43.5	824.2	29.07	6.76
<b>GWS</b>	9x5x3-DD	11.1	14.19	157.5	8,879	42	938.5	33.1	5.96
<b>GWS</b>	10x6-DD	11.1	15.41	171	8,842	50.2	1060.6	37.41	6.2
<b>GWS</b>	10x6x3-DD	11.1	19.94	221.3	8,388	47.7	1281.3	45.2	5.79
<b>GWS</b>	11x7-DD	11.1	23.67	262.8	8,184	54.3	1486.4	52.43	5.66
<b>GWS</b>	12x8-DD	11.1	33.5	371.8	7,358	55.7	1763	62.19	4.74
<b>MAS</b>	8x6x3	11.1	12.23	135.8	9,089	51.6	716.7	25.28	5.28
<b>MAS</b>	9x7x3	11.1	19.41	215.4	8,523	56.5	1096.2	38.67	5.09
<b>MAS</b>	10x5x3	11.1	17.21	191	8,699	41.2	1145	40.39	5.99
<b>MAS</b>	10x7x3	11.1	24.52	272.2	8,110	53.8	1416	49.95	5.2
<b>MAS</b>	11x7x3	11.1	28.87	320.5	7,748	51.4	1628.7	57.45	5.08
<b>MAS</b>	11x8x3	11.1	31.08	345	7,556	57.2	1663	58.66	4.82

## **APPENDIX C**

### **JUSTIFICATION OF AERODYNAMICAL OUTPUTS BY CFD CALCULATIONS**

As explained in methodology chapter, no CFD data is used in mathematical model considering the computational costs. Therefore, after the design phase, CFD calculations are performed in order to check the validity of the analytical calculations. Of course, CFD calculations have certain errors and they are not completely correct; but it is a good practice to compare the order of magnitudes of the numbers of both sources.

#### **Analysis Conditions**

The same physical conditions with the mathematical model are used in analysis. The temperature, density and the viscosity of the air are assumed to be constant. The effects of the propellers are not considered in the analysis, it is sure that the prop-wash changes the forces on the motor booms, especially at low velocities.

- Operating pressure: 88792 Pa
- Air viscosity:  $1.7547 \times 10^{-5}$  Pa.s
- Air temperature: 281.01 K
- Air density:  $1.101 \text{ kg/m}^3$

#### **Mesh and Boundary Conditions**

A rectangular prism shaped domain is used for calculations. The dimensions of the domain are about 20 times of the aircraft's maximum lengths at corresponding directions.

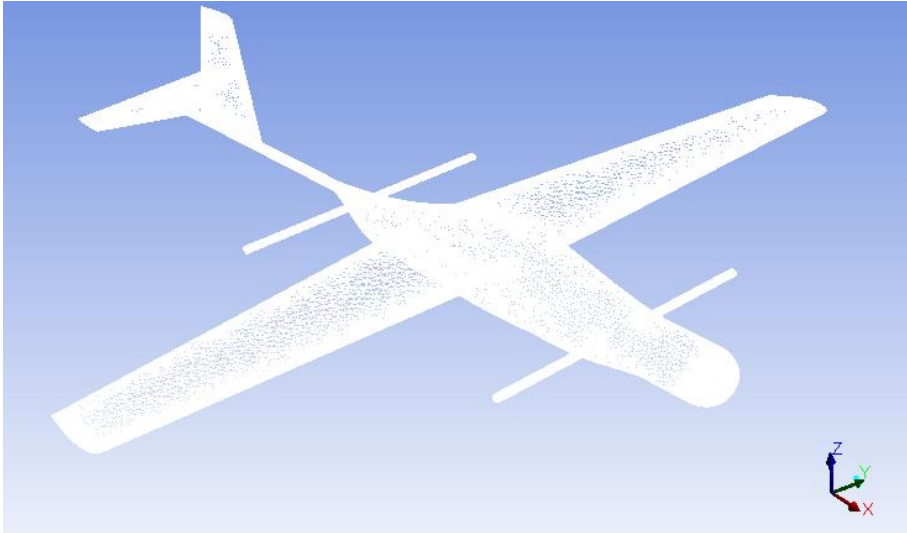


*Figure C.0.1 Boundary Mesh on the Wall Surfaces*

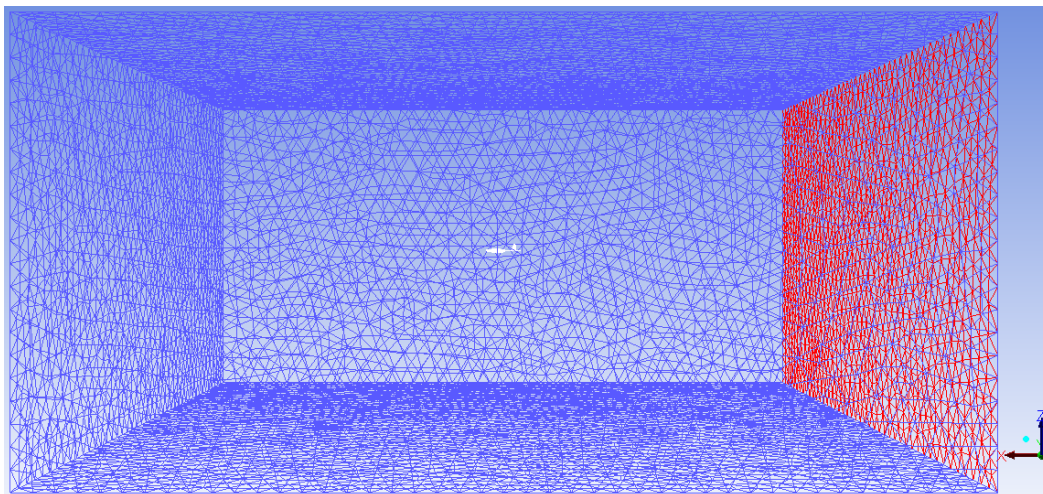


*Figure C.0.2 Computational Domain*

The number of the elements is limited to be about 4.5 million due to the computational source. A curvature based size function is used in meshing, which is typical for CFD meshing. 15 boundary layers around the wall surfaces are applied.

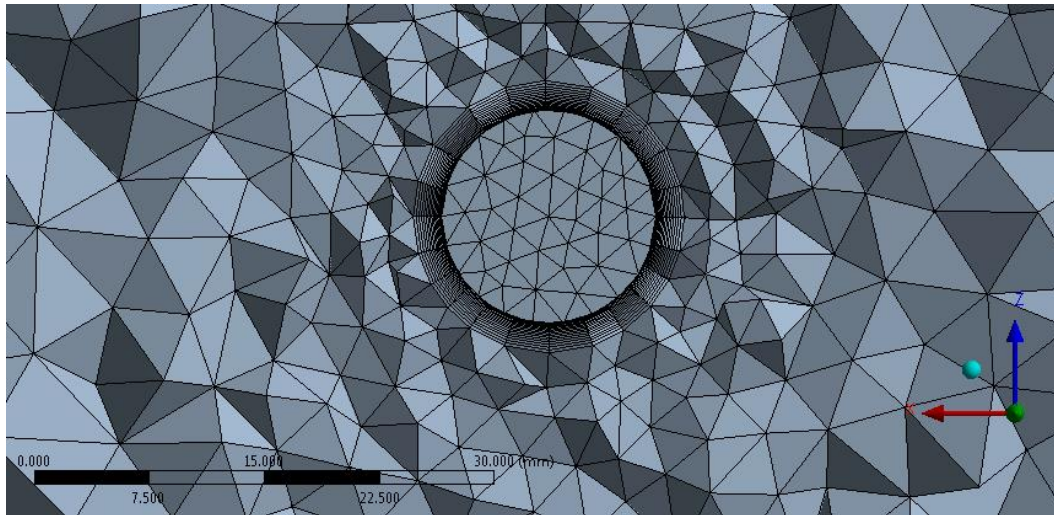


*Figure C.0.3 Cross-section of the motor boom in computational mesh*

There is one outlet at the back and the other faces of the domain are inlets. The velocity is specified at these inlets and it is 20 m/s. The faces of the aircraft are defined as wall.

Spalart-Almaras turbulence model is used.

**$\alpha$  Runs:**

Steady state analyses are performed by varying the angle of attack of the aircraft. -10, -5, 0, 5, 10, 13, 14, 15, 16 and 17 degrees of angles of attack cases are analysed.

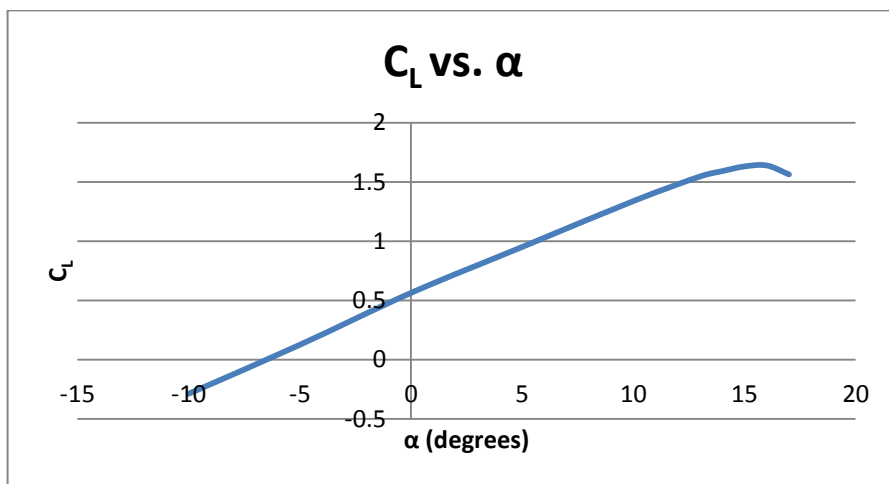


*Figure C.0.4 Lift Coefficient Variation of the Full Aircraft with Angle of Attack*

Estimated design lift coefficient at zero angle of attack is 0.655. (see Table 3.3) From the CFD data  $C_{L@\alpha=0^\circ}$  is found to be 0.613. At cruise velocity with zero angle of attack, the lift is about 4700 gf.

One of the most important characteristic of an aircraft is  $C_{L\alpha}$ . A typical linear curve of  $C_L$  vs.  $\alpha$  curve is obtained. After a point, flow separation starts and lift is reduced. At the linear region the slope, which is equal to  $C_{L\alpha}$ , is found to be  $4.83 \text{ rad}^{-1}$ . It is very close to the value calculated analytically. (see Table 3.3)

For the full aircraft, the lift begins to drop after  $16^\circ$  of angle of attack. Considering the incidence angle of the wing, it seems very late. The reason for this situation seems to be that the lift of the fuselage and tail is remarkable at high angle of attack values. At 16 degrees of angle of attack, the wing produces 116.1 N of lift. The fuselage and tail contribution is about 16 N in total. So the, maximum lift coefficient of the whole aircraft is calculated to be 1.7 (see Figure C.0.4), while the wing's maximum lift coefficient is calculated to be 1.55, which is a reasonable value considering the  $C_{l,max}$  of the wing airfoil.

Another output to be checked is zero lift angle of attack of the airfoil, which is used for the first estimate of the wing incidence angle. The zero lift angle of attack of the wing is found to be  $-3.91^\circ$  from CFD data. Comparing with the airfoil data, it is a very good value.

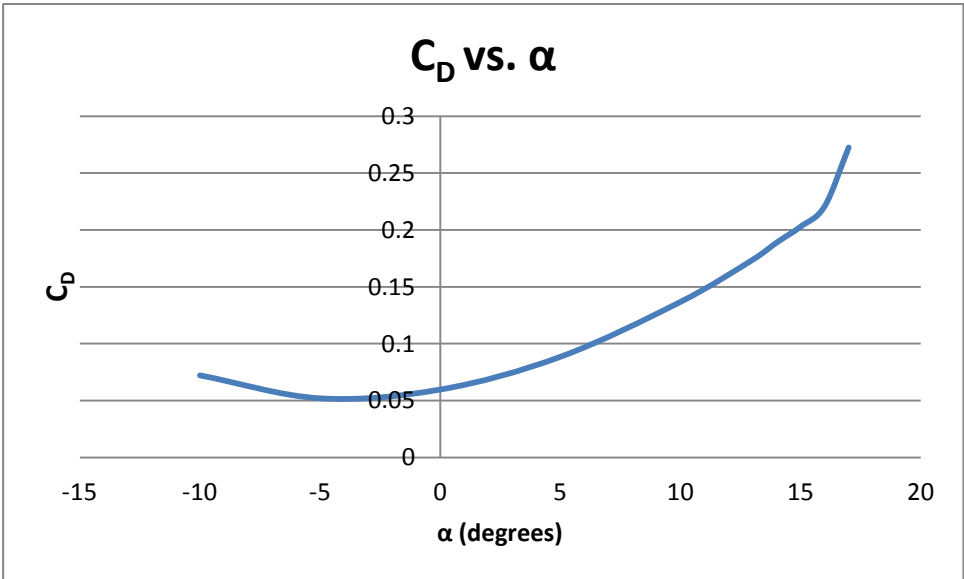


Figure C.0.5 Drag Coefficient Variation of the Full Aircraft with Angle of Attack

Another critical parameter is the drag coefficient of the aircraft, as the horizontal flight endurance directly depend on it. At zero angle of attack,  $C_D$  is found to be 0.062 from CFD calculations. Comparing with the value calculated by analytical methods (see Table 3.3), the drag estimation used in the model seems reasonable. Of course, this is a critical issue and more detailed CFD runs or wind tunnel tests are required to extract stability and control derivatives.

As it can be seen in Figure C.0.5, at the nose of the aircraft, flow stagnates and creates a high pressure area here, which contributes the total drag significantly. The payload is modelled as a rounded cylinder for simplicity, but the real geometry of the payload might create a different flow field. A model with higher fidelity may enhance the solution.

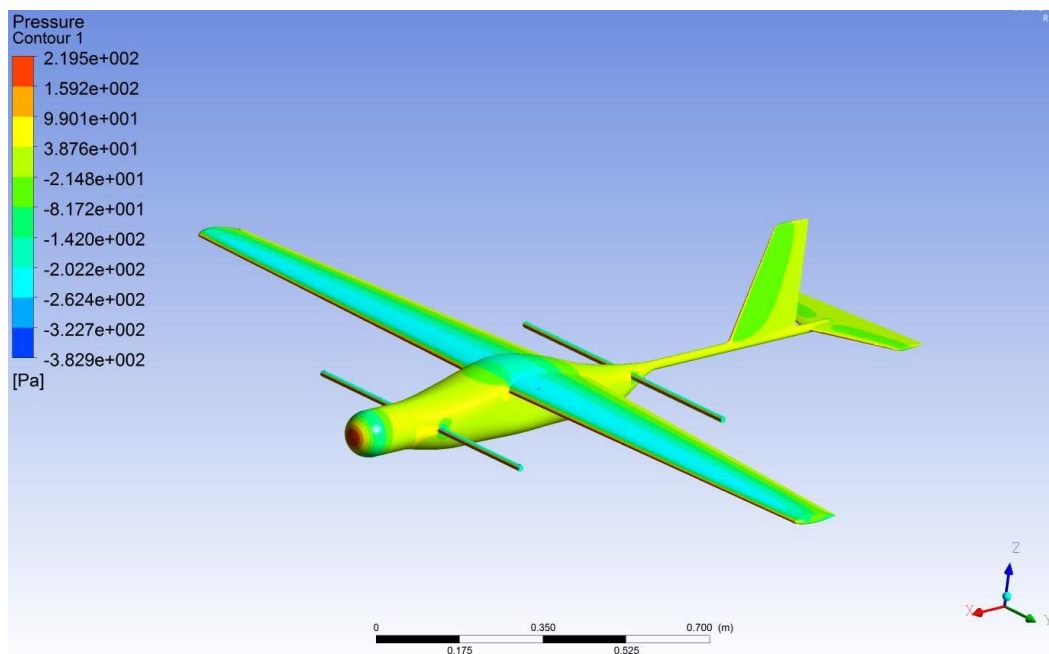


Figure C.0.6 Static Pressure Contours at 20 m/s and Zero Angle of Attack

In detail, the separate values of the components' drag forces are obtained from CFD data at zero angle of attack. For motor booms, the values are very close. As the flow separates behind the boom, it was thought be difficult to estimate the drag force on the motor booms. There are two possible reasons for the accuracy. Firstly, the reference value for analytical calculation, which is taken from [45], is an empirical value; so the estimation is good. Secondly, the CFD calculation is accurate enough.

Also for fuselage, which has a cylindrical-like shape, the values are close.  $C_{D,0}$  is not calculated for tail by using CFD data, because the drag on the tail boom is included in it. For the wing, the analytically calculated drag force is a bit lower than the CFD result. The parasite drag coefficient is not calculated for the wing also; because the proportion of the induced drag and parasite drag cannot be distinguished from the CFD data.

*Table C.1 Drag Force Comparison of CFD Results with Analytical Calculations*

	<b>DRAG (CFD) (N)</b>	<b>DRAG (ANALYTICAL) (N)</b>	<b><math>C_{D,0}</math> (CFD)</b>	<b><math>C_{D,0}</math> (Table 3.3)</b>
<b>MOTOR BOOMS</b>	1.834	1.887	0.024507	0.0252
<b>FUSELAGE</b>	0.4226	0.4035	0.005645	0.00539
<b>TAIL</b>	0.285	0.108 (without tail boom)	-	0.00145
<b>WING</b>	2.131	1.769	-	0.00541

In mathematical model,  $C_{M,\alpha}$  value is calculated analytically, and the static margin calculation is made accordingly. In addition to that,  $C_{M,\alpha}$  is the basic parameter to check the longitudinal stability of the aircraft. It can be considered as the damping of the change in angle of attack, so it must be negative to have a balancing effect [56]. As it is seen, it is monotonically decreasing with the angle of attack. The value calculated analytically is -0.38, while the slope of the graph in Figure C.0.7 between  $\alpha=0^\circ$  and  $\alpha=5^\circ$  is around -0.37.

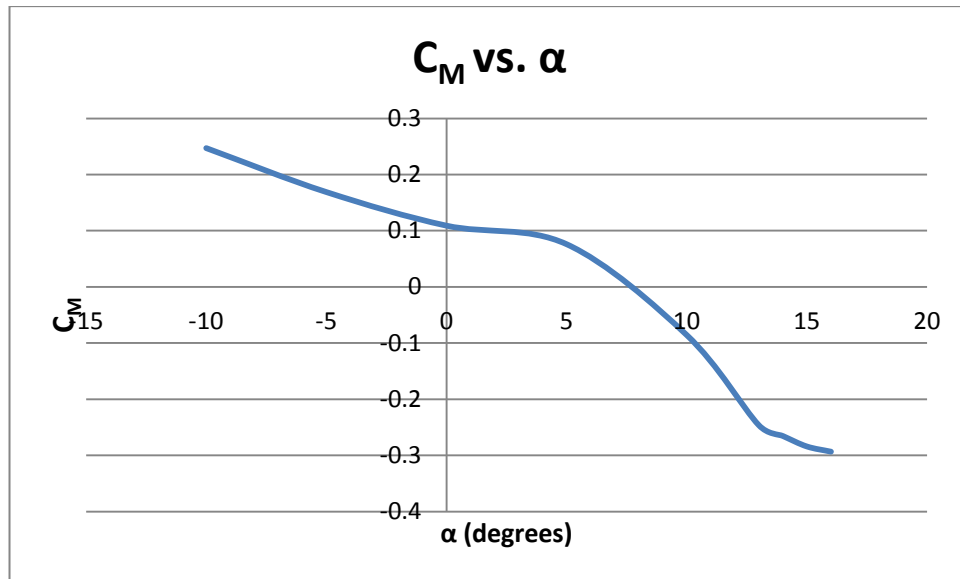


Figure C.0.7 Body-y Moment Coefficient Variation of the Full Aircraft with Angle of Attack (In Stability Axes [56])

### $\beta$ Runs:

Steady state analyses are conducted at side-slip angle of  $5^\circ$  and  $10^\circ$  to check the lateral static stability.

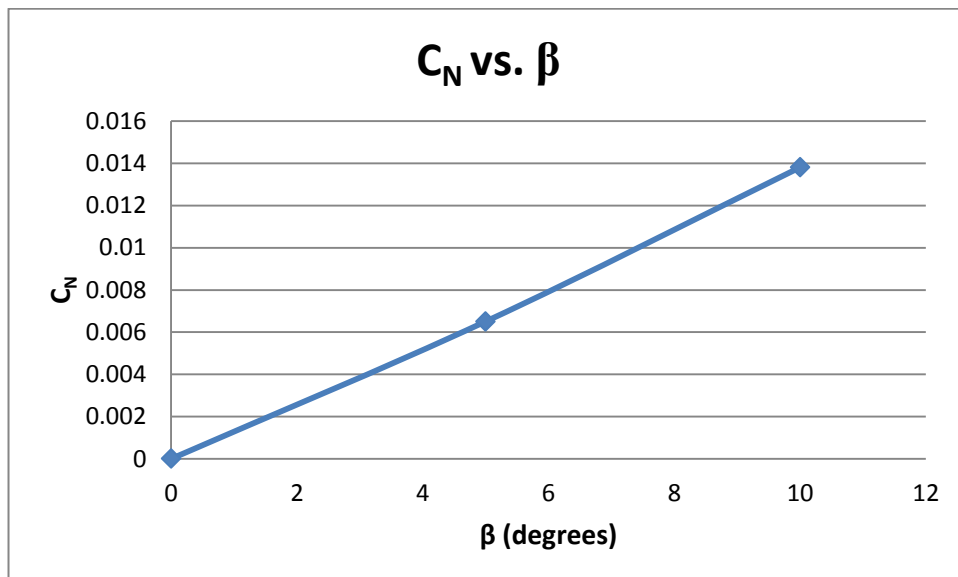


Figure C.0.8 Body-z Moment Coefficient Variation of the Full Aircraft with Angle of Attack (In Stability Axes [56])

Positive yaw stiffness is required to obtain weathercock stability [56]. As seen in Figure C.0.8, the moment coefficient in stability-z axis,  $C_N$ , is increasing with angle of attack. Thus,  $C_{N,\beta}$  is positive. Numerically, it is around 0.079.

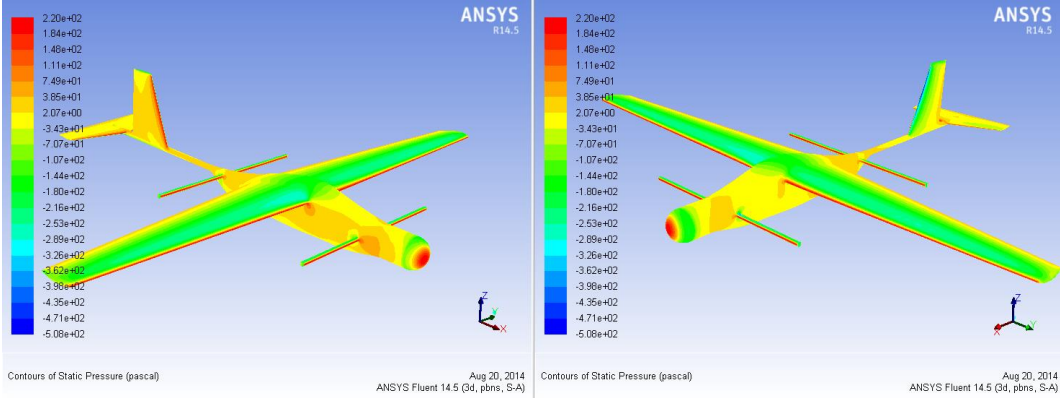


Figure C.0.9 Static Pressure Contours at 20 m/s and 10° Side-slip Angle

## APPENDIX D

### CONCEPTUAL PROBLEM: DRAG FORCE ON MOTOR BOOMS

Although the airframe concept of this study brings about many advantages, the most important handicap of the concept seems to be the high drag force on the motor booms in horizontal flight.

Due to the cylindrical shape of the booms, boundary layer separation behind the motor booms is seen very clearly. Considering the manufacturing ease, the booms have no special shape and during the production of the first prototype, they are left as they are. Some ideas have been generated during this study, but optimizing the shape of the motor booms is beyond the scope of this study.

In terms of stating the case clearly, it is good practice to examine the CFD data, which is in a good match with analytical calculations.

*Table D.1 Drag Forces on Components at 20 m/s with zero angle of attack*

	<b>DRAG FORCE (N)</b>
<b>WING</b>	2.131
<b>MOTOR BOOMS (TOTAL)</b>	1.834
<b>FUSELAGE</b>	0.4226

Looking at the Table D.1, it is very clear that the drag on the booms is very close to the wing's and four times of the fuselage's. Considering its surface area, an extraordinary contribution comes from the booms. This situation is already obvious from the parasite drag coefficients.

As it can be seen in Figure D.0.1, flow separates after a point near the top points of the cylinder, leaving a low pressure zone behind the boom (see Figure D.0.2) . It creates a high drag force on the boom.

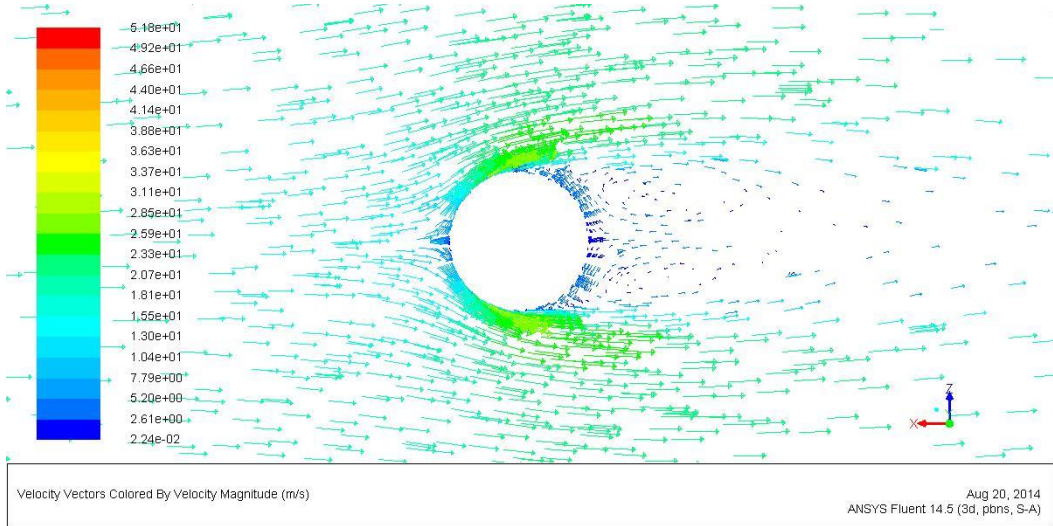


Figure D.0.1 Velocity Vectors around the Motor Boom at 20 m/s with zero angle of attack

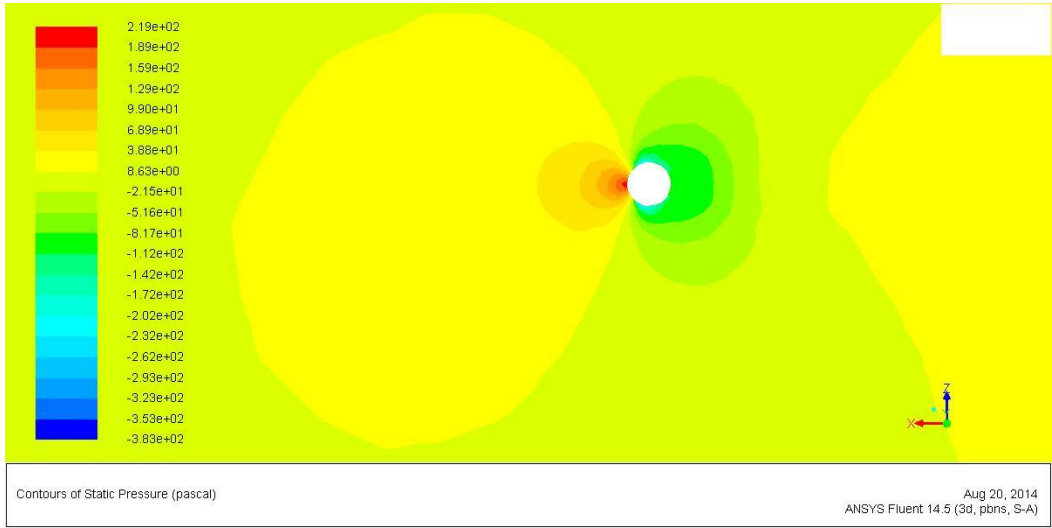


Figure D.0.2 Static Pressure Contours around the Motor Boom at 20 m/s with zero angle of attack

This situation drastically decreases the horizontal flight endurance of the aircraft. Almost 40 % of the total drag is due to the motor booms. If the booms are removed, the drag force reduces to 3.05 N according to the CFD data. (see Figure D.0.3) It can be also said that the motor booms decreases the horizontal flight endurance by almost

40 %. This cost is too much for sake of vertical flight capabilities; and also it is avoidable.

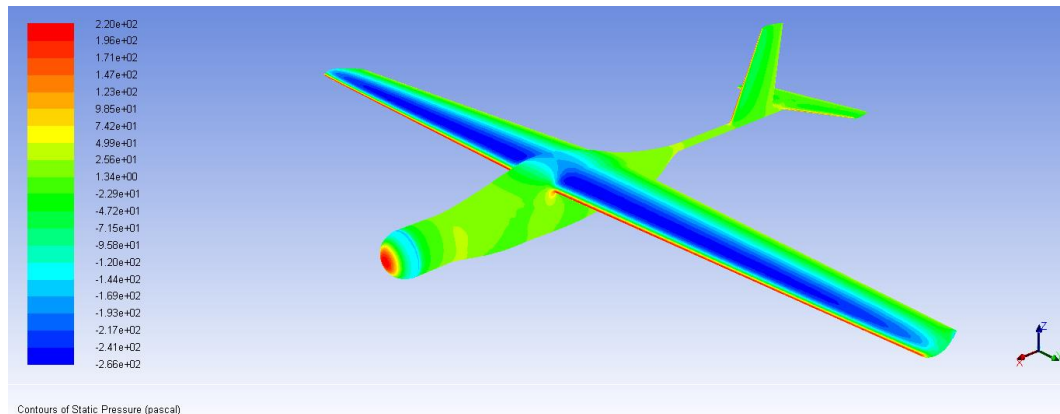


Figure D.0.3 Static Pressure Contours of the Aircraft Version without Motor Booms at 20 m/s with zero angle of attack

This is a very common problem in various disciplines of engineering. So, there are a lot of studies related with it. For this concept, there are two main approaches to solve the drag problem.

The first approach is to have streamline-shaped motor boom. A streamline-shaped boom prevents the flow separation and the form drag would decrease. [56]

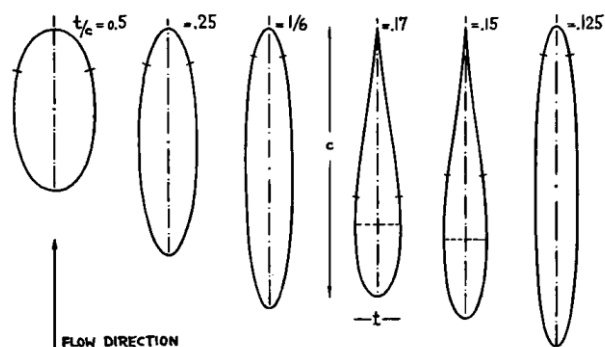
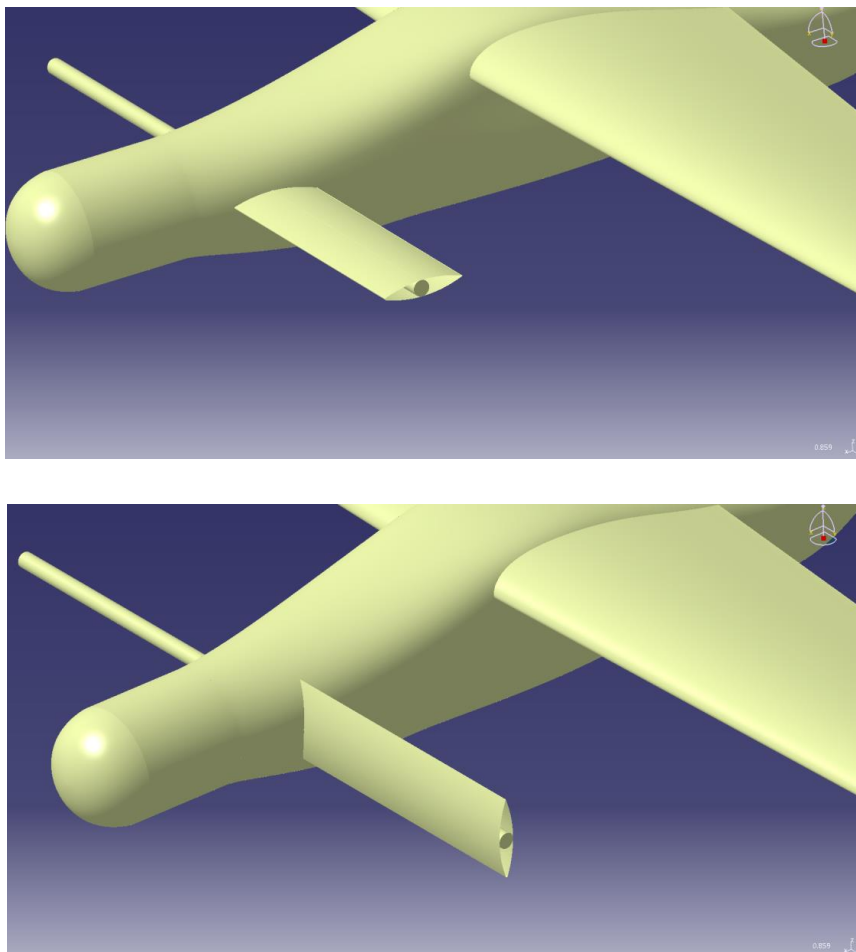


Figure D.0.4 Separation Points on several 2-d elliptical and Jukowsky shapes determined by theoretical analysis of the boundary layer flow (from [45])

It is simply placing fairings on motor booms. Coating the carbon fiber booms with a non-structural material is a solution. The diameter of the boom still must be large enough to have required strength, as it carries 1.5 kgf at its tip during the hovering.

On the other hand, if the thickness ratio is small, the length of the fairing becomes larger. Two disadvantages come with that. The first one is that in hovering downwash of the propeller is faced directly by the fairing. (see Figure 1.4) Out of the ground effect, this situation decreases the carrying capacity as explained before. On the other hand, this problem may be solved by tilting the fairing synchronously with the propellers like a tilt-wing aircraft. The second disadvantage is the possibility to distort the upstream of the wing. Eliminating and even turning it to an advantage is possible by an integrated servo controller, which tilts the fairing; but this would be a very complicated system. Besides, stability problems may arise due to these fairings.

Equivalently strong booms may be replaced. The diameter of the boom may be reduced or an elliptical boom may be used but the prices of the elliptical booms are very high and the production of them is rather hard.



*Figure D.0.5 A Possible Tilting-Fairing Solution to Reduce the Form Drag (Upper configuration in horizontal flight and lower configuration in hovering)*

The second approach is to obtain a thicker boundary layer and postpone the separation like in well-known golf ball example.

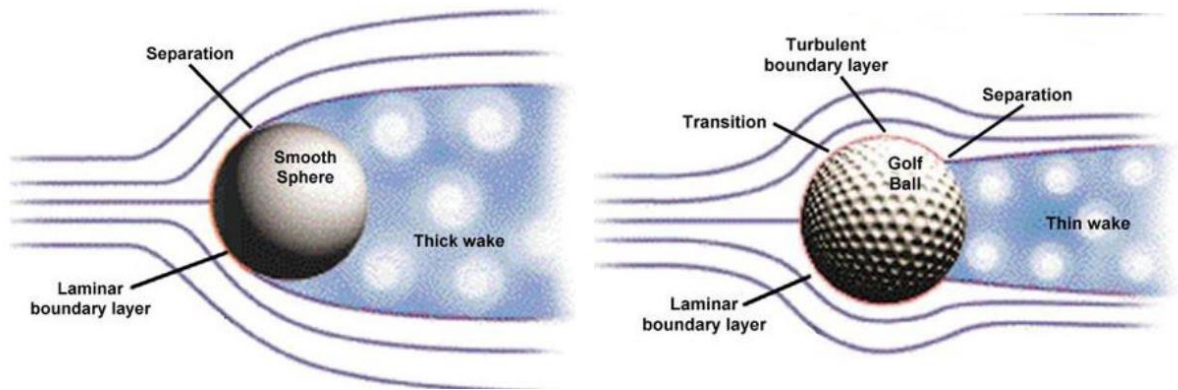


Figure D.0.6 Delay Separation on Golf Ball (from [57])

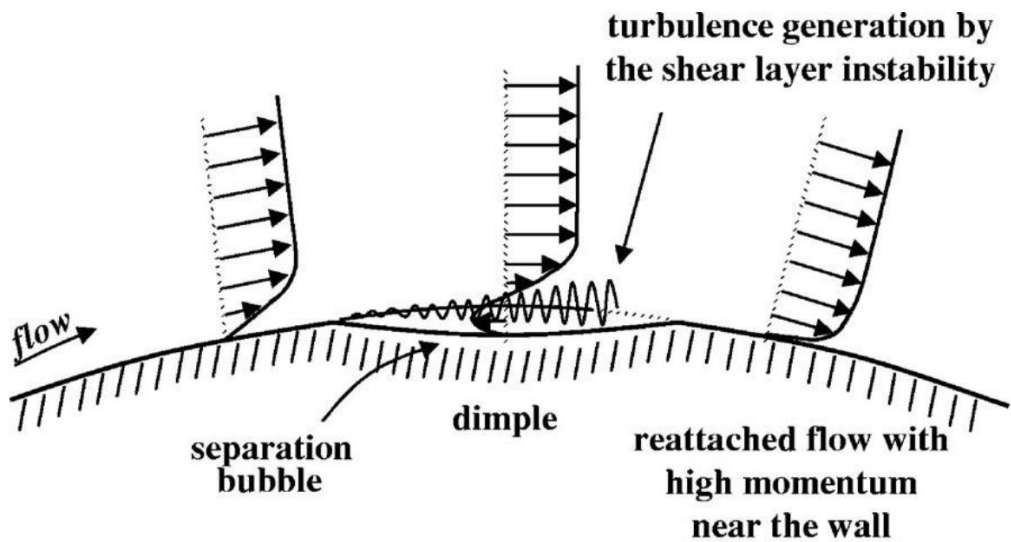


Figure D.0.7 The Mechanism of Flow Separation Delaying by Dimples on Surface (from [58])

Briefly, the flow separation occurs when the momentum of the flow is not enough to overcome the pressure gradient. Separation bubbles are generated in the dimples and this situation induces a turbulent boundary layer. The momentum of the turbulent boundary layer is higher than laminar. So the flow can reattach to the wall and the separation is delayed [58].

This phenomenon is dependent to Reynolds number. For a smooth circular cylinder, there is a critical Reynolds number that the drag coefficient dramatically changes. That point corresponds to the separation. It is between Reynolds number of  $1e+5$  and  $1e+6$  for a smooth sphere. In this studies' specific case, the flow on the motor booms would have a Reynolds number around 20000, in case there is no prop-wash on

them. On the other hand, considering that they are at a point that is very close to the propellers; it can be expected to have a close  $Re$  value to  $1e+5$  on the booms. Thus, it seems suitable to apply this methodology for reducing the drag. Besides, it should be taken into account that the prop-wash is a complex flow with high vortices, so the case may have different characteristics with golf ball or other simple cases.

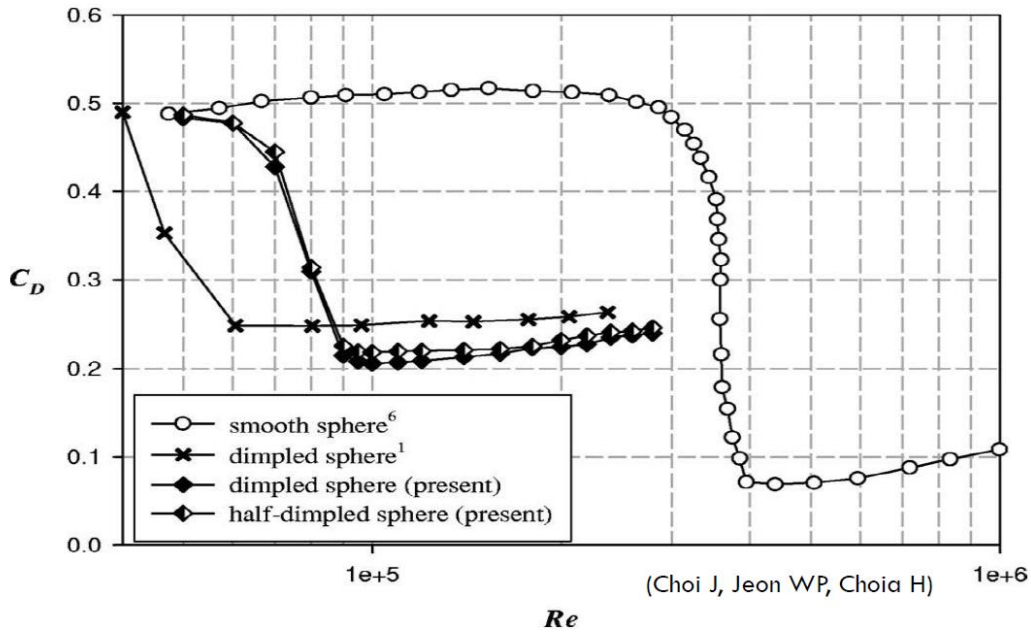


Figure D.0.8 Drag Coefficient Variation of Some Geometries with Reynolds Number ([from[58]])

Another study with similar logic but different practice is about manipulating the upstream flow. [59] Again, the same range of Reynolds numbers is investigated. A turbulator rod is set in front of the cylinder to increase the turbulence in upstream of the cylinder. In optimum conditions, it is said that a drag reduction of 63 % could be obtained as an outcome of this study.

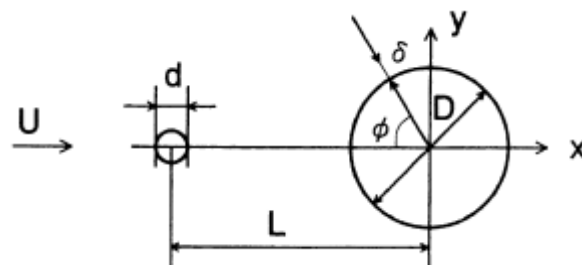


Figure D.0.9 Sketch of the Experimental Flow Geometry [59] (from [59])

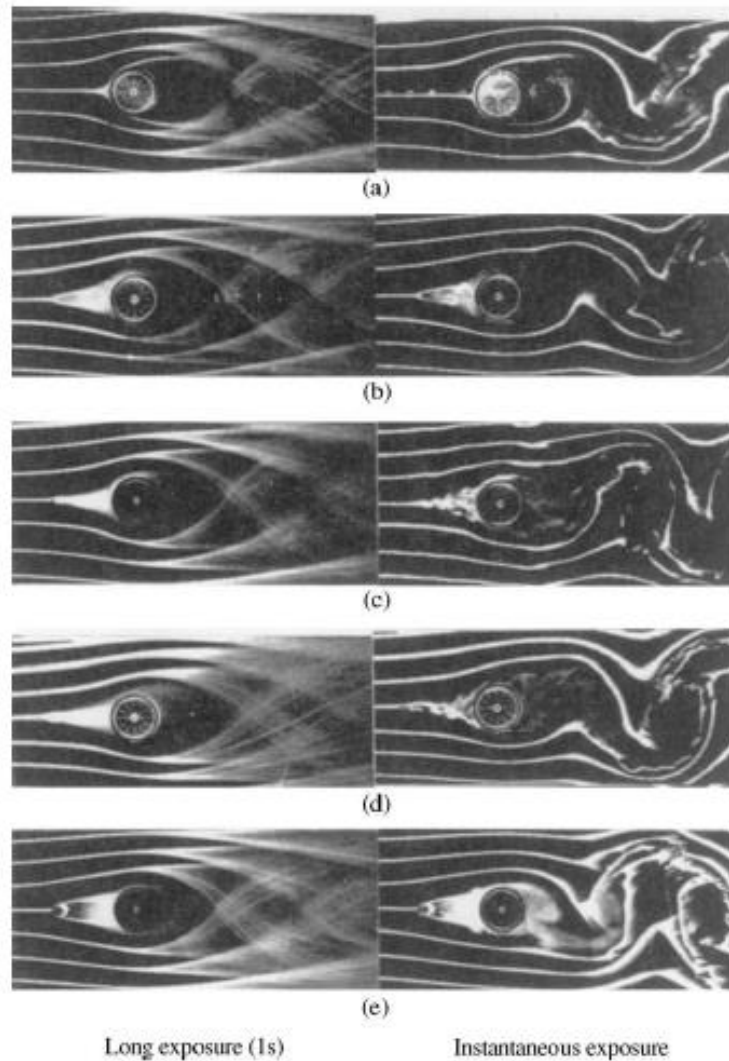


Fig. 2. Flow visualization by smoke tunnel. (a) Without rod,  $Re = 1.5 \times 10^4$ , (b) pattern B,  $d/D = 0.075$ ,  $L/D = 1.75$ ,  $Re = 1.5 \times 10^4$ , (c) pattern A,  $d/D = 0.075$ ,  $L/D = 1.75$ ,  $Re = 2 \times 10^4$  (d) pattern A,  $d/D = 0.075$ ,  $L/D = 2.0$ ,  $Re = 1.5 \times 10^4$  and (e) pattern B,  $d/D = 0.25$ ,  $L/D = 2.0$ ,  $Re = 1.5 \times 10^4$ .

*Figure D.0.10 Flow Visualization of the Experiment in [59] (from [59])*

This is a similar method used by radio control (R/C) modellers with same purpose. For the specific case of this aircraft, placing the manipulating rod in front of the boom can be hard due to physical limitations, but it would be a conceptually straightforward and cheap option.

On the other hand, aft of the boom is more available in terms of physical space. Placing a “splitter plate” would be an option to reduce the drag [45]. Theoretical background can be explained briefly as such: The motion characteristic of the vortex

street behind the circular cylinder is affected by placing a splitter plane at the centreline of it. Behind the cylinder, Strouhal number is decreased and the local pressure increase. [45], [60]. Thus, a higher pressure field is obtained behind the cylinder and the total form drag reduces, as the pressure difference between both sides is decreased.

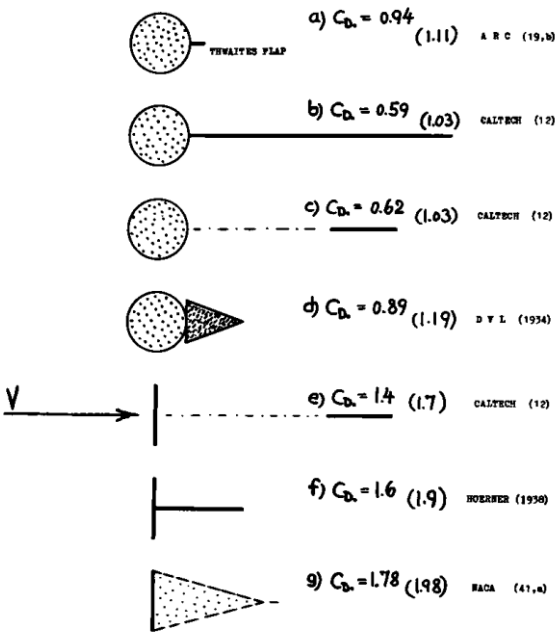


Figure 8. Influence of “splitter” plates (and similar devices) on the drag coefficient of vortex-street-producing shapes (tested between walls). The values in brackets are the drag coefficients without wake interference. The Reynolds numbers (on  $d$  or  $h$ ) are between  $10^4$  and  $10^5$ .

Figure D.0.11 Influence of Splitter Plates on Drag Coefficients of Several Geometries (from [45])

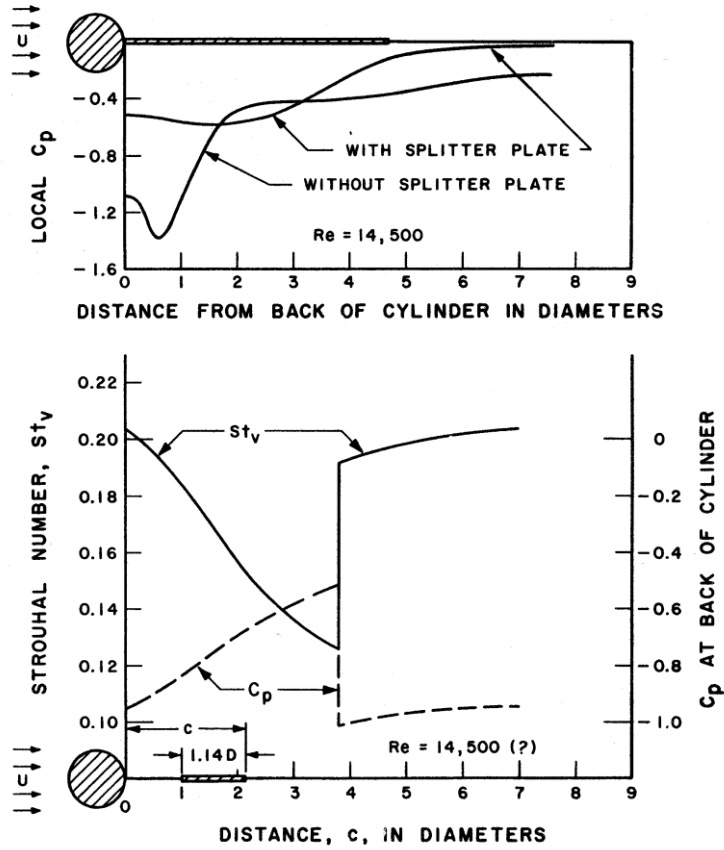


Figure D.0.12 Effects of Splitter Plates upon  $St_v$  and Localised Pressure Coefficient (from [61])

This method is good for being easy and cheap to manufacture; but the problem of decreasing carrying capacity in hovering may arise due to the downwash hitting the splitter plate. A careful splitter plate design with trade-off analyses should be made in case of using this method.



## APPENDIX E

### JUSTIFICATION OF THE STRUCTURAL DESIGN OF THE AIRCRAFT BY STATIC LOADING

The structural design of the aircraft is tested by static wing loading of 1g and 3g; and motor boom tip loading of 1.5 kgf. In wing loading tests, elliptical load distribution is assumed. The loads are calculated along the span by integrating the load per unit length,  $q$  [N/m]. A Riemann sum approach is used to calculate the loads at the stations. In below formula, “W” refers the total load on one wing in Newton, and “b”

refers the wing span. 
$$q(x) = \frac{4 \cdot W}{\pi \cdot b} \cdot \sqrt{1 - \frac{x^2}{b^2}}$$

Considering the mission concept of the aircraft, the maximum loading in a possible flight envelope is thought to be around 2g from past experiences. By applying a factor of safety of 1.5, 3g static wing loading test is realized.



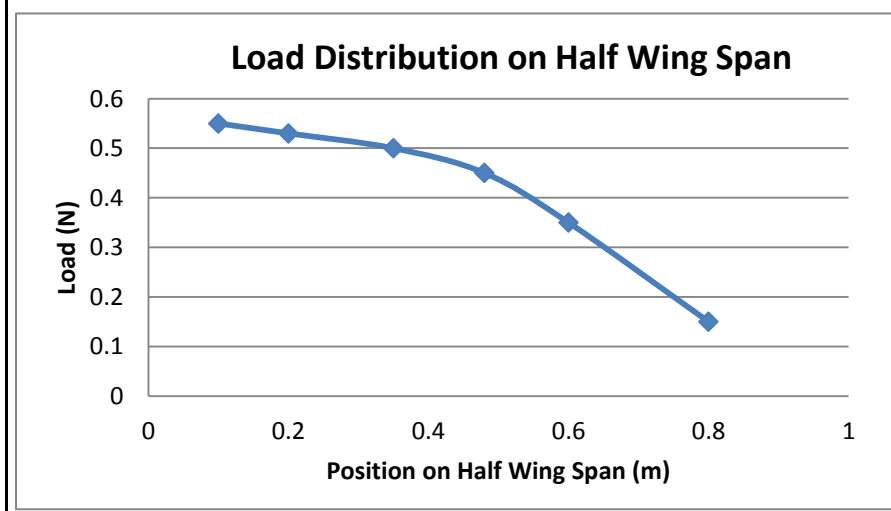
*Figure E.0.1 1g Static Wing Loading Test (about 2.5kg at each wing)*



Figure E. 0.2 1g Static Wing Loading Test (about 2.5kg at each wing)

Table E.1 Loads at the Stations in 1g Static Wing Loading Test

<u>Station #</u>	<u>Station position (from root)(m)</u>	<u>Load (kg)</u>
x1	0.8	0.15
x2	0.6	0.35
x3	0.48	0.45
x4	0.35	0.5
x5	0.2	0.53
x6	0.1	0.55
	<b>SUM</b>	<b>2.498</b>



In 1g test, a total load of 5 kg (2.5 kg at each wing) is applied from the quarter chord of the wing. About 3.5 mm of wing tip deflection is measured and no sign of fracture or surface buckling is observed.

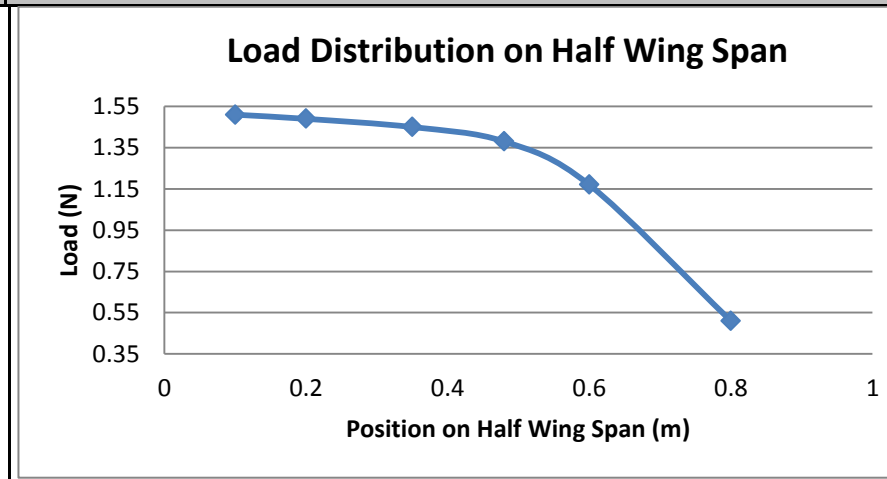


Figure E. 0.3 Wing Deformation in 1g Static Wing Loading Test

In 3g test, a total load of 15 kg (7.5 kg at each wing) is applied from the quarter chord of the wing. About 21.5 mm of wing tip deflection is measured and no sign of fracture or surface buckling is observed.

Table E.2 Loads at the Stations in 3g Static Wing Loading Test

<u>Station #</u>	<u>Station position (from root)(m)</u>	<u>Load (kg)</u>
x1	0.8	0.50
x2	0.6	1.17
x3	0.45	1.38
x4	0.35	1.45
x5	0.2	1.49
x6	0.1	1.51
<b>SUM</b>		<b>7.5</b>





*Figure E.0.4 3g Static Wing Loading Test (about 7.5 kg at each wing)*



*Figure E.0.5 Wing Deformation in 1g Static Wing Loading Test*

For the motor booms, 1.5 kgf, which is the maximum thrust value of the propellers, is applied at their tips. In average 1.5 mm of tip deflection is measured and no sign of fracture is observed.

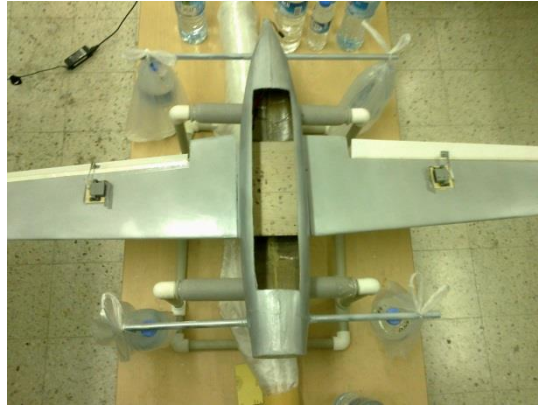


*Figure E.0.6 Static Loading of Motor Booms*